AN ANALYTICAL AND EXPERIMENTAL INVESTIGATION

OF BUBBLE WAITING TIME IN NUCLEATE BOILING

by

Ameer Ali, B.Eng. (Mech. Eng.)

A Thesis
Submitted to the School of Graduate Studies
In Partial Fulfilment of the Requirements
For the Degree
Master of Engineering

McMaster University

May 1980

AN ANALYTICAL AND EXPERIMENTAL INVESTIGATION
OF BUBBLE WAITING TIME IN NUCLEATE BOILING

TO MY PARENTS

11

MASTER OF ENGINEERING   McMaster University
(Mechanical Engineering)

TITLE: An Analytical and Experimental Investi-
                    gation of Bubble Waiting Time in Nucleate
                    Boiling

AUTHOR: Ameer Ali, B.Eng. (Mech. Eng.),
                    (McMaster University)

SUPERVISOR: Dr. Ross L. Judd

NUMBER OF PAGES: xii, 149

ABSTRACT

An analytical and experimental study of bubble waiting time for dichloromethane boiling on a glass surface is reported in this thesis. Bubble waiting time data for boiling at heat fluxes of approximately 8000, 10000, 12000, 14000, 16500 and 19000 BTU/hr ft^2 and subcooling values of 1.6, 14.7 and 30.0 $^{\circ}$F is presented.

In as much as bubble nucleation theory formulated on the basis of diffusion of heat to the thermal layer predicted results for bubble waiting time that were inconsistent with experimental data, a bubble nucleation theory incorporating both diffusion and convective transport of heat to the liquid in the vicinity of active sites was developed. The bubble waiting time results predicted by this theory agreed very well with experimental observations and therefore the evidence suggests that the convective contribution of heat transfer to the liquid layer adjacent to the heat transfer surface is a significant parameter in bubble nucleation.

ACKNOWLEDGEMENTS

TABLE. OF CONTENTS

LIST OF FIGURES

xi

LIST OF TABLES

CHAPTER 1

INTRODUCTION

Boiling heat transfer is the most efficient means of heat transfer in use. Modern technological devices such as nuclear reactors and space vehicles require the removal of tremendous quantities of thermal energy and the demand for a deeper understanding of the boiling phenomenon is now greater than ever. Boiling heat transfer has therefore become a very challenging field in contemporary heat transfer research.

Boiling heat transfer is defined as the mode of heat transfer that occurs with a change of phase from liquid to vapour within the bulk of a liquid. Boiling occurs when the liquid temperature exceeds its saturation temperature at a given pressure. The two basic types of boiling are forced convection boiling and pool boiling; forced convection boiling occurs in a flowing stream of liquid whereas pool boiling occurs on a heating surface submerged in a quiescent pool of liquid. Depending on the heat flux transferred to the liquid by the heating surface, either individual vapour bubbles (nucleate boiling) or a continuous vapour film (film boiling) will appear on the surface.

A unique characteristic of nucleate boiling is the presence of active sites on the heat transfer surface. These

1.

active sites, called nucleation sites, have the ability to
initiate and support the nucleation of vapour bubbles. Nucle-
ation sites have been demonstrated conclusively to be tiny
pits,-scratches and other imperfections on the heat transfer
surface. The rate of heat transfer in nucleate boiling de-
pends on the number of active sites per unit area. As the
temperature of the heat transfer surface is raised above the
liquid saturation temperature, the number of active sites
increases and this is accompanied by increased heat transfer
rates.

In the process of nucleate boiling, bubbles nucleate
at active sites, grow rapidly and eventually detach themselves
from the heating surface. Depending on whether the liquid is
subcooled or saturated the bubbles will either collapse in
the bulk of the liquid or continue to grow and rise all the
way to the free surface. 'In both cases, however, the genera-
tion and departure of bubbles are thought to produce strong
hydrodynamic currents in the boiling liquid which lead to
extremely high rates of heat transfer.

The behaviour of vapour bubbles at active sites consti-
tute one aspect in the systematic study of nucleate boiling.
Although intensive experimental and theoretical investiga-
tions have been performed over the past few decades in every
aspect of boiling, much remains to be learned.

CHAPTER 2

LITERATURE SURVEY

2.1. Nucleation Phenomena and Active Site Distribution

Theoretical considerations [1, 2, 3, 4] have shown that nucleation of gas or vapour bubbles occurs preferentially from surface cavities as opposed to nucleation from plane surfaces and surface projections and that systems with poor wetting characteristics promote nucleation much easier than well wetted systems. Thus, poorly wetted surface cavities should hold the greatest promise of being active sites. These considerations further show that poorly wetted cavities have a strong tendency to entrap gases or vapour. From these arguments most cases of nucleation should occur at poorly wetted surface cavities with a pre-existing gas or vapour phase. The experimental evidence [5, 6, 7, 8, 9] in support of these theories is quite convincing and it is now generally accepted that naturally occuring pits, and to a lesser extent scratches, do indeed serve as active nucleation sites in pool boiling.

In 1959, Clark, Strenge and Westwater [7] studied active sites in nucleate boiling and demonstrated that grain boundaries and regions of special atomic densities on a heating surface do not necessarily act as active nucleation sites.

3.

Berenson [10] studied the characteristic pool boiling curve, which is a plot of heat flux versus wall superheat, for different surface materials and found that the temperature difference required to produce a given heat flux for the same surface finishing technique depends on the surface material. It was postulated that this difference in behaviour is caused by the difference in material hardness which tends to change cavity size and distribution, and the difference in thermal properties of the surface. A subsequent investigation [11] confirmed these results.

The effect of surface roughness on boiling characteristics has been investigated extensively over the past four decades. In 1936, Jakob [12] demonstrated that increasing surface roughness progressively shifts the boiling characteristic curve to the left as shown in Figure 1. Corty and Foust [13] made measurments of nucleate boiling coefficients for a variety of liquids on a horizontal heated surface of different roughnesses. They found that both the position and slope of the boiling characteristic curves varied with surface roughness and that the wall superheat generally decreased as r.m.s. roughness increased. Kurihara and Myers [14] conducted similar experiments and observed a greater number of active sites on a rough surface than on a smooth one. Their results imply that a rougher surface yields a higher heat transfer coefficient than a smooth one. The

Curve No.   State of Heating Surface

1   Recently Roughened by a Sand Blast

2   Same, Oxidized by Longer Use

3   Same, Roughened Once More by Sand Blast

4   Same, After Long Use

5   Recently Fitted with a Roughness Screen
     and Cleaned

6   Same, After 4 Hours of Boiling, Followed by
     24 Hours of Lying in Water

7   Same, After 8 More Hours of Boiling, Followed
     by Another 24 Hours of Lying in Water
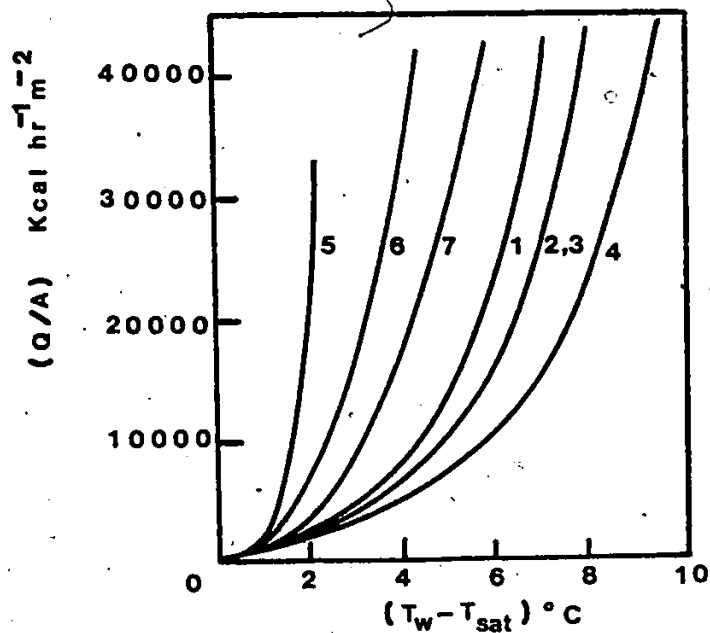
Figure 1   Effect of Surface Roughness on the
            Boiling of Water According to Jakob [12].

experimental results of Nishikawa [15] and Hsu and Schmidt [16] agreed with those of Kurihara and Myers.

Subsequent to this, Hatton and Hall [17] did a photographic study of boiling on prepared surfaces and found that

$$N/A = Constant \times P^{2.5} \qquad 2.1$$

For a given heat flux the Constant increased with rougher grades of surface finish and for a given surface finish it increased with heat flux.

Vachon, Tanger, Davis and Nix [18] presented pool boiling data in 1966 which showed an increase and subsequent decrease in heat transfer with increasing r.m.s. roughness for polished surfaces. The investigators demonstrated that surfaces of the same r.m.s. roughness but with different surface preparation techniques, produce markedly different boiling curves.

In 1970, Nix, Vachon and Hall [8] conducted a scanning and electron microscopy study of pool boiling surfaces and came to the conclusion that an increase in r.m.s. roughness does not necessarily mean an increase in active nucleation sites and heat transfer. They concluded that both r.m.s. roughness and surface preparation technique combine to influence the number of sites activated. The investigators pointed out that a profilometer, which measures surface roughness by interpretting the motion of a diamond tip needle as it moves across a surface, can give a very misleading picture of the

surface with respect to the dimensions of nucleation sites because of the size of the profilometer tip. The tip could bridge many of the depressions and cavities, thus giving an erroneous indication of the nucleation characteristics of the surface. Nucleation sites are microsopic imperfections in a surface and r.m.s. roughness values are estimates of macroscopic conditions. It is felt that no reliable accurate measuring technique or scale of micro-roughness suitable for boiling studies exists at this time.

In 1962, Gaertner [19] presented a statistical analysis of the only existing data at that time of the spatial distribution of boiling nucleation sites. As shown in Figure 2, Gaertner demonstrated excellent agreement between the data and the prediction of a Poisson's distribution of the form

$$P_U(Na) = \frac{a}{A} Z_{Na} = [e^{-\bar{N}a}(\bar{N}a)^{Na}]/(Na)! \qquad 2.2$$

It was therefore concluded that active nucleation sites are randomly distributed. Gaertner went on to perform a statistical analysis of nearest neighbor distances between active sites and showed by theoretical considerations that

$$S_{mp} = \frac{1}{\sqrt{2\pi}} \left(\frac{\bar{N}}{A}\right)^{-\frac{1}{2}} \qquad 2.3$$

$$\bar{S} = \frac{1}{2} \left(\frac{\bar{N}}{A}\right)^{-\frac{1}{2}} \qquad 2.4$$

$$\sqrt{\bar{S}^2} = \frac{1}{\sqrt{\pi}} \left(\frac{\bar{N}}{A}\right)^{-\frac{1}{2}} \qquad 2.5$$
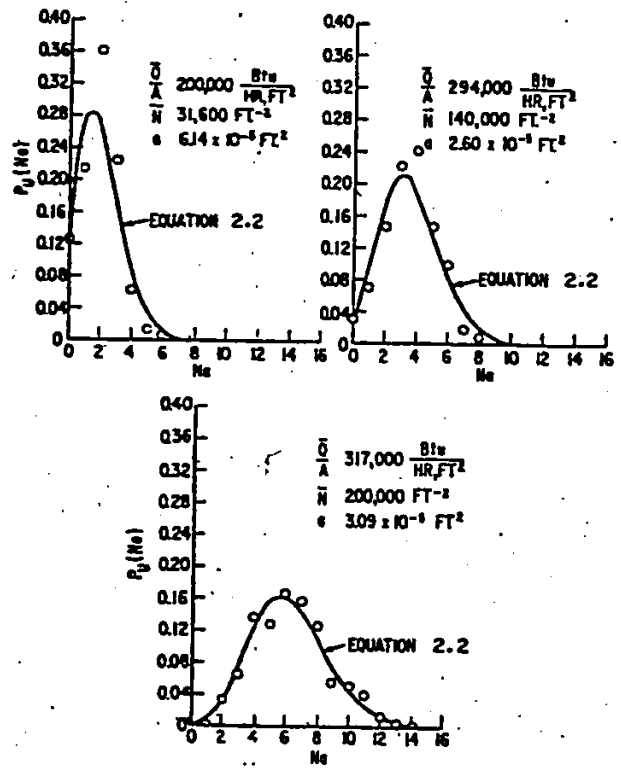
Figure 2   Distribution of Local Active Site
Populations According to Gaertner [19].

where S_{mp} is the most probable nearest neighbor distance
between active sites, $\bar{S}$ is the mean nearest neighbor dis-
tance between active sites and $\sqrt{\bar{S^2}}$ is the root-mean-square
nearest neighbor distance between active sites. Figure 3
shows fair agreement between the experimental data analyzed
by Gaertner and equations 2.3, 2.4 and 2.5.

More recently, Sultan [20] investigated spatial dis-
tribution of active sites at different levels of heat flux
and subcooling. In accordance with the procedure devised
by Gaertner, the heat transfer surface was divided into a
number of small squares and the probability of finding a
local population Na was calculated as

$$P_U(Na) = \frac{a}{A} Z_{Na} \qquad\qquad 2.6$$

Good agreement was shown with the Poisson's distribution,
thus confirming that active nucleation sites are randomly
distributed. By making a refinement in the procedure of
calculating nearest neighbor distance, Sultan was able to
show a better agreement between his data and the predictions
of equations 2.3, 2.4 and 2.5 as shown in Figure 3.

2.2. Characteristics of Active Sites

Figure 4 shows a vapour-liquid interface in a conical
cavity. Assuming that the curved interface is part of a
sphere and that isothermal equilibrium conditions exist, it
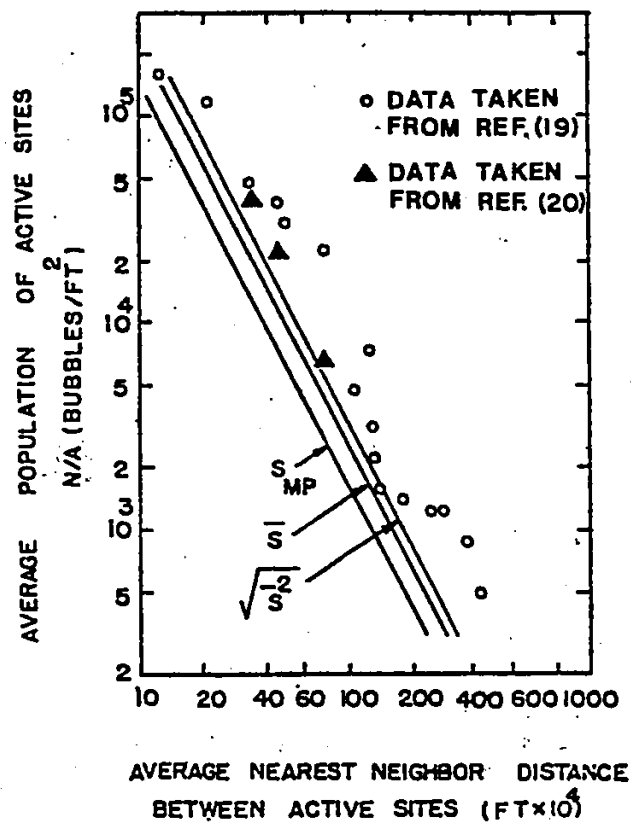
Figure 3   Average Nearest-Neighbor Distance
Between Active Sites According to
Gaertner [19] and Sultan [20].

Liquid Vapor

(4)

(*)

L
V

$\beta = 90°$

(1)

r_4

r^*

r

(0)

r_1

o

θ
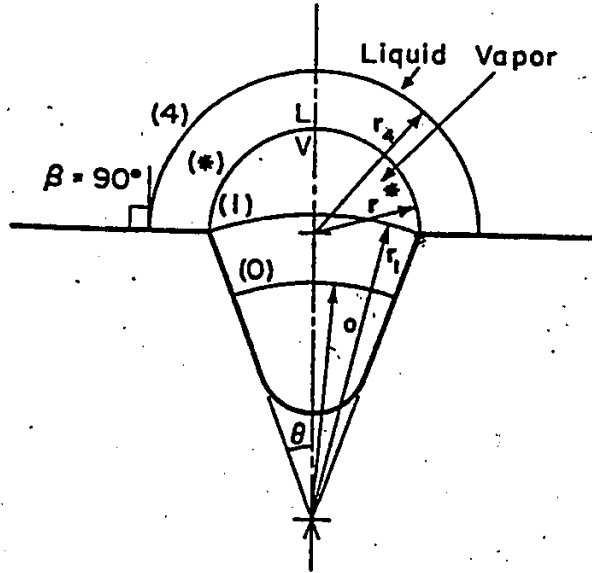
Figure 4   Conical Cavity with Vapour Nucleus According
to Griffith and Wallis. [6].

$\frac{1}{r}$

$\frac{1}{r}^{*}$

(0) (1)   (*)   .(4) Volume
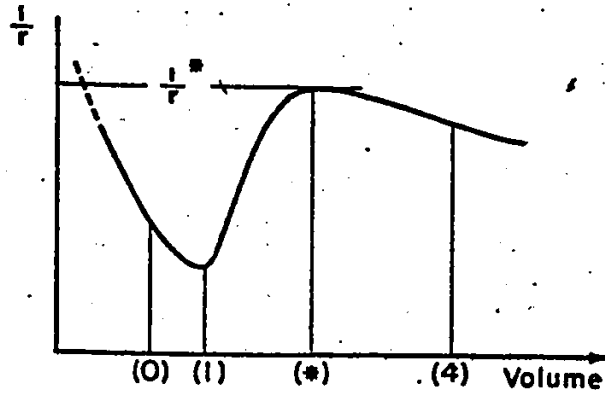
Figure 5   Plot of the Inverse of Bubble Nucleus Versus
Bubble Volume According to Griffith and
Wallis [6]..

can be shown that

$$P_v - P_\ell = \frac{2\sigma}{r} \qquad\qquad 2.7$$

According to the Clausius-Clapeyron relationship

$$\frac{dP}{dT} = \frac{h_{fg}}{v_{fg}T} \qquad\qquad 2.8$$

Equation 2.8 can be approximated by the form

$$\frac{P_v - P_\ell}{T_v - T_{sat}} = \frac{h_{fg}\rho_v}{T_{sat}} \qquad\qquad 2.9$$

Elimination of $(P_v - P_\ell)$ from equations 2.7 and 2.9 results in

$$T_v - T_{sat} = \frac{2\sigma T_{sat}}{r\rho_v h_{fg}} \qquad\qquad 2.10$$

Assuming that the vapour is in thermal equilibrium with the solid surface

$$T_w = T_v \qquad\qquad 2.11$$

and equation 2.10 becomes

$$T_w - T_{sat} = \frac{2\sigma T_{sat}}{r\rho_v h_{fg}} \qquad\qquad 2.12$$

from which it may be deduced that

$$r = \frac{2\sigma T_{sat}}{\rho_v h_{fg}(T_w - T_{sat})} \qquad\qquad 2.13$$

Figure 5 shows a plot of 1/r versus bubble volume with a contact angle of $90°$. The diagram shows that when the bubble arrives at the lip of the cavity its radius of curvature begins to decrease with increasing bubble volume. Finally when the bubble projects beyond the cavity with the shape of

a hemisphere, further increases in volume results in an increase in the radius of curvature of the bubble once again. With this trend of behaviour, the minimum radius of curvature of the bubble is equal to the radius of the cavity mouth and is called the critical radius r_c. Equation 2.12 shows that r_c determines the minimum superheat needed to initiate the growth of a bubble.

Griffith and Wallis [6] conducted extensive experiments on specially prepared surfaces in which they investigated nucleation characteristics of single artificial cavities. They concluded that the theory of nucleation embodied in equation 2.12 is substantially correct when the liquid is uniformly superheated and that the specification of a single dimension r_c for the characterization of a nucleation site is sufficient. The authors postulated that for surfaces of the same material treated in the same way a single curve should result when the number of active sites per unit area N/A is plotted versus theoretical cavity radius $2\sigma T_{sat}/[\rho_v h_{fg}(T_w - T_{sat})]$, regardless of the type of fluid or its pressure. Figure 6, taken from Reference [6], shows that this is exactly the case. It was therefore concluded that the nucleation characteristics of a surface is fixed if the size distribution of the cavities on the surface is known.

Shoukri [21] later investigated nucleation phenomena and concluded that the parameter group $2\sigma T_{sat}/\rho_v h_{fg}(T_w - T_{sat})]$ is
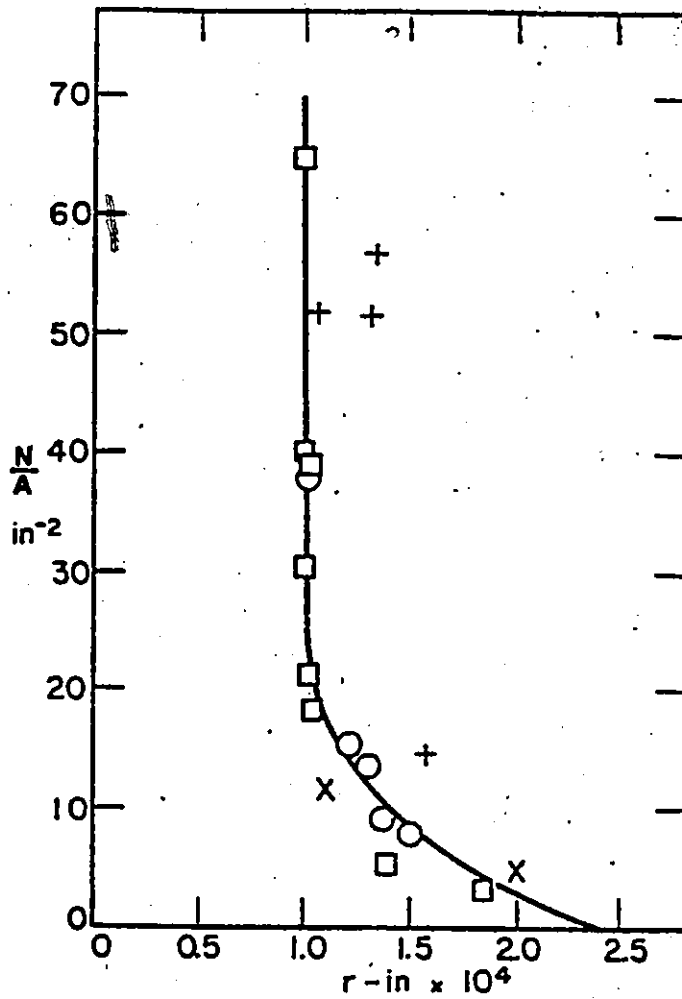
Figure 6   Plot of the Number of Active Sites per Unit
Area as a Function of Theoretical Cavity Radius
According to Griffith and Wallis [6].

generally capable of predicting the minimum nucleation cavity
radius and that this parameter group, together with Brown's
correlation [22]

$$\left(\frac{N}{A}\right)_{r_c} = C\left(\frac{1}{r_c}\right)^m$$ 2.14

constitute a sufficient method of describing boiling nuclea-
tion characteristics.

In 1962, Hsu [23] formulated a nucleation model to
predict the size range of active cavities. By assuming the
existence of favourable cavity geometry, the pre-existence
of a vapour nucleus sitting at the mouth of a cavity and a
limiting thermal layer thickness δ adjacent to the heat
transfer surface, he derived the following expressions:

$$r_{c,max} = \frac{\delta}{2C_1}\left\{\left(1 - \frac{\theta_{sat}}{\theta_w}\right) + \left[\left(1 - \frac{\theta_{sat}}{\theta_w}\right)^2 - \frac{4AC_3}{\delta\theta_w}\right]^{\frac{1}{2}}\right\}$$ 2.15

$$r_{c,min} = \frac{\delta}{2C_1}\left\{\left(1 - \frac{\theta_{sat}}{\theta_w}\right) - \left[\left(1 - \frac{\theta_{sat}}{\theta_w}\right)^2 - \frac{4AC_3}{\delta\theta_w}\right]^{\frac{1}{2}}\right\}$$ 2.16

For a cavity to be active

$$r_{c,min} < r_c < r_{c,max}$$ 2.17

Hsu tested his nucleation model on the experimental
data of Clark et al [7] and obtained good agreement. In a
later boiling experiment, Heled and Orell [24] identified
active sites in the range 5.9×10^{-4} to 2×10^{-3} inches. The theo-
retical size range predicted by Hsu's model with an assumed

value of 3000 micro-inches for δ is 2×10^{-4} to 1.3×10^{-3} inches.
The experimental and theoretical results are therefore in
reasonably good agreement.

In a recent investigation, Wiebe and Judd [25] measured
the thermal layer thickness δ for water boiling on a copper
surface. They found that thermal layer thickness increases
as heat transfer coefficient decreases and subcooling increases,
and that thermal layer thickness and active site density are
interrelated so that δ is not a constant as previously assumed.

Han and Griffith [26] also presented a theoretical treat-
ment of the mechanism of nucleate boiling. With the same
assumptions as those underlying the Hsu's model but with a
change of one of the boundary conditions, they developed the
following expressions for the most favourable cavity range

$$r_{c,max} = \frac{\delta(\theta_w - \theta_{sat})}{3\theta_w} \left\{ 1 + \left[1 - \frac{6A\theta_w}{(\theta_w - \theta_{sat})^2 \delta} \right]^{\frac{1}{2}} \right\} \qquad 2.18$$

$$r_{c,max} = \frac{\delta(\theta_w - \theta_{sat})}{3\theta_w} \left\{ 1 - \left[1 - \frac{6A\theta_w}{(\theta_w - \theta_{sat})^2 \delta} \right]^{\frac{1}{2}} \right\} \qquad 2.19$$

In 1974, Shoukri [21] compared both theoretical models
with experimental data and found good agreement with a ten-
dency for active nucleation sites to fall in the lower portion
of the predicted range of cavity radii.

2.3 Thermal Boundary Layer and Bubble Formation Process

Among the parameters recognized as significant in

nucleate boiling is the thickness of the superheated boundary layer adjacent to the heat transfer surface and the temperature profile within it. Generally, there exits two distinctive types of thermal boundary layer [23] as shown in Figure 7. The first type, whose thickness is denoted by δ_1 in Figure 7, is governed by the gross action of all the nucleation sites. It is believed that this type of thermal layer is important in predicting the gross heat transfer. The second type of thermal layer, which is transient in nature and whose thickness is denoted by δ_2 in Figure 7, exists in the close vicinity of the active nucleation site and is the governing factor for bubble nucleation as discussed in References [23], [26] and [29]. Because of the relatively short duration of time allowed for its growth, the thickness of the local thermal boundary δ_2 is about an order of magnitude less than δ_1.

Yamagata, Nishikawa and Matsouka [28] measured the thermal boundary layer thickness, which should be δ_1 in Figure 7, by means of an optical technique and found it to be of the order of 10^{-2} inches.

In 1965, Marcus and Dropkin [29] investigated the temperature profile within the superheated layer δ_1 adjacent to a nickel plated copper surface in saturated nucleate pool boiling of water and demonstrated that very near to the heating surface the temperature profiles are essentially linear and beyond the linear region it varies with some power in
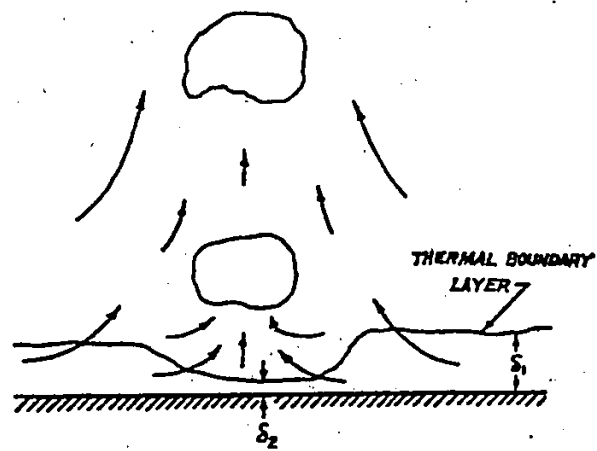
Figure 7   Thermal Boundary Layers and Temperature and
           Velocity Fields in the Layer of Liquid Adjacent
           to a Heat Transfer Surface According to Hsu [23].

accordance with

$$T - T_\infty \propto y^{-a} \qquad\qquad 2.20$$

Although the thermal boundary layer ξ was previously
defined as the height above the surface beyond which the
average bulk temperature is uniform, Marcus and Dropkin
observed from their temperature profile diagrams, Figure 8
and Figure 9, that it would be difficult to define such a
height precisely since the temperature gradient approaches
the bulk liquid temperature very slowly. This, coupled with
the fact that the highly superheated region very near to the
heating surface is most responsible for bubble dynamics,
prompted the authors to introduce a new definition for super-
heat layer thickness. They defined a thickness δ as the
height of the intersection between the tangent to the tempera-
ture profile at the surface and the constant liquid bulk-
temperature line as depicted in Figure 10. The tangent line
defining δ is actually an extrapolation of the linear portion
of the temperature distribution to the bulk liquid temperature
and δ is therefore called the "extrapolated superheat layer
thickness". This parameter is usually an order of magnitude,
less than ξ but it is a more useful one since it reflects the
thickness of the very important and highly superheated region
of the thermal boundary layer. Marcus and Dropkin observed
that δ decreased with increasing heat flux.

More recently, Wiebe and Judd [25] studied the temper-
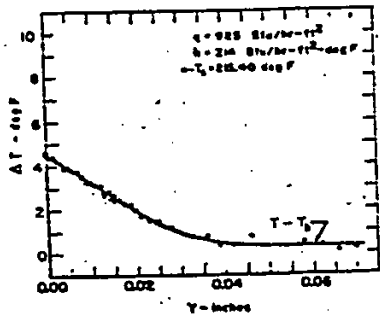
Figure 8   Temperature Profile at
Low Heat Flux According
to Marcus and Dropkin
[29].
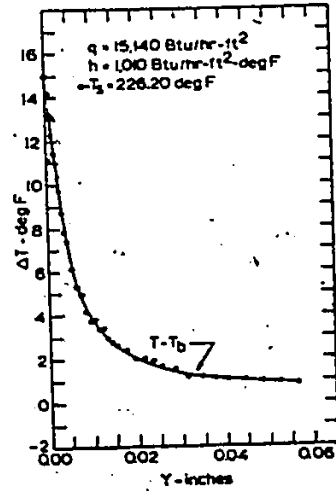
Figure 9   Temperature Profile
at High Heat Flux
According To Marcus
and Dropkin [29].
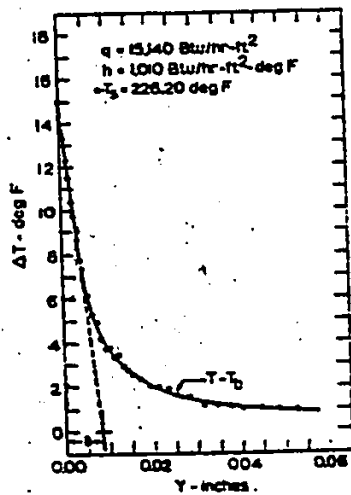
Figure 10   Temperature Profile and Defina-
tion of "Extrapolated Superheat
Layer Thickness" According to
Marcus and Dropkin [29].

ature profiles in saturated and subcooled boiling of water on a copper surface. The authors confirmed the results of Marcus and Dropkin and established that increasing the heat flux and decreasing subcooling has the effect of reducing the extrapolated superheat layer thickness.

In 1961, Hsu and Graham [27] did a detailed analytical and experimental investigation of the thermal boundary layer and bubble emission cycle in nucleate boiling and concluded that a cycle of bubble nucleation and growth consists of the following stages:

a) Growth of the local thermal boundary layer

b) Bubble growth

c) Detachment of the bubble from the heating surface. Bubble detachment at the end of the growth period is invariably followed by the destruction of the thermal layer as relatively cold liquid from the liquid bulk rushes in to fill the void left by the departed bubble. A new cycle begins as the thermal layer begins to recover. The authors observed from their experimental data that the bubble waiting period, which is the time required for the local thermal layer to recover after a bubble has left an active site, is generally larger than the growth period and is dependent upon cavity size r_c as well as the local thermal boundary layer thickness δ.

In the model which Hsu [23] developed in 1962 for

bubble nucleation, it was assumed that at the beginning of a
cycle a bubble nucleus sits at the mouth of a cavity of
favourable geometry. The nucleus can be assumed to be the
residual vapour left behind by the preceding bubble and is
surrounded by relatively cold bulk liquid. As time passes,
the cold liquid is warmed up by transient conduction and
the local thermal boundary layer thickness increases. When
the surrounding liquid becomes warmer than the bubble nucleus
the waiting period comes to an end and the bubble begins to
grow. Hsu postulated that the waiting period ends and the
growth period begins when the temperature in the local thermal
boundary layer at a height corresponding to the height of the
vapour nucleus achieves the temperature inside the nucleus.
After the bubble has grown to a sufficient size it detaches
from the heating surface and rises towards the free surface
of the liquid. Relatively cold liquid from the bulk liquid
then rushes into the void left behind by the departed bubble,
the local thermal boundary layer is destroyed and the bubble
cycle begins again.

Best, Burow and Beer [30] investigated bubble dynamics
through laser interferometry and have presented a set of inter-
ferograms which show that the temperature distribution in the
layer of liquid adjacent to the heat transfer surface cannot
be accounted for by conduction alone. It appears that, in
addition to conduction, there is a convective component of

heat transfer operating in the local thermal boundary layer that cannot be neglected in any analysis.

2.4 Bubble Emission Frequency and Departure Diameter

Nucleate boiling is characterized by high intensity heat transfer. Although several mechanisms of heat removal - vapour liquid exchange, turbulization of the liquid layer at the heat transfer surface, microlayer evaporation - may contribute in some proportion to the total heat transfer, bubble activity is a common feature of all of them. Bubble emission frequency f and bubble departure diameter D are important parameters in predicting heat transfer and they arise in such correlation as the Rohsenow equation [31]

$$\frac{Q}{A} = h_{fg} \rho_v \frac{N}{A} \frac{\pi}{6} D^3 f \qquad 2.21$$

McFadden and Grassman [32] investigated the relationship between bubble emission frequency and departure diameter and showed by dimensional analysis that

$$\frac{f D^2 \rho_\ell^{\frac{1}{2}}}{(\sigma D)^{\frac{1}{2}}} \; \alpha \; \left(\frac{g \Delta \rho D^2}{\sigma}\right)^a \qquad 2.22$$

where

$$\Delta \rho = \rho_\ell - \rho_v.$$

They then showed that their experimental data, taken over a wide range of frequencies and diameters, fitted equation 2.22 when $a \cong \frac{1}{2}$. This implied that

$$f D^{\frac{1}{2}} \cong 0.56 \left(\frac{g \Delta \rho}{\rho_\ell}\right)^{\frac{1}{2}} \qquad 2.23$$

for a given fluid. Assuming that $\Delta\rho \cong \rho_\ell$, then

$$fD^{\frac{1}{2}} \cong 0.56\sqrt{g} = 17.6 \text{ cm}^{\frac{1}{2}}/\text{sec} \qquad (2.24)$$

This result was confirmed by Cole [33].

In a more recent investigation [34] of the relation-ship between bubble emission frequency and departure dia-meter for water and sodium chloride, it was demonstrated that for water

$$Df^{0.5} = C \qquad \text{for } f > 20/\text{sec} \qquad (2.25)$$

$$fD^{0.3} = C \qquad \text{for } f < 20/\text{sec} \qquad (2.26)$$

and for sodium chloride solution

$$Df^{0.15} = C \qquad (2.27)$$

At this point in time there seems to be some controversy over the exact relationship between D and f and the value of the constant C.

In an experimental investigation of 1966, Cochran and Aydelott [35] demonstrated that bubble lifetime, which is the reciprocal of bubble emission frequency, decreases as liquid subcooling increases. This result was confirmed by Ellion [36] and Gunther [37]. However, in 1968 Judd [38] reported that his experimental data indicated that bubble lifetime increases, instead of decreasing, as liquid subcooling increases. More recently, Shoukri [39] advanced theoretical models which predicted a decrease of bubble emission frequency with a decrease of surface superheat,

with an increase of liquid subcooling and an increase in nucleation cavity size. Although the different models incorporated different equations for bubble growth period, they show very close agreement. The author's experimental data for water and iso-propyl alcohol boiling on a copper surface with two different surface finishes showed good agreement with the proposed models.

CHAPTER 3

THEORY

3.1 Introduction

In the course of nucleate boiling, periodic streams of bubbles are emitted from active cavities on the heat transfer surface. The time elapsed between two consecutive bubble departures from a given cavity is defined as the bubble period. The study of bubble period is divided into two parts: the study of the waiting period t_w, which is the time from the last bubble departure to the beginning of the next bubble formation and the growth period t_g, which is the time from the beginning of the bubble formation to its departure or collapse. The sum of the waiting period and growth period amounts to the bubble period or bubble lifetime.

In the sections to follow, models of bubble nucleation will be formulated and used to predict bubble waiting time for a given set of conditions. However, before proceeding to theoretical considerations it is appropriate to discuss at this point the conditions under which nucleation is thought to occur. A cavity is believed to be able to serve as an active nucleation site if it has the ability to hold gas or vapour in it [1, 2, 3, 4, 5, 6, 7, 8, 9]. The conditions necessary for the entrapment of a gas have been considered by Bankoff [4]. For simplicity, a semi-infinite

sheet of liquid was considered to be advancing during the
filling process unidirectionally towards a groove as shown
in Figure 11. If the contact angle β of the liquid were
greater than the wedge angle ϕ, the advancing liquid front
would strike the opposite wall of the cavity before it had
completed its advance down the near wall. A residue of
gas would therefore be trapped which could serve as a nucleus
for the formation of subsequent bubbles. Hence, the condi-
tion necessary for the entrapment of a gas is

$$\beta > \phi \qquad\qquad (3.1)$$

If the contact angle β is less than the wedge angle ϕ, the
vapour will be completely displaced by the advancing liquid
and the cavity will be deactivated.

Lorenz, Mikic and Rohsenow [40] assumed the exist-
ence of an idealized conical cavity and the vapour trapping
mechanism proposed by Bankoff and, on the basis of geometri-
cal considerations alone, generated a set of curves represent-
ing the relationship between the nucleus/cavity radii ratio
(r_n/r_c), the contact angle β and the cone angle ϕ. These
curves, shown in Figure 12, indicate that for a given cone
angle ϕ, there is a maximum value of contact angle β above
which the radius of curvature of the nucleus r_n in a cavity
is always identical with the cavity mouth radius r_c. It
means therefore that for liquids with relatively large
contact angles, or cavities with relatively small cone angles,
the radius of curvature of the vapour nucleus will always be
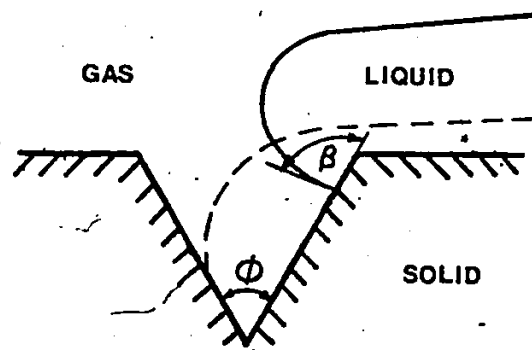
Figure 11   Conditions for the Entrapment of a Gas in the
Spreading of a Liquid Across a Groove According
to Bankoff [4].
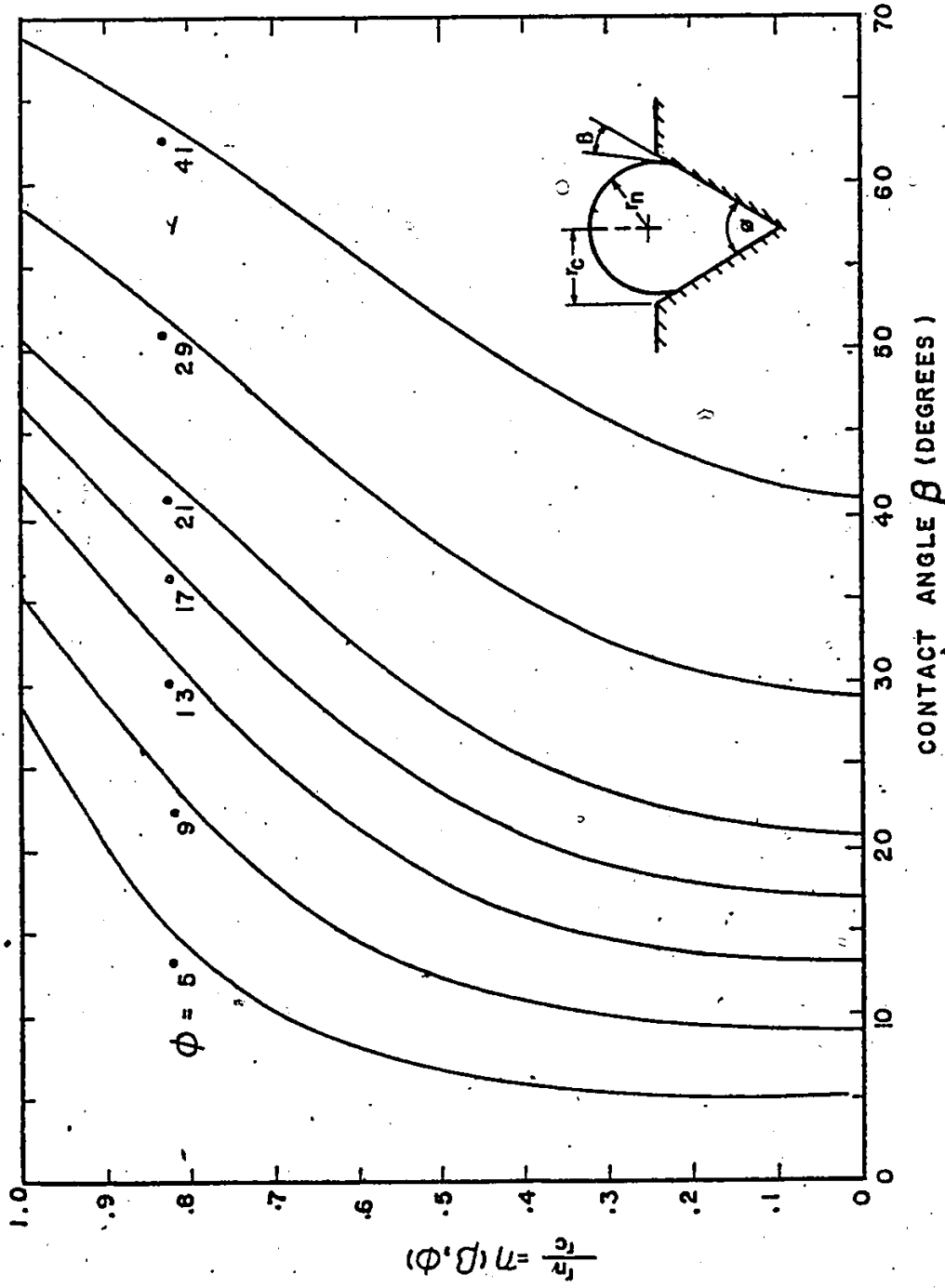
Figure 12 Relationship Between Effective Radius of Nucleation and Cavity Geometry
According to Reference [40].

identical with the cavity mouth radius. On the other hand,
if the liquid contact angle is too small or cavity too large,
the liquid-vapour interface may exist some distance in the
cavity mouth. The authors' own experimental data is in good
agreement with the proposed model.

Hsu [23] proposed a model for bubble nucleation
which assumed that at the beginning of an emission cycle
a bubble nucleus sits at the mouth of a cavity of favourable
geometry. The nucleus can be considered to be the residual
vapour left behind by the preceding bubble and is surrounded
by relatively cold bulk liquid at temperature T_∞. As time
passes, the cold liquid is heated up by transient conduction
and the local thermal boundary layer thickness increases;
when it grows to the extent that the surrounding liquid
becomes warmer than the vapour in the nucleus, the bubble
waiting time ends and the bubble begins to grow. After
achieving sufficient size the bubble detaches from the heat
transfer surface and leaves a residue of vapour behind in
the cavity that will act as the nucleus for the formation of
the next bubble. As the bubble leaves the heating surface,
bulk liquid at temperature T_∞ rushes in and fills the void
left behind and the local thermal boundary layer is destroyed.
A nucleus is once again surrounded by relatively cold bulk
liquid and another bubble cycle is about to begin.

3.2   Growth and Temperature Distribution in
       the Thermal Boundary Layer

In the formulation of bubble nucleation models

[23, 26] it was commonly assumed that the local thermal boundary layer grew as a result of diffusion from the heat transfer surface to the liquid. However, experimental data [30] indicates that the actual temperature distribution in the thermal layer in the near vicinity of an active nuclea- tion site cannot be accounted for by diffusion alone. Figure 13, taken from Reference [30] depicts the temperature dis- tributions at 0 m s, 4 m s and 8 m s after bubble detachment for water boiling on a copper surface. If it can be assumed that the wall temperature is instantaneously raised from bulk liquid temperature T_∞ to wall temperature T_w at the commence- ment of the thermal layer growth, then assuming conduction to be the only mode of heat transfer into the liquid it can be shown [41] that the temperature distribution in the thermal layer should be

$$\frac{T - T_\infty}{T_w - T_\infty} = erfc \frac{y}{2\sqrt{\kappa_\ell t}} \qquad (3.2)$$

Figure 14 shows a plot of T versus y at 4 m s and 8 m s after bubble detachment for the situation depicted in Figure 13. On the same diagram, the temperature distribu- tions according to equation (3.2) are also shown. The figure clearly shows that conduction alone seriously under- estimates the growth of the thermal layer and the temperature distribution in it. The optical investigations of Best, Burow and Beer [30] pointed to a convective contribution of heat transfer in the thermal boundary layer which cannot be neglected in any meaningful formulation of a bubble nucleation
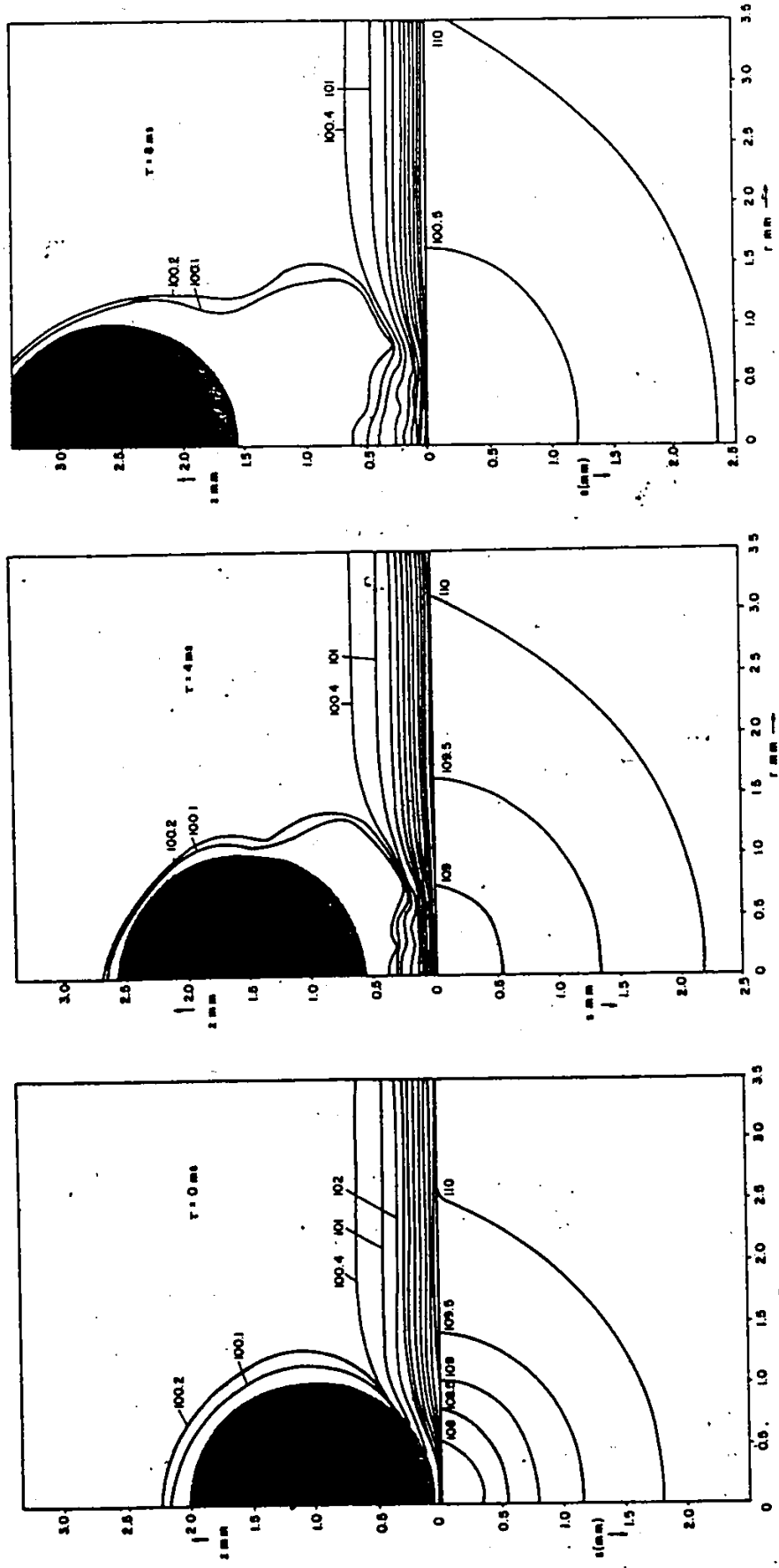
Figure 13 Isotherm Patterns in Liquid and in Wall at 0 ms, 4 ms and 8 ms After Bubble Departure
$(T_w - T_{sat} = 10^oC)$ According to Best, Burow and Beer [30].

32.
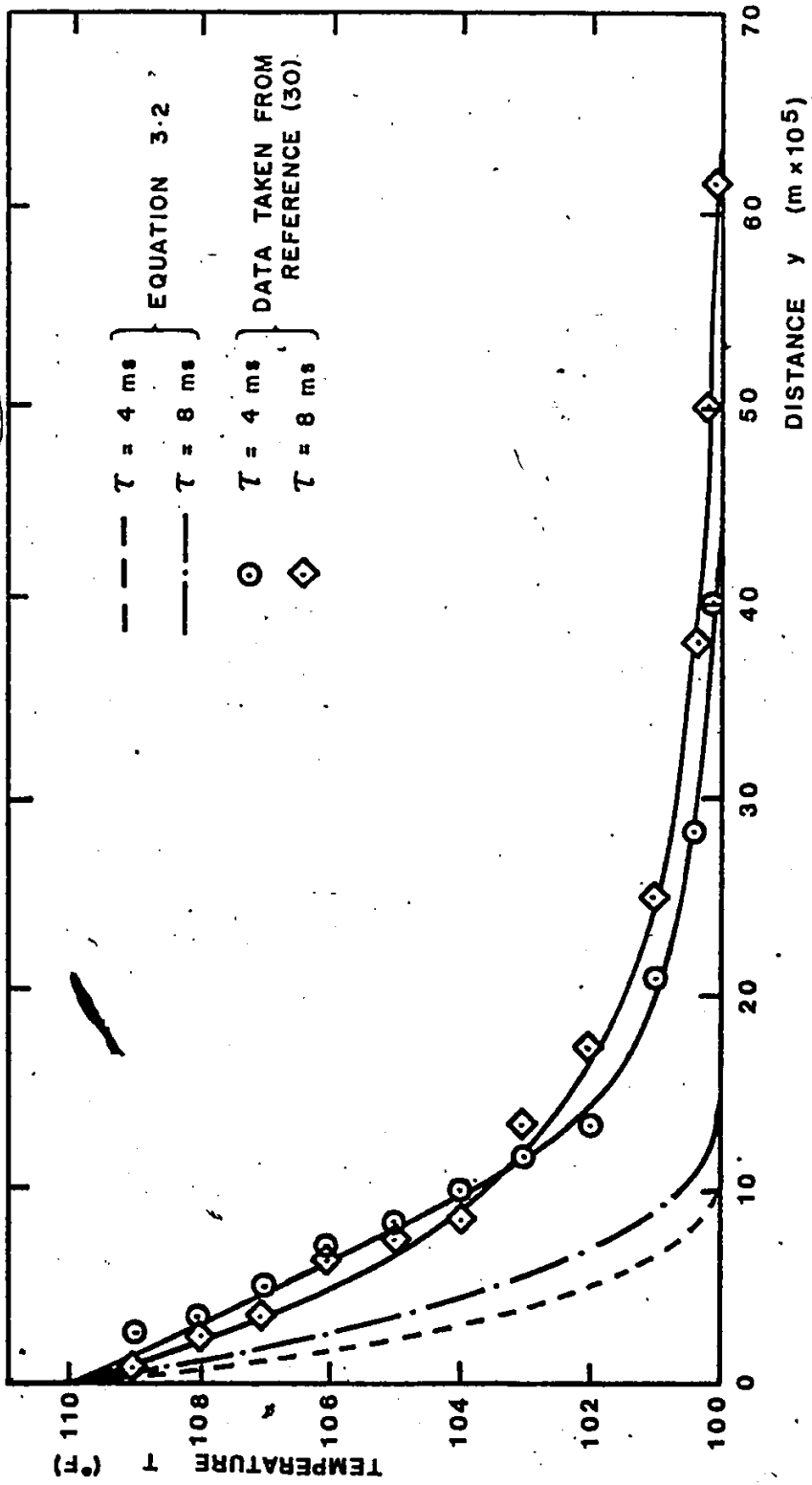
Figure 14   Temperature Distribution in Liquid Layer Adjacent to Heat Transfer Surface at 4 ms and 8 ms After Bubble Departure.

model. It is therefore suggested that a flow of liquid exists in the vicinity of an active site promoted by the departing bubble, which is inwardly directed towards the active site, that results in the convective component of heat transfer in the thermal layer formation. In the following theoretical analyses the growth of, and temperature distribution in, the local thermal boundary layer as controlled by diffusion only and by diffusion combined with convection will be examined.

3.2.1 Thermal Boundary Layer Growth-Diffusion Controlled

Consider a heat transfer surface delivering a net heat flux Q/A into a liquid at temperature T_∞ that has suddenly come into contact with it, Figure 15. Assuming the liquid to be semi-infinite in extent and that conduction occurs unidirectionally into it, the conduction equation can be written as

$$\frac{\partial T}{\partial t} = \kappa_\ell \frac{\partial^2 T}{\partial y^2} \qquad (3.3)$$

where κ_ℓ is the thermal diffusivity of the liquid. The initial condition of the liquid is

$$T(y,0) = T_\infty \qquad (3.4)$$

and the boundary conditions are

$$Q/A = - k_\ell \frac{\partial T(0,t)}{\partial y} \qquad (3.5)$$

$$T(\infty,t) = T_\infty \qquad (3.6)$$
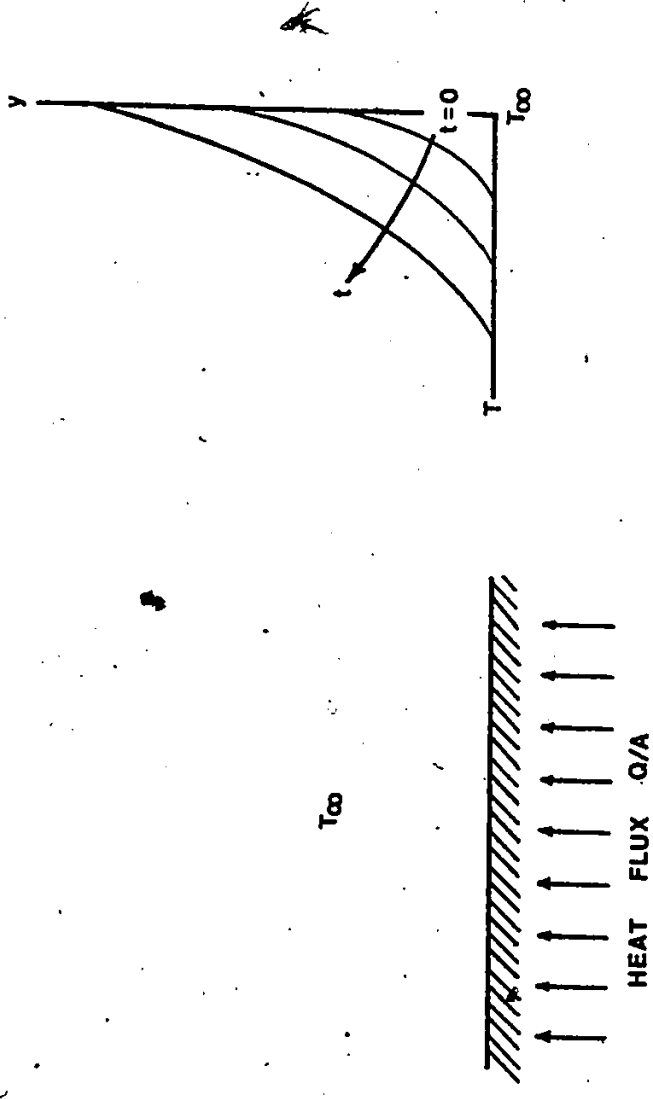
Figure 15   Unidirectional Conduction of Heat From a Heat Transfer Surface to a Liquid
Contacting it.

Writing the dependent variable

$$\theta(y,t) = T(y,t) - T_\infty \qquad (3.7)$$

the conduction equation can be written as

$$\frac{\partial \theta}{\partial t} = \kappa_\ell \frac{\partial^2 \theta}{\partial y^2} \qquad (3.8)$$

while the initial condition becomes

$$\theta(y,t) = 0 \qquad (3.9)$$

and the boundary conditions become

$$Q/A = - k_\ell \frac{\partial \theta(0,t)}{\partial y} \qquad (3.10)$$

$$\theta(\infty,t) = 0 \qquad (3.11)$$

The Laplace transformation of equation (3.8) with time can be written as

$$\frac{d^2 \bar{\theta}}{dy^2} - q^2 \bar{\theta} = 0 \qquad (3.12)$$

where $\quad q = \sqrt{\dfrac{s}{\kappa_\ell}} \qquad (3.13)$

The general solution of equation (3.12) is

$$\theta(y,s) = A_1 e^{-qy} + A_2 e^{qy} \qquad (3.14)$$

where $\quad A_1$ and A_2 are constants.

The Laplace transformation of the boundary conditions can be written as

$$\frac{Q/A}{k_\ell s} + \frac{d\theta(0,s)}{dy} = 0 \qquad (3.15)$$

$$\overline{\theta}(\infty, s) = 0 \qquad (3.16)$$

The constants A_1 and A_2 are determined by substituting the boundary conditions, equations (3.15) and (3.16), into equation (3.14)

$$A_1 = \frac{Q/A}{k_\ell sq} = \frac{(Q/A)\sqrt{\kappa_\ell}}{k_\ell \ s\sqrt{s}}$$

$$A_2 = 0$$

Substitution for A_1 and A_2 into equation (3.14) gives the solution to equation (3.12)

$$\theta(y,s) = \frac{(Q/A)\sqrt{\kappa_\ell}}{k_\ell s\sqrt{s}} \ e^{-\sqrt{\frac{s}{k_\ell}}\, y} \qquad (3.17)$$

After inverse Laplace transforming, equation (3.17) becomes

$$\theta(y,t) = \frac{Q/A}{k_\ell} \left\{ 2\left(\frac{\kappa_\ell t}{\pi}\right)^{1/2} e^{-\frac{y^2}{4\kappa_\ell t}} - y \ \mathrm{erfc}\ \left[\frac{y}{2(\kappa_\ell t)^{1/2}}\right] \right\}$$

$$(3.18)$$

Substituting of equation (3.7) into equation (3.18) and rearranging gives

$$\frac{T(y,t) - T_\infty}{(Q/A)\sqrt{\kappa_\ell t}/k_\ell} = 2 \left\{ \frac{1}{\sqrt{\pi}} e^{-\left(\frac{y}{2\sqrt{\kappa_\ell t}}\right)^2} - \frac{y}{2\sqrt{\kappa_\ell t}} \ \mathrm{erfc}\ \left(\frac{y}{2\sqrt{\kappa_\ell t}}\right) \right\} \qquad (3.19)$$

Defining $\qquad Z = \dfrac{y}{2\sqrt{\kappa_\ell t}} \qquad (3.20)$

equation (3.19) can be written in the form

$$\frac{T(y,t) - T_{\infty}}{(Q/A)\sqrt{\kappa_{\ell} t}/k_{\ell}} = 2 \left[\frac{1}{\sqrt{\pi}} e^{-Z^2} - Z \, \text{erfc} \, Z\right] \qquad (3.21)$$

or

$$\frac{T(y,t) - T_{\infty}}{(Q/A)\sqrt{\kappa_{\ell} t}/k_{\ell}} = 2 \, \text{ierfc} \, Z \qquad (3.22)$$

Figure 16 shows a plot of dimensionless temperature $[T(y,t) - T_{\infty}]/[(Q/A)\sqrt{\kappa_{\ell} t}/k_{\ell}]$ versus Z according to equation (3.22).

3.2.2 Thermal Boundary Layer Growth - Diffusion and Convection Controlled

The flow which is established in the wake of a rising bubble is admittedly very complicated and only recently has it become possible to predict the unsteady velocity components adjacent to the surface from which a bubble is rising with any confidence [30]. However, in this study, an approximate analysis is just as useful and the derivation which follows is such an analysis which predicts the development of the unsteady hydrodynamic field and temperature field in the wake of a bubble accelerating away from a horizontal heating surface [42].

Consider a bubble of hemispherical shape rising in an incompressible liquid of constant properties at temperature T_{∞} and moving away from a heat transfer surface that is delivering a net heat flux Q/A to the liquid as shown in Figure 17. An idealized hemispherical shape is assumed
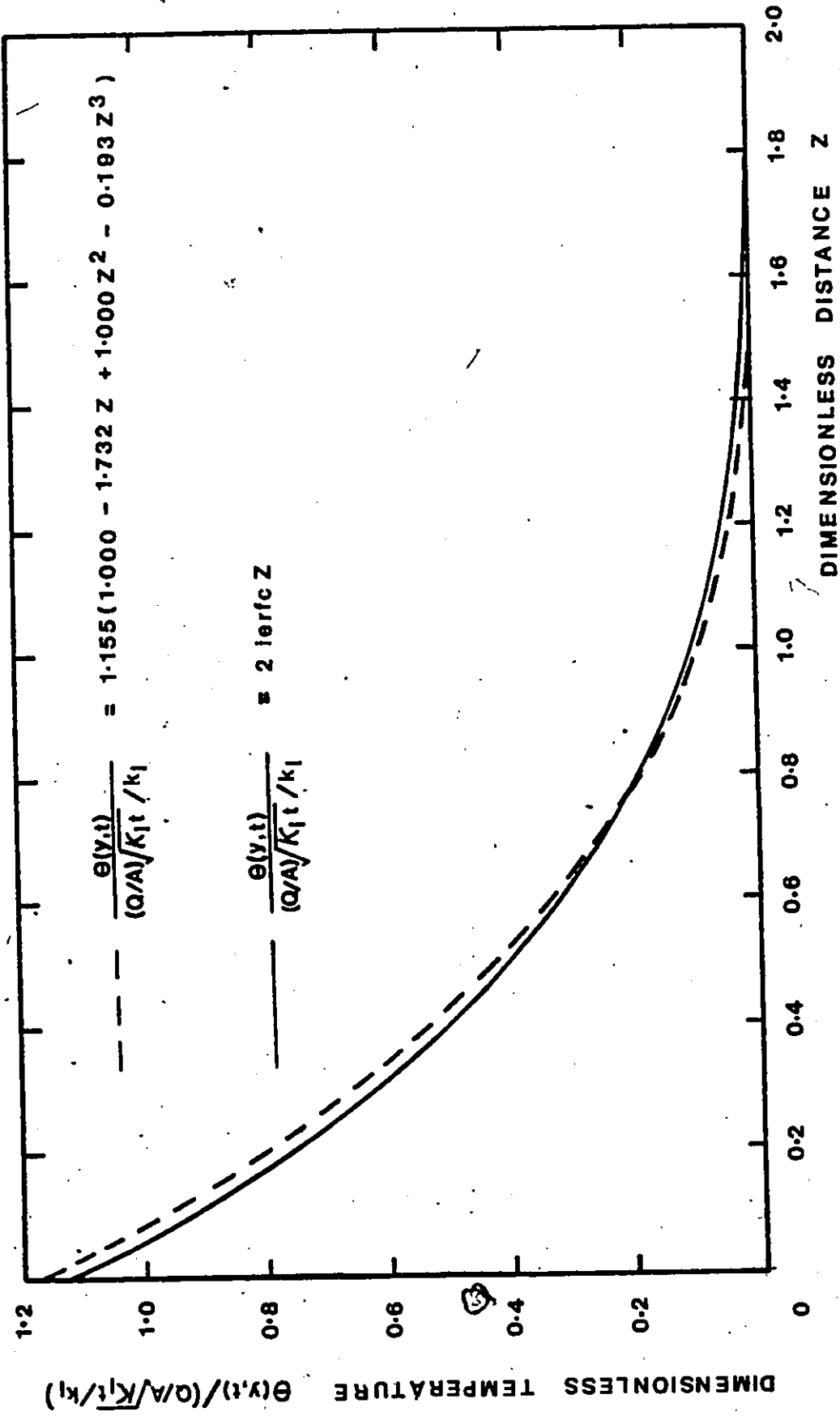
Figure 16 Plot of Dimensionless Temperature Versus Dimensionless Distance for a Liquid Receiving Heat by Conduction.
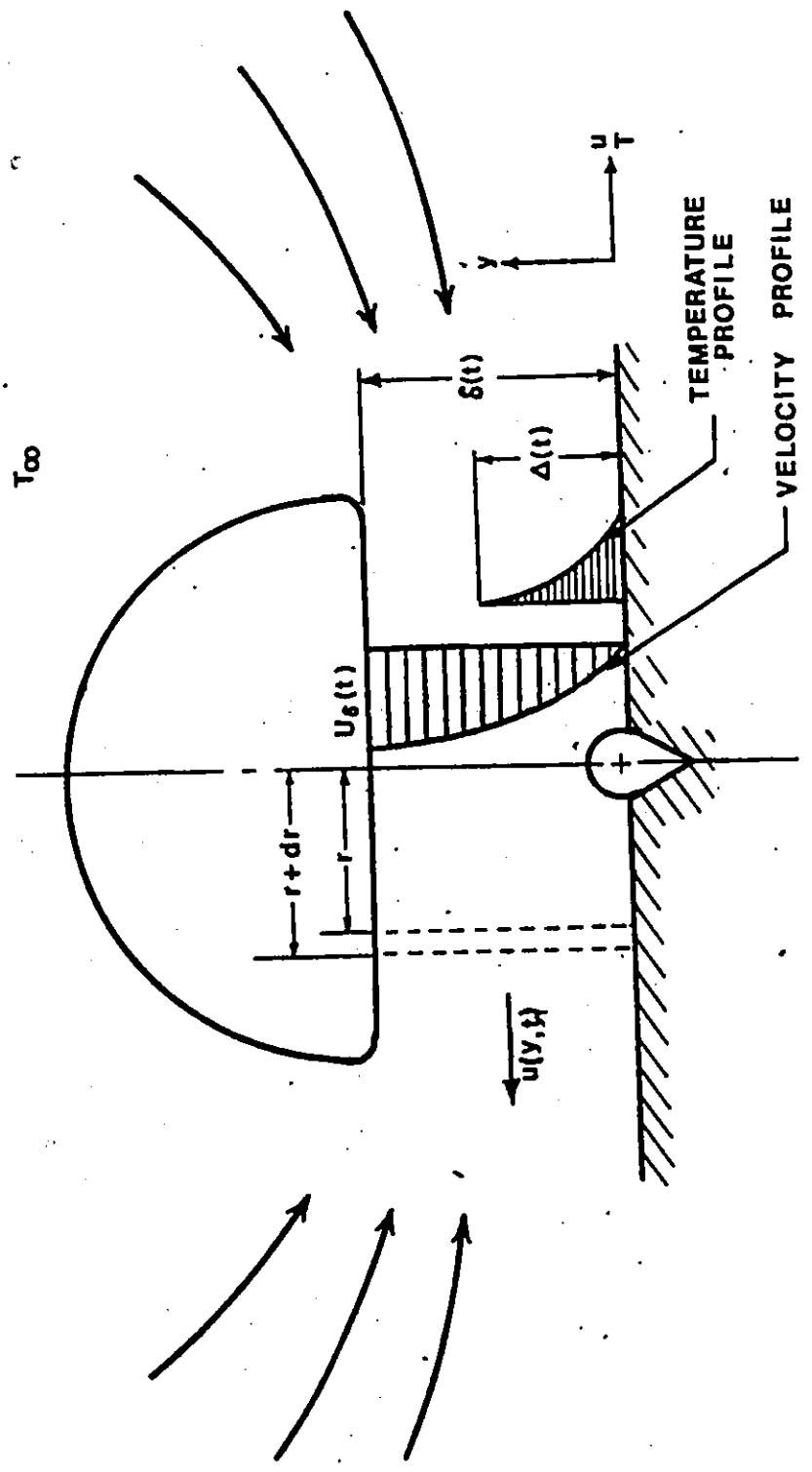
Figure 17 Thermal and Hydrodynamic Boundary Layer Growth in the Wake of a Rising Bubble.

for simplicity in the analysis, although bubbles of this
shape have actually been observed experimentally [43].
As the bubble rises, liquid moves in with a horizontal velocity
component u (y,t) to fill the void that is left behind and
an unsteady flow field is therefore set up in the vicinity
of the surface. One of the features of the flow field is
the formation and growth of a wake region whose thickness
is shown as $\delta(t)$ in Figure 17. As a result of heat being
conducted to the liquid from the heat transfer surface and
convective transport of energy caused by the flow behind the
bubble, a thermal boundary layer, whose thickness is shown
as $\Delta(t)$ in Figure 17, develops in the wake region. The
hydrodynamic boundary conditions are

$$u(y,t) = 0 \quad \text{at } y = 0 \tag{3.23(a)}$$

$$u(y,t) = -U_\delta(t) \quad \text{at } y = \delta(t) \tag{3.23(b)}$$

where $U_\delta(t)$ is the velocity of the flow at the base of the
bubble.

The thermal boundary conditions are

$$T(y,t) = T_w(t) \quad \text{at } y = 0 \tag{3.24(a)}$$

$$T(y,t) = T_\infty \quad \text{at } y = \Delta(t) \tag{3.24(b)}$$

and the initial conditions associated with the problem are

$$\delta(t) = 0 \quad \text{at } t = 0 \tag{3.25(a)}$$

$$\Delta(t) = 0 \quad \text{at } t = 0 \tag{3.25(b)}$$

The analysis begins by developing the conservation of mass equation appropriate to the present flow system. Consider a cylindrical shell of liquid, shown in Figure 17, with an inner radius r and an outer radius (r + dr) under the base of the bubble. The mass flow rate of liquid out of the elemental shell is

$$\dot{m}_{out} = -2\pi\rho r \int_0^{\delta(t)} u(y,t)\,dy \qquad (3.26)$$

and the mass flow rate of liquid into the elemental shell is

$$\dot{m}_{in} = -\left\{2\pi\rho(r+dr)\left[\int_0^{\delta(t)} u(y,t)dy + \frac{\partial}{\partial r}\left(\int_0^{\delta(t)} u(y,t)dy\right)dr\right]\right\} \qquad (3.27)$$

Neglecting insignificant terms, equation 3.27 can be expanded to give

$$\dot{m}_{in} = -2\pi\rho\left[r \int_0^{\delta(t)} u(y,t)dy + r \frac{\partial}{\partial r}\left(\int_0^{\delta(t)} u(y,t)dy\right)dr\right.$$

$$\left. + dr \int_0^{\delta(t)} u(y,t)dy\right] \qquad (3.28)$$

The rate of growth of the elemental shell as a result of the bubble departure from the surface is

$$\dot{m}_{\delta(t)} = 2\pi r\rho\frac{d\delta(t)}{dt}\,dr \qquad (3.29)$$

From the principle of conservation of mass

$$\dot{m}_{\delta(t)} = \dot{m}_{in} - \dot{m}_{out} \qquad (3.30)$$

Substituting equations 3.26, 3.28 and 3.29 into equation 3.30 and simplifying the result gives the conservation of mass equation in the form

$$- \frac{1}{r} \frac{\partial}{\partial r} \left[r \int_{0}^{\delta(t)} u(y,t)dy \right] = \frac{d\delta(t)}{dt} \qquad (3.31)$$

To solve equation 3.31 it is first necessary to be able to describe the velocity distribution $u(y,t)$ and the thickness $\delta(t)$. Any expressions assumed for $u(y,t)$ and $\delta(t)$ must satisfy the appropriate boundary conditions.

For the velocity distribution, assume that

$$\frac{u(y,t)}{U_{\delta}(t)} = -(2\xi - 2\xi^3 + \xi^4) \qquad (3.32)$$

where $\qquad \xi = \frac{y}{\delta(t)} \qquad (3.33)$

From equation 3.32

$$u(y,t) = 0 \quad \text{at} \quad y = 0$$
$$u(y,t) = -U_{\delta}(t) \quad \text{at} \quad y = \delta(t)$$

Equation 3.32 therefore satisfies the necessary hydrodynamic boundary conditions as described by equations 3.23(a) and 3.23(b).

Having an expression for $u(y,t)$, equation 3.31 can now be solved

$$\int_{0}^{\delta(t)} u(y,t)dy = -U_{\delta}(t) \int_{0}^{\delta(t)} (2\xi - 2\xi^2 + \xi^4)dy$$

$$= -U_\delta(t) \; \delta(t) \int_0^1 (2\xi - 2\xi^3 + \xi^4)d\xi$$

$$= -0.70 \; U_\delta(t) \; \delta(t) \tag{3.34}$$

For the wake region thickness, assume that

$$\frac{d\delta(t)}{dt} = V_\infty(1 - e^{-t/t_c}) \tag{3.35}$$

where V_∞ and t_c are unspecified constants.

Integrating equation 3.35 with respect to time gives

$$\delta(t) = V_\infty t + V_\infty t_c \; e^{-t/t_c} + Constant \tag{3.36}$$

From the initial condition, equation 3.25(a), the value of the Constant is determined as

$$Constant = -V_\infty t_c$$

Substituting for the constant in equation 3.36 and rearranging the result gives

$$\delta(t) = V_\infty t_c \left[\frac{t}{t_c} - (1 - e^{-t/t_c})\right] \tag{3.37}$$

Defining dimensionless time τ according to

$$\tau = \frac{t}{t_c} \tag{3.38}$$

equation 3.37 can be expressed as

$$\delta(t) = V_\infty t_c \left[\tau - (1 - e^{-\tau})\right] \tag{3.39}$$

Combining equations 3.35 and 3.39 gives

$$\frac{1}{\delta(t)} \frac{d\delta(t)}{dt} = \frac{1}{t_c} \frac{1-e^{-\tau}}{\tau-(1-e^{-\tau})} \tag{3.40}$$

Now, substituting equation 3.34 into equation 3.31 and rearranging the result gives

$$\frac{0.7}{r} \frac{\partial}{\partial r} \left[r U_\delta(t) \right] = \frac{1}{\delta(t)} \frac{d\delta(t)}{dt} \tag{3.41}$$

Substituting equation 3.40 into equation 3.41 and rearranging again gives the conservation of mass equation in the following form

$$\frac{1}{r} \frac{\partial}{\partial r} \left[r \, U_\delta(t) \right] = \frac{1.429}{t_c} \frac{1-e^{-\tau}}{\tau-(1-e^{-\tau})} \tag{3.42}$$

The conservation of energy equation must now be developed. Consider again the cylindrical shell of liquid described earlier and depicted in Figure 17. The heat conducted into the element is

$$Q_{cond} = -2\pi r dr k_\ell \left(\frac{\partial \theta(y,t)}{\partial y} \right)_{y=0} \tag{3.43}$$

where $\theta(y,t) = T(y,t) - T_\infty$ $\tag{3.44}$

The heat convected out of the element is

$$Q_{conv,out} = -2\pi\rho Cr \int_0^{\Delta(t)} [u(y,t)\theta(y,t)] dy. \tag{3.45}$$

and the heat transported into the element by convection is

$$Q_{conv,in} = -2\pi\rho C(r+dr)\left\{\int_0^{\Delta(t)} \left[u(y,t)\theta(y,t)dy\right]\right.$$

$$\left. + \frac{\partial}{\partial r}\left[\int_0^{\Delta(t)} u(y,t)\theta(y,t)dy\right]dr\right\} \quad (3.46)$$

Neglecting insignificant terms, equation 3.46 can be written in the form

$$Q_{conv,in} = -2\pi\rho C\left\{r\int_0^{\Delta(t)} u(y,t)\theta(y,t)dy + r\frac{\partial}{\partial r}\left[\int_0^{\Delta(t)} u(y,t)\theta(y,t)dy\right]dr\right.$$

$$\left. + dr\int_0^{\Delta(t)} u(y,t)\theta(y,t)dy\right\} \quad (3.47)$$

The heat stored in the element is

$$Q_{stored} = 2\pi r dr\rho C \frac{\partial}{\partial t}\int_0^{\Delta(t)} \theta(y,t)dy \quad (3.48)$$

From the principle of conservation of energy

$$Q_{cond} + Q_{conv,in} - Q_{conv,out} = Q_{stored} \quad (3.49)$$

Substituting equations 3.43, 3.45, 3.47 and 3.48 into equation 3.49 and simplifying the result gives the energy

equation in the form

$$\frac{\partial}{\partial t} \int_0^{\Delta(t)} \theta(y,t)dy + \frac{1}{r}\frac{\partial}{\partial r}\left[r \int_0^{\Delta(t)} u(y,t)\theta(y,t)dy\right] = \kappa\left(\frac{\partial\theta(y,t)}{\partial y}\right)_{y=0} \quad (3.50)$$

In order to solve equation 3.50 an expression for $\theta(y,t)$ is required. A suitable polynomial expression for the temperature distribution across the thermal boundary layer is

$$\frac{T(y,t) - T_\infty}{T_w(t) - T_\infty} = \frac{\theta(y,t)}{\theta_w(t)} = 1-3\eta+ 3\eta^2-\eta^3 \quad (3.51)$$

where $\qquad \eta = \frac{y}{\Delta(t)} \qquad\qquad (3.52)$

From equation 3.51

$$T(y,t) = T_w(t) \quad \text{at} \quad y = 0$$
$$T(y,t) = T_\infty \quad \text{at} \quad y = \Delta(t)$$

The assumed expression for the temperature distribution, equation 3.51, therefore satisfies the thermal boundary conditions as described by equations 3.24(a) and 3.24(b). Further justification for using equation 3.51 will be provided later.

Having an expression for $\theta(y,t)$, equation 3.50 can now be solved

$$\frac{\partial}{\partial t} \int_0^{\Delta(t)} \theta(y,t)dy = \frac{\partial}{\partial t} \int_0^{\Delta(t)} \theta_w(t)(1-3\eta+3\eta^2-\eta^3)d\eta \quad (3.53)$$

$$= \frac{\partial}{\partial t}\left(\theta_w(t)\Delta(t)\right) \int_0^1 (1-3\eta+3\eta^2-\eta^3)d\eta = \frac{1}{4}\frac{d\left(\theta_w(t)\Delta(t)\right)}{dt}$$

Similarly

$$\int_0^{\Delta(t)} u(y,t)\theta(y,t) = -U_\delta(t)\theta_w(t) \int_0^{\Delta(t)} \left[2(\tfrac{y}{\delta})-2(\tfrac{y}{\delta})^3+(\tfrac{y}{\delta})^4\right]\left[1-3(\tfrac{y}{\Delta})+3(\tfrac{y}{\Delta})^2-(\tfrac{y}{\Delta})^3\right]dy$$

$$(3.54)$$

where both δ and Δ are understood to be functions of t.

Expanding equation 3.54 results in

$$\int_0^{\Delta(t)} u(y,t)\theta(y,t) = -U_\delta(t)\theta_w(t)\left\{\int_0^{\Delta(t)} \left[2(\tfrac{y}{\delta})-6(\tfrac{y^2}{\delta\Delta})+6(\tfrac{y^3}{\delta\Delta^2})-2(\tfrac{y^4}{\delta\Delta^3})\right]\right.$$

$$-\left[2(\tfrac{y}{\delta})^3-6(\tfrac{y^4}{\delta^3\Delta})+6(\tfrac{y^5}{\delta^3\Delta^2})-2(\tfrac{y^6}{\delta^3\Delta^3})\right]$$

$$\left.+\left[(\tfrac{y^4}{\delta^4})-3(\tfrac{y^5}{\delta^4\Delta})+3(\tfrac{y^6}{\delta^4\Delta^2})-(\tfrac{y^7}{\delta^4\Delta^3})\right]\right\}dy \qquad (3.55)$$

Carrying out the integration and then imposing the limits gives

$$\int_0^{\Delta(t)} u(y,t)\theta(y,t) = -U_\delta(t)\theta_w(t)\Delta(t) \left\{\left[(\tfrac{\Delta}{\delta})-2(\tfrac{\Delta}{\delta}) + \tfrac{3}{2}(\tfrac{\Delta}{\delta}) + \tfrac{2}{5}(\tfrac{\Delta}{\delta})\right]\right.$$

$$\left.-\left[\tfrac{1}{2}(\tfrac{\Delta}{\delta})^3-\tfrac{1}{.5}(\tfrac{\Delta}{\delta})^3+(\tfrac{\Delta}{\delta})^3-\tfrac{2}{7}(\tfrac{\Delta}{\delta})^3\right]+\left[\tfrac{1}{5}(\tfrac{\Delta}{\delta})^4-\tfrac{1}{2}(\tfrac{\Delta}{\delta})^4+\tfrac{3}{7}(\tfrac{\Delta}{\delta})^4-\tfrac{1}{8}(\tfrac{\Delta}{\delta})^4\right]\right\}$$

$$= U_\delta(t)\theta_w(t)\Delta(t) \left[0.100(\tfrac{\Delta}{\delta}) - 0.014(\tfrac{\Delta}{\delta})^3 + 0.004(\tfrac{\Delta}{\delta})^4\right] \quad (3.56)$$

Now, from equation 3.51

$$\left(\tfrac{\partial\theta}{\partial y}\right)_{y=0} = -\frac{3\theta_w(t)}{\Delta(t)} = -\frac{Q/A}{k_\ell} = \text{Constant} \qquad (3.57)$$

Substituting equation 3.53, 3.56 and 3.57 into equation

3.50 and rearranging the resulting expression, the energy equation becomes

$$\frac{1}{4}\frac{d[\theta_w(t)\Delta(t)]}{dt} - \Delta(t)\theta_w(t)\left[0.100(\tfrac{\Delta}{\delta}) - 0.014(\tfrac{\Delta}{\delta})^3 + 0.004(\tfrac{\Delta}{\delta})^4\right]\frac{1}{r}\frac{\partial}{\partial r}\left(rU_\delta(t)\right)$$

$$= -3\kappa_\ell\frac{\theta_w(t)}{\Delta(t)} \qquad\qquad (3.58)$$

Substituting the conservation of mass equation, equation 3.42, into the conservation of energy equation, equation 3.58, gives the result

$$\frac{1}{4}\frac{d[\theta_w(t)\Delta(t)]}{dt} - 1.429\theta_w\frac{\Delta(t)}{t_c}\frac{1-e^{-\tau}}{\tau-(1-e^{-\tau})}\left\{0.100\left(\frac{\Delta(t)}{\delta(t)}\right) + 0.014\left(\frac{\Delta(t)}{\delta(t)}\right)^3\right.$$

$$\left. - 0.004\left(\frac{\Delta(t)}{\delta(t)}\right)^4\right\} = -3\kappa_\ell\frac{\theta_w(t)}{\Delta(t)} \qquad (3.59)$$

However, equation 3.57 gives $\theta_w(t) = \frac{1}{3}\frac{Q/A}{k_\ell}\Delta(t)$ so that equation 3.59 can be re-arranged to give

$$\frac{1}{\kappa_\ell}\frac{d[\Delta(t)]^2}{dt} - \frac{[\Delta(t)]^2}{\kappa_\ell t_c}\frac{1-e^{-\tau}}{\tau-(1-e^{-\tau})}\left\{0.574\left[\frac{\Delta(t)}{\delta(t)}\right] - 0.082\left[\frac{\Delta(t)}{\delta(t)}\right]^3 + 0.020\left[\frac{\Delta(t)}{\delta(t)}\right]^4\right\}$$

$$= 12 \qquad\qquad (3.60)$$

Defining $\quad \phi = \frac{\Delta(t)}{\sqrt{\kappa_\ell t_c}}$ $\qquad\qquad\qquad\qquad (3.61)$

and $\quad \chi = \frac{\delta(t)}{\sqrt{\kappa_\ell t_c}} = V_\infty t_c\frac{\tau-(1-e^{-\tau})}{\sqrt{\kappa_\ell t_c}} = C\frac{\tau-(1-e^{-\tau})}{\sqrt{\kappa_\ell t_c}}$ $\quad(3.62)$

where $V_\infty t_c$ has been re-written as a constant C, which can be interpreted as the distance above the heat transfer surface

at which the terminal velocity of the bubble is achieved
and is thought to be independent of heat flux and subcooling,
then

$$\frac{d\phi^2}{d\tau} - \frac{1-e^{-\tau}}{\tau - (1-e^{-\tau})}\phi^2 \left[0.574(\frac{\phi}{X})-0.082(\frac{\phi}{X})^3 + 0.020(\frac{\phi}{X})^4\right] = 12 \quad (3.63)$$

Solution of equation 3.63 provides the dimensionless time τ
at which a dimensionless thermal layer thickness ϕ is achieved
as a result of diffusion and convection of heat in the layer
of liquid adjacent to the heat transfer surface.

If there were no flow in the system then

$$u(y,t) = 0 \quad (3.64)$$

and the conservation of energy equation, equation 3.50, would
become

$$\frac{\partial}{\partial t} \int_0^{\Delta(t)} \theta(y,t)dy = -\kappa_\ell \left(\frac{\partial \theta(y,t)}{\partial y}\right)_{y=0} \quad (3.65)$$

Substituting equations 3.53 and 3.57 into equation
3.65 and rearranging results in

$$\frac{1}{4}\frac{d[\Delta(t)\theta_w(t)]}{dt} = \kappa_\ell \frac{3\theta_w(t)}{\Delta(t)}$$

so that $\quad d[\Delta(t)]^2 = 12 \kappa_\ell dt$

Carrying out the integration gives

$$[\Delta(t)]^2 = 12 \kappa_\ell t$$

from which

$$\Delta(t) = \sqrt{12\kappa_\ell t} \quad (3.66)$$

Now $\quad Q/A = -k_\ell \left.\dfrac{\partial \theta(y,t)}{\partial y}\right|_{y=0}$ (3.67)

The temperature distribution in the thermal layer was assumed to be

$$\frac{\theta(y,t)}{\theta_w} = 1 - 3\left[\frac{y}{\Delta(t)}\right] + 3\left[\frac{y}{\Delta(t)}\right]^2 - \left[\frac{y}{\Delta(t)}\right]^3 \qquad (3.51)$$

so

$$\left(\frac{\partial \theta(y,t)}{\partial y}\right)_{y=0} = -\frac{3\theta_w}{\Delta(t)} \qquad (3.68)$$

Substitution of equation 3.68 into equation 3.67 gives

$$Q/A = k_\ell \frac{3\theta_w}{\Delta(t)} \qquad (3.69)$$

From equation 3.69

$$\theta_w = \frac{(Q/A)\Delta(t)}{3k_\ell} \qquad (3.70)$$

Now, substitution of equation 3.66 into equation 3.70 gives

$$\theta_w = \frac{(Q/A)}{3k_\ell}\sqrt{12\kappa_\ell t} \qquad (3.71)$$

Substituting equations 3.71 and 3.66 into the assumed temperature distribution expression, equation 3.51, gives

$$\frac{T(y,t) - T_\infty}{(Q/A)\sqrt{\kappa_\ell t}/k_\ell} = \frac{\sqrt{12}}{3}\left[1 - 3\left(\frac{y}{\sqrt{12\kappa_\ell t}}\right) + 3\left(\frac{y}{\sqrt{12\kappa_\ell t}}\right)^2 - \left(\frac{y}{\sqrt{12\kappa_\ell t}}\right)^3\right]$$

which can be simplified to give

$$\frac{T(y,t) - T_\infty}{(Q/A)\sqrt{\kappa_\ell t}/k_\ell} = 1.155\left[1 - 1.732\,Z + 1.000\,Z^2 - 0.193\,Z^3\right] \qquad (3.72)$$

where

$$Z = \frac{y}{2\sqrt{\kappa_\ell t}}$$ (3.20)

Now, equation 3.72 is an expression for the temperature distribution in the thermal layer in the absence of flow and convection currents. Since diffusion is the only prevailing mode of heat transfer into the liquid, then if the assumed temperature distribution expression, equation 3.51, adequately describes the temperature field in the thermal layer, a plot of the function $[T(y,t)-T_\infty]/[(Q/A)\sqrt{\kappa_\ell t}/k_\ell]$ versus Z according to equation 3.72 should closely follow the curve derived from equation 3.22, which represents the temperature distribution in the thermal layer derived on diffusion theory. Figure 16 shows that this is exactly the case and further justification is therefore provided for using equation 3.51 to describe the temperature distribution in the thermal boundary layer.

3.3 Criterion for Bubble Growth

In accordance with Hsu [23] it is assumed that at the beginning of a bubble emission cycle, a nucleus of vapour sits near the mouth of a cavity of suitable geometry as depicted in Figure 18. The nucleus is surrounded by bulk liquid at temperature T_∞ and can be assumed to be the residual vapour left behind in the cavity by the preceding bubble. By com-

Figure 18 Bubble Nucleus at Active Site
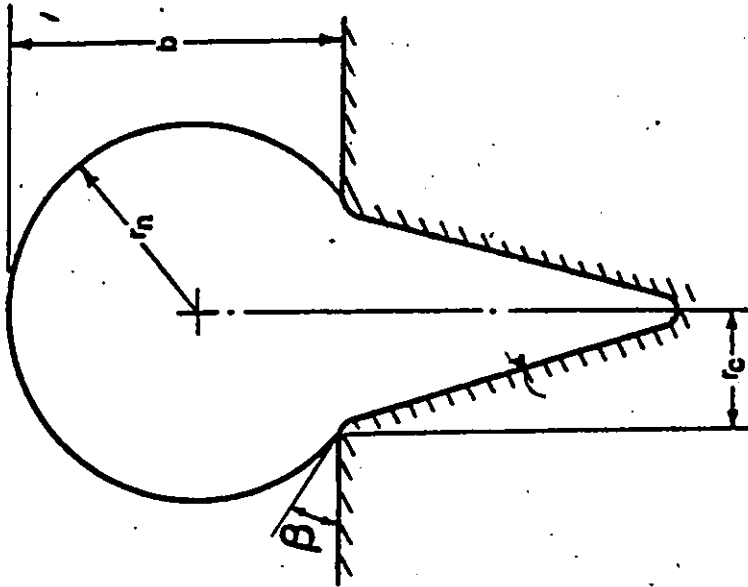
Figure 18(a) Bubble Nucleus Sitting at
Cavity Mouth.
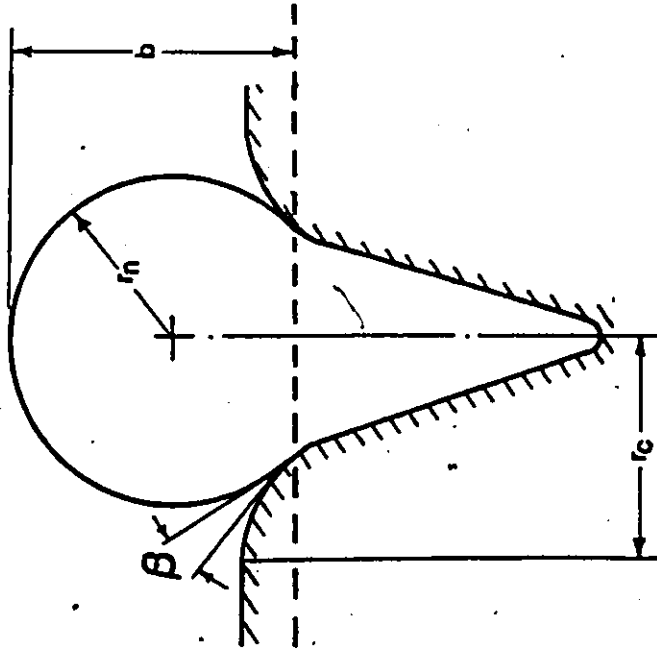
Figure 18(b) Bubble Nucleus Sitting
Within Cavity.

bining the equation of thermostatic equilibrium and the
Clausius - Clapeyron relationship, it can be shown that

$$T_v = T_{sat} + \frac{2\sigma T_{sat}}{\rho_v h_{fg}} \frac{1}{r_n} \tag{3.73}$$

Defining $\quad A = \dfrac{2\sigma T_{sat}}{\rho_v h_{fg}} \tag{3.74}$

the nucleus equilibrium temperature T_v can be written as

$$T_v - T_\infty = T_{sat} - T_\infty + \frac{A}{r_n} \tag{3.75}$$

or

$$\theta_v = \theta_{sat} + \frac{A}{r_n} \tag{3.76}$$

As time passes, the cold liquid surrounding the
bubble nucleus is warmed up as heat is delivered to it and
the local thermal boundary layer thickness increases in
accordance with equation 3.22 or equation 3.63, depending
on whether the mode of heat transfer is pure conduction or
conduction combined with convection. The bubble will start
to grow when the liquid surrounding the bubble nucleus has
been heated sufficiently that its temperature becomes equal
to or exceeds the vapour temperature over the entire liquid-
vapour interface. Mathematically, bubble growth begins when

$$\theta(b,t) = \theta_v \tag{3.77}$$

where b is the height of the bubble nucleus above the point
of contact with the heat transfer surface. Equation 3.77 is
satisfied when the thermal boundary layer has grown to a

sufficient thickness.

3.4 Determination of Bubble Waiting Time

After the criterion equation for bubble growth,
equation 3.77, is satisfied the bubble begins to grow and,
after achieving a sufficient size, it detaches from the
heat transfer surface and rises in the bulk of the liquid.
The bubble leaves behind in the active cavity a residue of
vapour that will serve as a nucleus for the next bubble
formation and as it departs from the heating surface, liquid
from the bulk at temperature T_∞ rushes in and fill the void
that is left behind. The local thermal boundary layer is
therefore completely destroyed. The waiting time for the
next bubble is determined by finding the time necessary for
the local thermal boundary layer to achieve the thickness
whereby the criterion equation, equation 3.77, is once again
satisfied. The waiting time is therefore the time taken from
the moment the local thermal boundary layer is destroyed to
the time it grows to the extent that equation 3.77 is satis-
fied. As stated before, the thermal boundary layer can
grow according to equation 3.22 or 3.63, depending on whether
heat is transferred by conduction alone or conduction combined
with convection. In subsequent sections, expressions will be
derived for bubble waiting time for these two different cases.

3.4.1 Waiting Time Determination for Diffusion Controlled
Thermal Boundary Layer Growth

Consider a bubble nucleus situated near the mouth of a cavity as shown in Figure 18(a). Assuming that a bubble has just left the cavity, that the nucleus is now surrounded by relatively cold liquid at temperature T_∞, the temperature distribution in the liquid is predicted by Equation 3.22.

$$\frac{T(y,t) - T_\infty}{(Q/A)\sqrt{\kappa_\ell t}/k_\ell} = 2 \text{ ierfc } Z \tag{3.22}$$

At the critical distance b from the heat transfer surface the temperature is

$$T(b,t) - T_\infty = \theta(b,t) = 2 \frac{(Q/A)\sqrt{\kappa_\ell t}}{k_\ell} \text{ ierfc}\left(\frac{b}{2\sqrt{\kappa_\ell t}}\right) \tag{3.78}$$

As mentioned in Section 3.4, the waiting time ends when the criterion equation for nucleation

$$\theta(b,t) = \theta_v \tag{3.77}$$

is satisfied. Substitution of equation 3.76 and equation 3.78 into equation 3.77 results in the waiting time equation

$$\theta_{sat} + \frac{A}{r_n} = 2 \frac{(Q/A)\sqrt{\kappa_\ell t}}{k_\ell} \text{ ierfc}\left(\frac{b}{2\sqrt{\kappa_\ell t}}\right) \tag{3.79}$$

The waiting time t_w comes to an end whenever equation 3.79 is satisfied. A solution of equation 3.79 for t therefore provides the bubble waiting time t_w for a given liquid.

nucleus size r_n and heat flux Q/A.

For the special case of a nucleus in the form of a truncated sphere sitting at the mouth of a cavity, it can be shown from geometrical considerations that

$$r_n = \frac{r_c}{\sin \beta} \tag{3.80}$$

$$b = \frac{1+\cos \beta}{\sin \beta} r_c \tag{3.81}$$

Defining

$$c_1 = \frac{1+\cos \beta}{\sin \beta} \tag{3.82}$$

$$c_2 = \frac{1}{\sin \beta} \tag{}$$

the waiting time equation, equation 3.79, can be written as

$$\theta_{sat} + \frac{A}{c_2 r_c} = 2 \frac{(Q/A)\sqrt{\kappa_\ell t}}{k_\ell} \text{ ierfc} \left(\frac{c_1 r_c}{2\sqrt{\kappa_\ell t}}\right) \tag{3.84}$$

For the case on which a nucleus sits within a cavity, it can be seen that for small contact angles β such as those associated with organic liquids

$$b \cong 2 r_n$$

and this is the assumption which was used throughout the analysis. Substituting equation 3.85 into equation 3.79 gives the waiting time equation in the form

$$\theta_{sat} + \frac{A}{r_n} = 2 \frac{(Q/A)\sqrt{\kappa_\ell t}}{k_\ell} \text{ ierfc} \left(\frac{2 r_n}{2\sqrt{\kappa_\ell t}}\right) \tag{3.86}$$

Therefore, with conduction being the only mode of heat transfer into the liquid from the heat transfer surface a solution of equation 3.84 or 3.86 provides the bubble waiting time t_w.

Figure 19 shows a history of the waiting period. Figure 20 shows a plot of waiting time t_w versus heat flux Q/A with subcooling θ_{sat} as a parameter according to equation 3.84.

3.4.2 Waiting Time Determination for Diffusion and Convection Controlled Thermal Boundary Layer Growth

As in the preceding section consider a nucleus of vapour situated near the mouth of a cavity of suitable geometry as depicted in Figure 18(b). The nucleus is surrounded by relatively cold liquid at temperature T_∞ indicating the beginning of a bubble emission cycle. Because of both conduction and convection in the liquid layer adjacent to the heat transfer surface, the local thermal boundary layer grows in accordance with equation 3.63.

$$\frac{d\phi^2}{d\tau} - \frac{1-e^{-\tau}}{\tau-(1-e^{-\tau})} \, \phi^2 \left[0.574\left(\frac{\phi}{\chi}\right) - 0.082\left(\frac{\phi}{\chi}\right)^3 - 0.020\left(\frac{\phi}{\chi}\right)^4 \right] = 12 \qquad (3.63)$$

The temperature distribution in the liquid is predicted by equation 3.51

$$\frac{T(y,t)-T_\infty}{T_w(t)-T_\infty} = \frac{\theta(y,t)}{\theta_w(t)} = 1 - 3\left(\frac{y}{\Delta(t)}\right) + 3\left(\frac{y}{\Delta(t)}\right)^2 - \left(\frac{y}{\Delta(t)}\right)^3 \qquad (3.51)$$

Figure 19 History of Bubble Waiting Time.
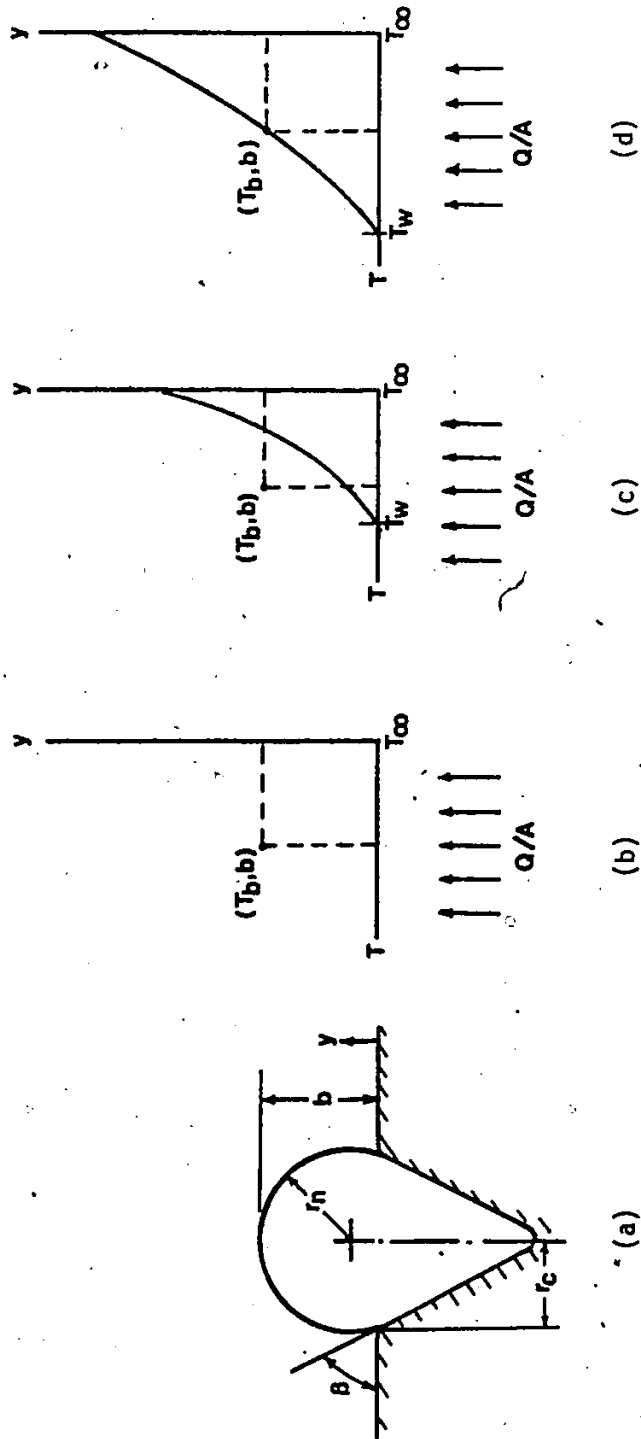
Figure 19(a) Bubble Nucleus Sitting at the Mouth of an Active Cavity.

Figure 19(b) Temperature Profile in Thermal Boundary Layer at $t = 0$, Beginning of Waiting Period.

Figure 19(c) Temperature Profile in Thermal Boundary Layer at $0 < t < t_w$.

Figure 19(d) Temperature Profile in Thermal Boundary Layer at $t = t_w$, End of Waiting Period.

59.
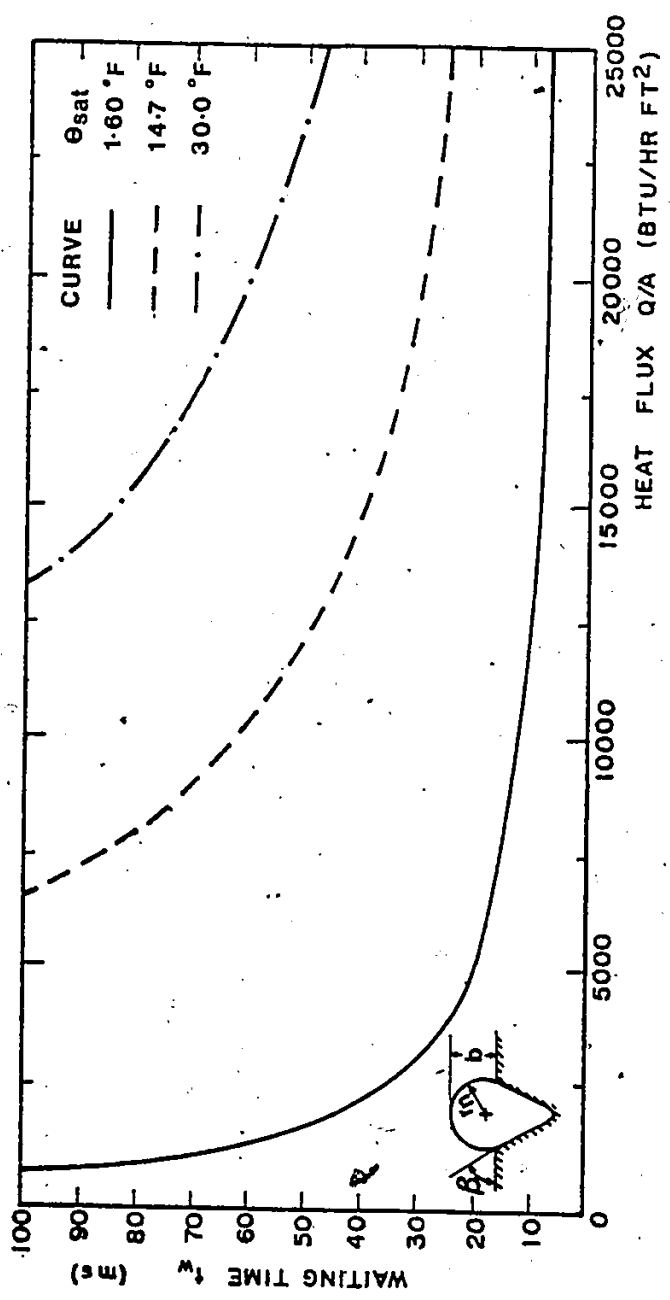
Figure 20 Plot of Bubble Wait Waiting Time as a Function of Heat Flux According
to Conduction Model of Bubble Nucleation.

Nucleation occurs and the waiting period comes to an end when

$$\theta(b,t) = \theta_v \qquad (3.77)$$

From equation 3.51

$$\theta(b,t) = 1 - 3\left(\frac{b}{\Delta(t)}\right) + 3\left(\frac{b}{\Delta(t)}\right)^2 - \left(\frac{b}{\Delta(t)}\right)^3 \qquad (3.87)$$

Substituting equations 3.76 and 3.51 into equation 3.77 along with $\theta_w(t) = \frac{1}{3}\frac{Q/A}{k_\ell}\Delta(t)$ leads to the waiting time equation

$$\frac{1}{3}\frac{Q/A}{k_\ell}\Delta(t)\left\{1 - 3\left(\frac{b}{\Delta(t)}\right) + 3\left(\frac{b}{\Delta(t)}\right)^2 - \left(\frac{b}{\Delta(t)}\right)^3\right\} = \theta_{sat} + \frac{A}{r_n} \qquad (3.88)$$

where $\Delta(t)$ is obtained by solving equation 3.63. Whenever equation 3.88 is satisfied the bubble waiting time for a given liquid, heat flux Q/A and nucleus size r_n comes to an end.

As in section 3.4.1, for the special case of a nucleus in the form of a truncated sphere sitting at the mouth of a cavity

$$r_n = \frac{r_c}{\sin \beta} \qquad (3.80)$$

$$b = \frac{1+\cos \beta}{\sin \beta} r_c \qquad (3.81)$$

For the case of organic liquid in which the nucleus is thought to be situated slightly below the cavity mouth, Figure 18(b), for small contact angles

$$b \cong 2 r_n \qquad\qquad (3.85)$$

Figure 21 shows a representative plot of waiting time t_w versus heat flux Q/A with θ_{sat} and t_c as parameters.
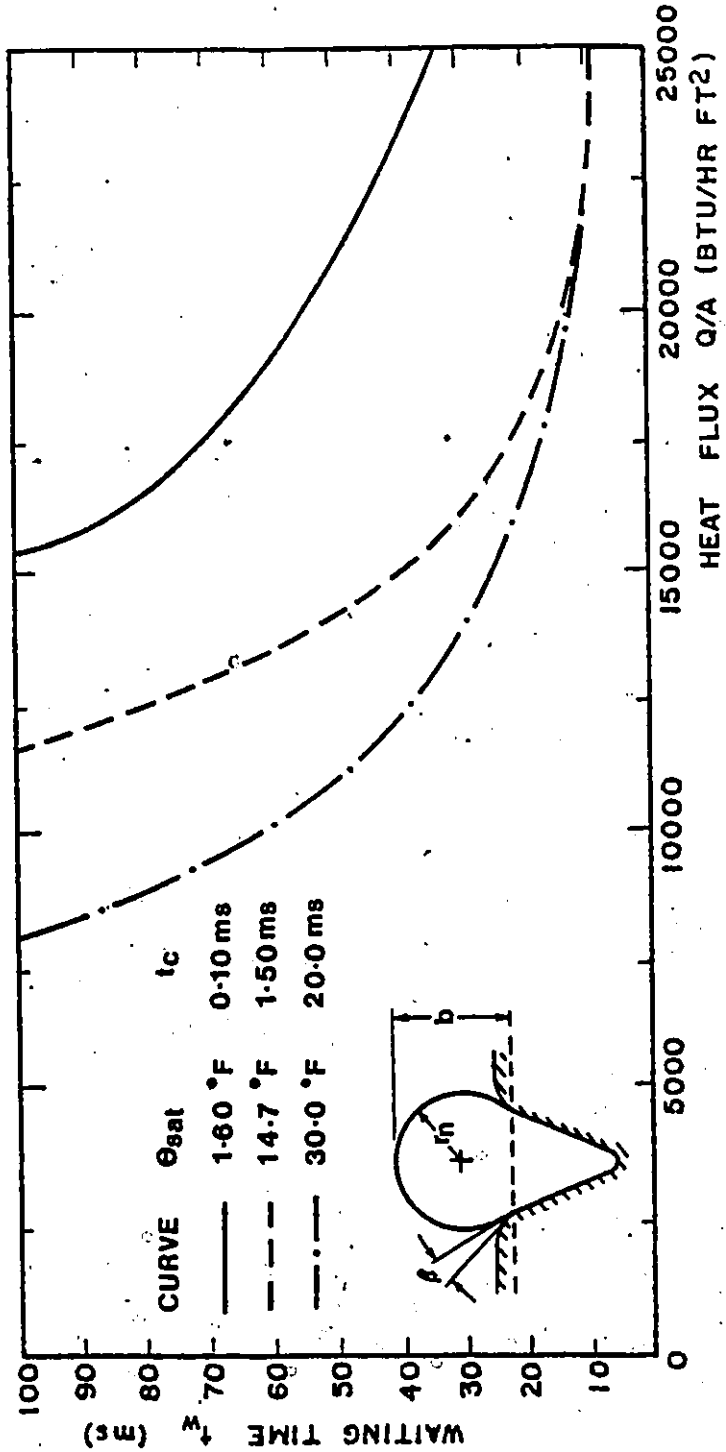
Figure 21 Plot of Bubble Waiting Time as a Function of Heat Flux According to
Conduction-Convection Model of Bubble Nucleation.

CHAPTER 4

EXPERIMENTAL APPARATUS

4.1 Introduction

In this experimental investigation, dichloromethane (methylene chloride) was boiled on a borosilicate glass heating surface coated with a half-wavelength thickness of stannic oxide which conducted electric current and generated heat causing the liquid to boil. Boiling was carried out at six levels of heat flux ranging from 8000 BTU/hr ft^2 to 20000 BTU/hr ft^2 and three levels of subcooling ranging from 1.6^{0}F to 30.0^{0}F.

At the commencement of the research, an experimental apparatus constructed by Voutsinos [44] to investigate micro-layer evaporation at various levels of heat flux and subcooling already existed. The apparatus was quite adequate in fulfilling the requirements of the present investigation and, except for using a newly acquired power supply unit as the energy source, the entire apparatus was used without any modification.

The major components of the apparatus, which is shown in Figure 22, were the test assembly, the power supply unit, the temperature measuring system and the optical system. Details of the design and operation of these components are
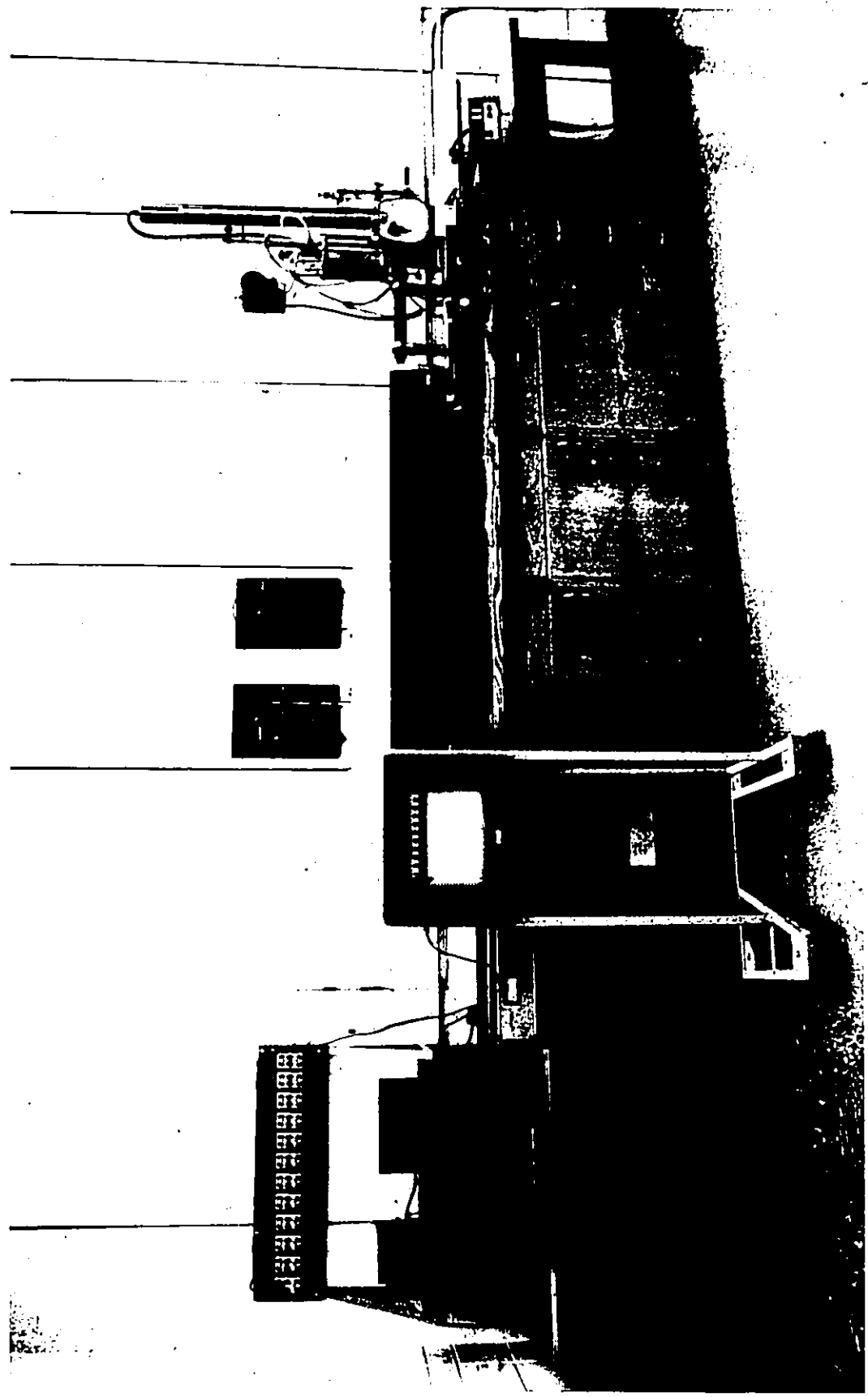
Figure 22 Photographic View of Experimental Apparatus.

presented in the sections which follow.

4.2 Test Assembly

A photograph of the test assembly is seen in Figure 23 and a detailed drawing is shown in Figure 24. The test assembly was constructed of a 6" diameter by 8" long type 304 stainless steel pipe closed by a base plate and a cover plate, both of the same material, resting on gaskets. The glass specimen heating surface was comprised of a 2 7/16" by 1 5/16" wide borosolicate glass coated with a half wavelength thickness of stannic oxide and was arranged in the vessel on the base plate. The oxide coating on the glass surface received electric power through two bus bars making electrical contact with it at metallic silver deposits on each end. The details of the base plate and glass heating surface are shown in Figure 25.

Subcooling of the liquid was carried out by means of a single pass heat exchanger (cooling coil) located in the bulk liquid. The desired levels of subcooling were achieved by using a needle valve to adjust the flow rate of cold water going through the cooling coil. An electric heater was also located in the bulk liquid. This element was used to supply heat directly to the bulk liquid such that, in combination with the cooling coil, a desired level of bulk liquid temperature could be achieved and maintained.
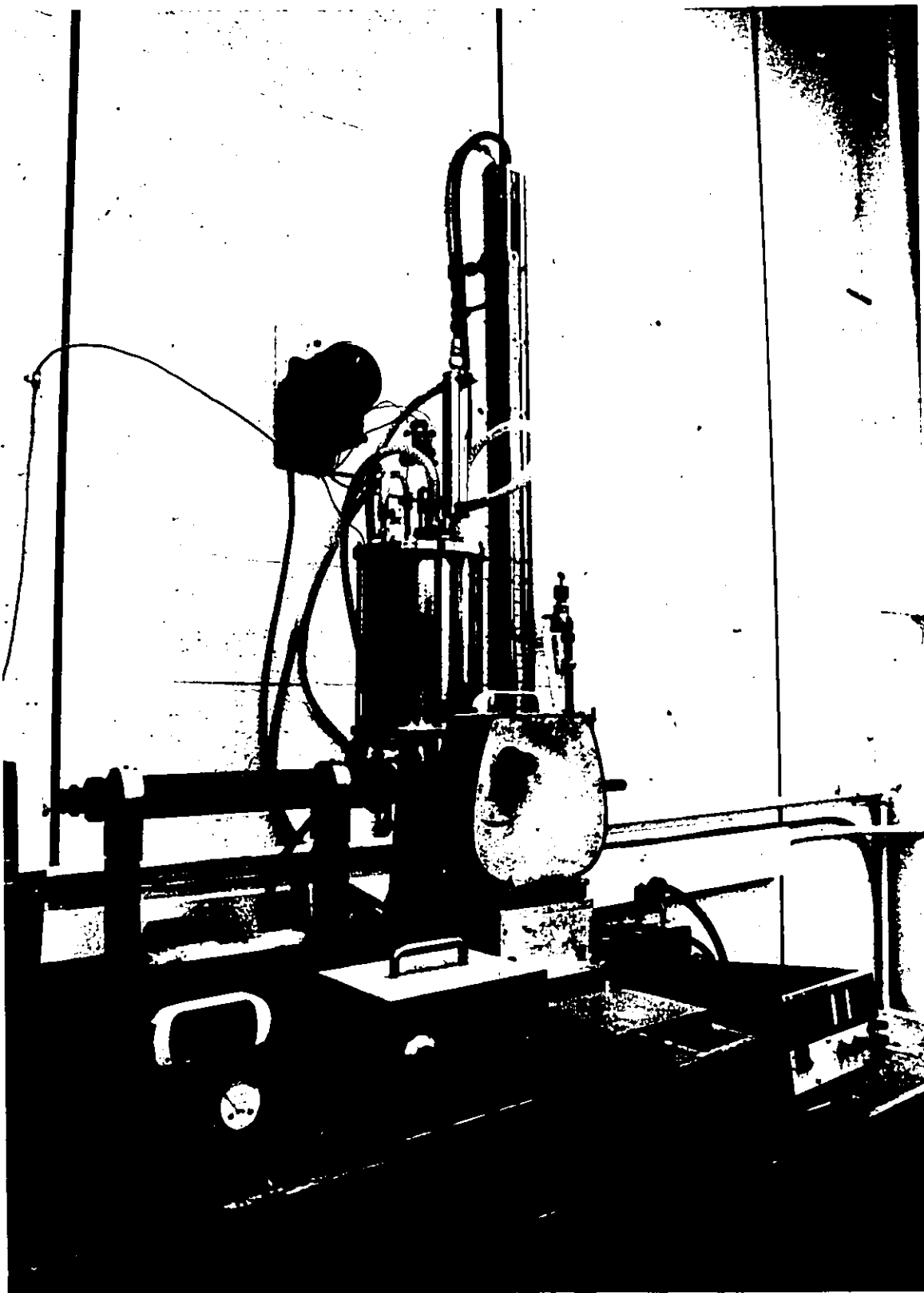
Figure 23   Photographic View of Test Assembly, High Speed Camera,
Timing Mark Generator and Power Supply.

Figure 24   Test Assembly

AREA OBSERVED BY CAMERA

SILVER DEPOSIT

HEATING SURFACE

GASKET

SUBCOOLING COIL

BUS BARS

TEST VESSEL
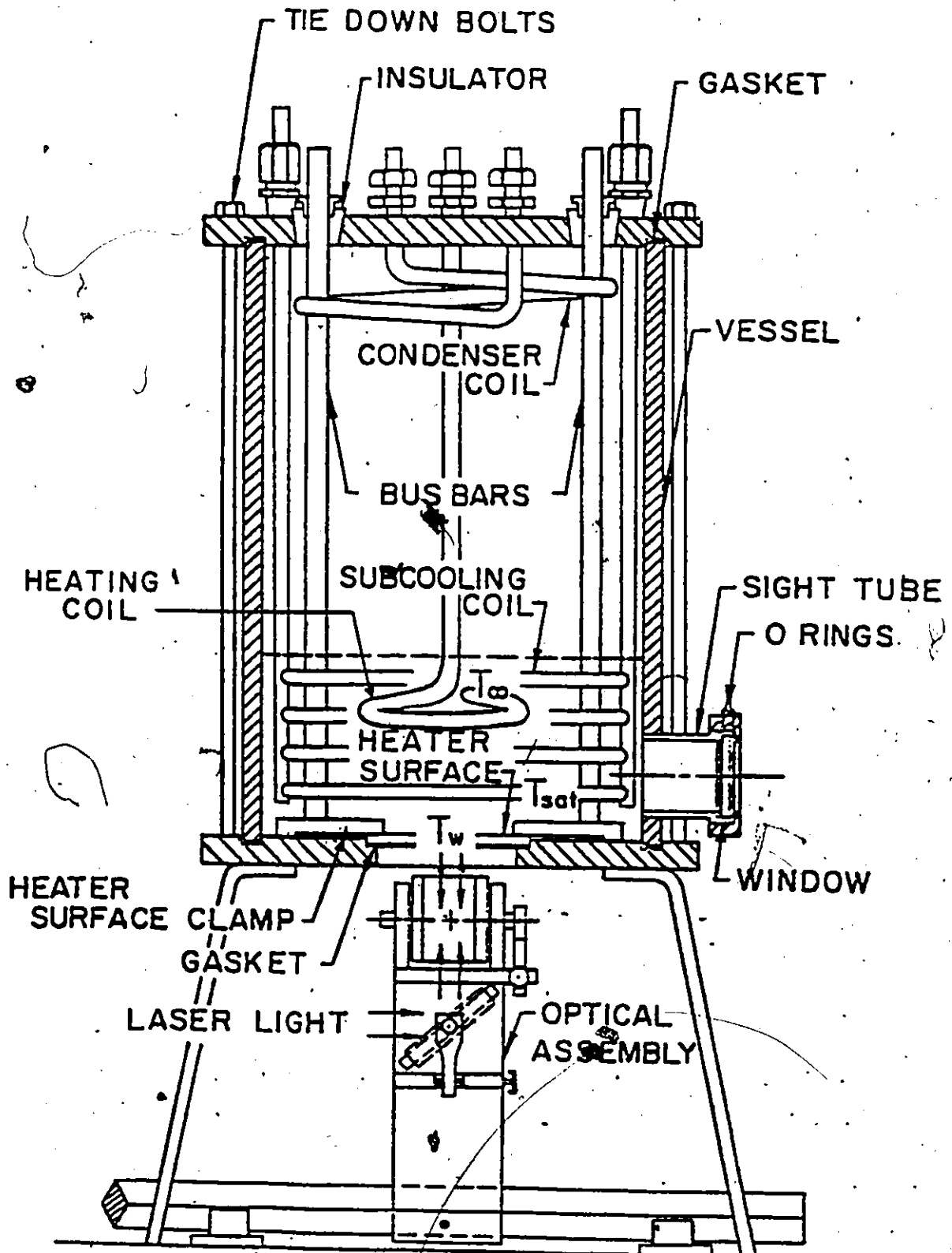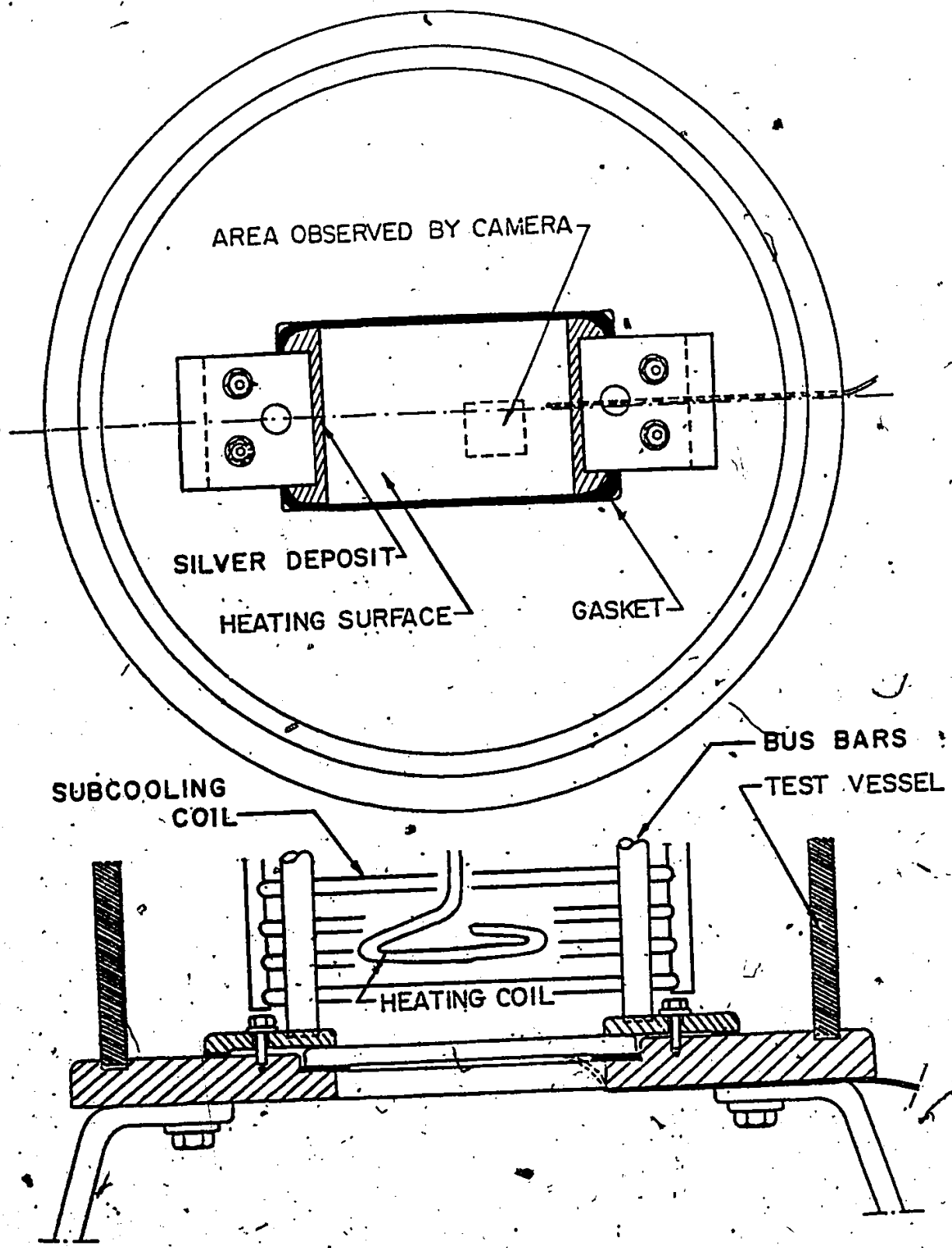
HEATING COIL

Figure 25   Vessel Base Plate and Heating Surface.

A condenser coil, constructed of stainless steel tubing wound in spiral form, was supported beneath the cover plate to condense the dichloromethane vapour formed during the experiments. A needle valve was used to adjust the flowrate of cold water going through the condenser. A reflux condenser, through which the test vessel was opened to the atmosphere was constructed on the cover plate to condense any dichloromethane vapour trying to escape to the atmosphere.

The experiment was carried out with the test vessel partially filled with one litre of dichloromethane such that the liquid level was a little more than 1" above the heating surface.

4.3 Power Supply

The stannic oxide coating on the glass surface received electric power for heating purposes from a KEPCO POWER SUPPLY (Model JQE 150 - 3.5 (M)). This DC power supply unit was capable of supplying a potential difference ranging from 0 - 150 volts to the heating surface and had the ability of independently setting the upper limit of the output voltage. The stannic oxide coating on the glass surface could only withstand a certain maximum potential difference beyond which it would burn itself out and the facility on the power supply allowing for setting an upper limit on voltage outputs served as a useful precautionary measure. The secondary

heater, located in the bulk liquid and used to add heat

directly to the bulk liquid, received power through a variac.

4.4 Temperature Measuring System

The temperature measuring system was comprised essentially of four chromel-constantan thermocouples. Three of these were used to measure the temperature of the bulk liquid and one was used to measure the wall temperature of the heat transfer surface. The thermocouples used to measure the bulk liquid temperature T_∞ were supported by the cover plate and arranged such that they were 120° apart with their hot junctions immersed in the bulk liquid at approximately the same level. The output signals of these thermocouples were directed by knife switches to a high resolution GUILDLINE POTENTIOMETER type 9160G (Serial No. 29425) where they were accurately measured. The hot junction of the thermocouple used for measuring the wall temperature T_w was "epoxied" on the underside of the heating surface and it was assumed that the temperature measured here represented the heating surface temperature. The output voltage from this thermocouple was directed by a knife switch to a MINNEAPOLIS HONEYWELL RECORDER where it was recorded continuously for at least ten minutes for each test. The E.M.F. produced by each of the four thermocouples were converted to temperature in degrees Fahrenheit by use of a conversion table published by the

National Bureau of Standards.

4.5   Illumination System and High Speed Camera

The source of illumination used for high speed photo-
graphy was a SPECTRAPHYSICS HELIUM NEON LASER Model 125A
(λ = 0.6328 μm) specified by the manufactured to produce a
highly collimated beam of 50 mW light. A schematic diagram
of the optical system is shown in Figure 26. Light from the
laser was directed through a diverging lens and then through
a collimating lens which together enlarged the beam ten times.
The emerging collimated and monochromatic beam of high inten-
sity light was then reflected upwards by a first surface
mirror and after passing through a rhomboidal prism it illu-
minated the glass plate where the bubbling phenomena occurred
on the upper surface. Images from the boiling surface were
reflected downwards and deflected into the objective lens
of the high speed camera for photgraphy.

High speed photography was accomplished by a 16 mm
Hycam motion picture camera (HYCAM Model K2001R) having a
film capacity of 100 feet and a maximum framing rate of
8500 frames/second. Kodak Double X negative film was used
at a framing rate of approximately 1000 frames/second. To
determine the framing rate more accurately a timing mark
generator was used in conjunction with the camera and pro-
duced timing dots on the edge of the film. The high speed
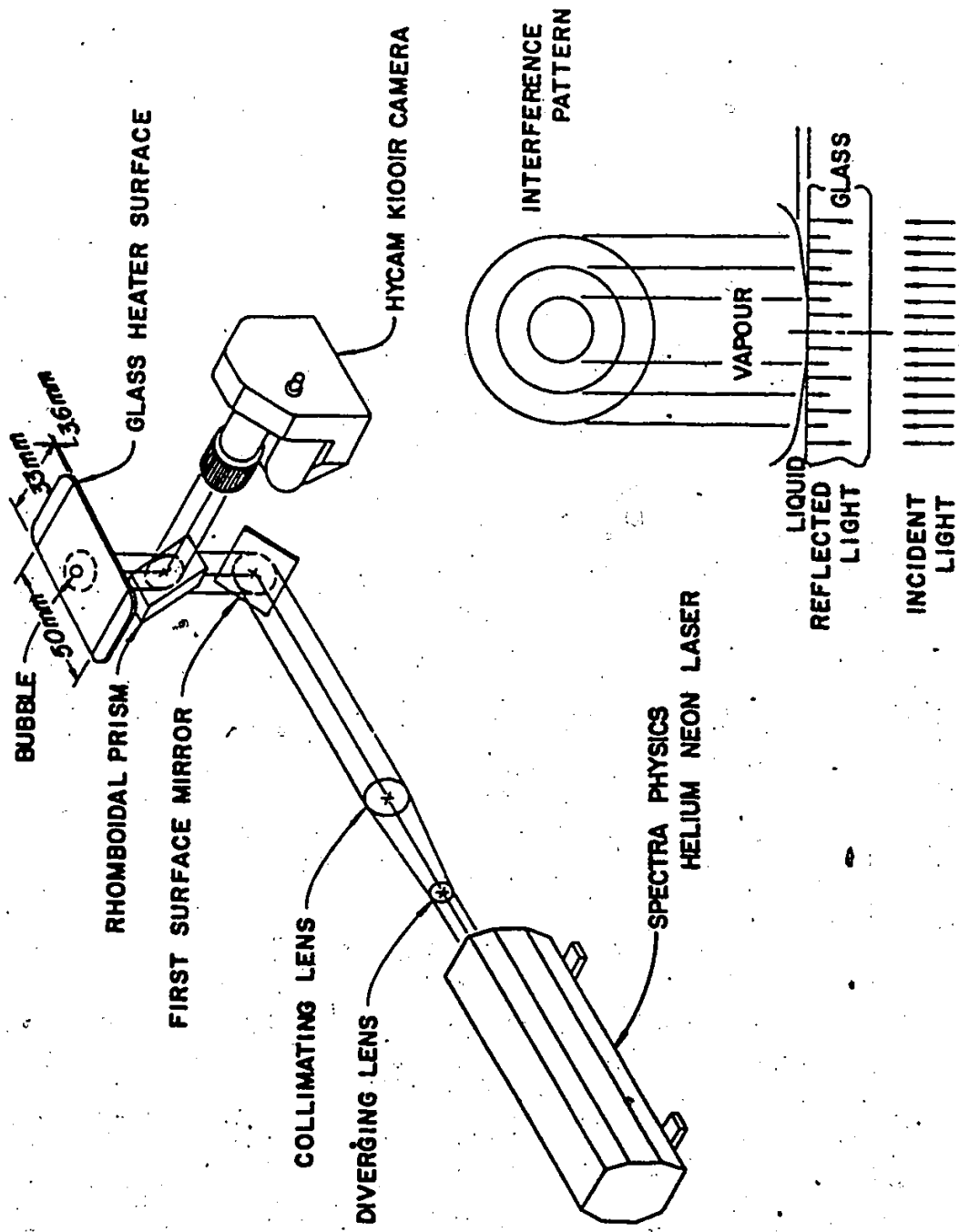
Figure 26 Schematic Representation of the Optical System.

camera, timing mark generator and power supply for the camera
are seen in Figure 23.

CHAPTER 5

TEST CONDITIONS

The·test fluid selected for this investigation was
dichloromethane (methylene chloride). Water is commonly
used in boiling experiments but was unsuitable for this
research because of its incompatability with the stannic
oxide coating on the glass surface. Experiments [38] have
shown that boiling water has a tendency to attack the oxide
coating in an electrolytic manner during testing and destroy
its usefulness in a matter of minutes. Although methanol,
carbon tetrachloride,·freon·and dichloromethane were all
known to have no destructive effect on the oxide coating,
dichloromethane was preferred because of its less hazardous
properties and the fact that it boils at a relatively low
· temperature.

During testing, the junctions of the thermocouples
used to measure liquid bulk temperature were positioned at
approximately one inch from the heat transfer surface. Prior.
experiments have shown that the response of these thermo-
couples were not affected in any significant way by their
position in the bulk liquid so long as they were not very
near to the heat transfer surface. A position of one inch
above the heating surface was therefore arbitrarily selected.

75.

as representative of the liquid bulk temperature. The average

reading of these three thermocouples was taken as the bulk

temperature. The hot junction of the thermocouple used to

measure the wall temperature of the heat transfer surface

was "epoxied" on the underside of the glass surface since it

was assumed that the temperature here represented the tempera-

ture of the boiling surface.

All tests were performed with the same liquid-surface

combination at atmospheric pressure. The atmospheric pressure

was measured at the time of testing with a mercury barometer

from which the saturation temperature of the liquid was

determined using the vapour-pressure saturation curve shown

in Appendix 1. Subcooling was computed by taking the differ-

ence between the saturation temperature and the average bulk

liquid temperature.

The desired levels of subcooling were achieved by

adjusting the flowrate of cold water going through the sub-

cooling coil. However it was sometimes necessary to use the

heating coil to add small amounts of heat directly to the

bulk liquid to maintain a desired level of subcooling.

Three levels of subcooling and six levels of heat

flux were investigated for their individual effect on bubble

waiting time. Eighteen individual tests were performed and

the corresponding photographic data was recorded on six rolls

of 100 feet Kodak Double X negative film during three

individual filming episodes. Photographic data was therefore recorded on approximately one-third of a film, which corresponds to approximately 1500 frames, for each test. Since the framing rate at filming was set at 1000 frames/second, the duration of filming per test was approximately 1.5 seconds. The levels of subcooling, together with the sequence of filming, are shown in Table 5.1.

TABLE 5.1.   FILMING SEQUENCE AND TEST CONDITIONS

SUBCOOLING θ_{SAT} (°F)	HEAT FLUX Q/A (BTU/hr ft^2)					
	7903	9757	11806	14050	16490	19124
1.60	FILM 2	FILM 2	FILM 2	FILM 1	FILM 1	FILM 1
14.7	FILM 4	FILM 4	FILM 4	FILM 3	FILM 3	FILM 3
30.0	FILM 6	FILM 6	FILM 6	FILM 5	FILM 5	FILM 5

CHAPTER 6

TEST PROCEDURE

Prior to the commencement of the research, high speed motion pictures of boiling at the heat transfer surface were taken at various framing rates. The objective of the experimental investigation was to determine bubble waiting times at different sites under different conditions and it was therefore desirable to photograph a number of bubble cycles per site whose average waiting time would reasonably represent the actual waiting time. The preliminary data indicated that although bubble waiting time varied considerably from site to site and from one test condition to another, a framing rate of 1000 frames/second would enable the determination of representative values of waiting times without significant losses in precision.

From personal experience developed with the apparatus it was known that the main and reflux condensers kept the loss of liquid as a result of vapourization during boiling to a minimum. However, at the beginning of each test sequence the dichloromethane was drained, measured and then poured back into the vessel. It was found that losses between test sequences were negligible and therefore the same charge, and practically the same volume, of liquid was used throughout the investigation. Similarly, the same glass heating surface was used in every test.

The air vent above the reflux condenser was then opened to the atmosphere so that the system pressure, as monitored by a mercury manometer, would remain constant at atmospheric pressure during testing. The cooling water valve controlling the flow to the condenser coils was fully opened and the power supply unit connected to the heat transfer surface switched on. Power was then gradually increased until the highest level of heat flux desired for the sequence of tests was attained. Boiling was allowed to take place for at least one hour such that steady state conditions could be achieved.

While allowing for the establishment of steady state boiling conditions, the temperature recorder and the pot-entiometer were calibrated against a standard cell of known E.M.F. The camera was then set up, loaded with 100 feet of Kodak Double X negative film, set at a framing rate of 1000 frames/second and the timing mark generator set at 100 pulses per second.

After boiling was fully established, the needle valve controlling the water flow-rate to the subcooling coil and the variac controlling the power supply to the secondary heater submerged in the liquid bulk were simultaneously adjusted to achieve and maintain the desired level of sub-cooling. Steady state conditions for any combination of heat flux and subcooling were considered to have been achieved when each of the bulk liquid temperature measurements was within $\pm 0.3°F$ of the desired subcooling for at least ten minutes

When it was certain that boiling was fully established, the output voltage of each of the bulk liquid thermocouples was measured sequentially and the wall temperature thermocouple was connected to the recorder where its output was recorded for approximately ten minutes. The high speed camera was then activated.

Power was then reduced to correspond to the next level of heat flux in the sequence. The bulk liquid temperature was monitored continuously on the potentiometer and necessary adjustments were made to the system to preserve the level of subcooling. When stability of boiling was established once again, the thermometric and photographic data were taken. This procedure was repeated for the next four test conditions in the sequence of tests. After taking photographic data at the last test condition in the sequence, the heat flux was further lowered in steps while the level of subcooling was maintained in order that further thermometric data would be obtained to plot the boiling characteristic curve.

CHAPTER 7

DATA REDUCTION

This chapter is concerned with a description of the methods used in calculating the heat flux Q/A, the saturation temperature T_{sat}, the surface temperature T_w, the bulk liquid temperature T_∞, the liquid subcooling θ_{sat} and the bubble waiting time t_w.

Heat Flux

The heat flux Q/A was calculated from the total power dissipation at the heat transfer surface. Although some of this energy was lost from the glass surface to the air under the heating surface and through the rubber gasket separating the heating surface from the test vessel, the total loss was estimated to be approximately 6% and was neglected in the calculation of the heat flux. The heat flux was calculated using the expression

$$Q/A = 3.414 \frac{E^2/R}{A} \qquad (7.1)$$

where   Q/A = heat flux, BTU/hr ft^2

     E = potential difference across heat transfer surface, Volts

     A = area of the oxide coating on the glass surface, 0.2188 ft^2

     R = electrical resistance of the oxide coating on the glass surface, 48 Ohms

Saturation Temperature

The saturation temperature T_{sat} of the liquid could not be measured directly. However, boiling was done at atmospheric pressure and by measuring this pressure directly with a mercury manometer, the saturation temperature was determined from the saturation curve shown in Appendix 1.

Surface Temperature

The temperature at the heat transfer surface T_w was assumed to be the same as that measured by the thermocouple epoxied to the underside. For each test, the output of this thermocouple was recorded for ten minutes and the average reading was taken as the temperature of the heat transfer surface under the conditions of testing.

The assumption as stated above is a reasonable one because the temperature drop across the thickness of the glass specimen as a result of conduction through it and a negligible heat transfer coefficient at the underside was practically insignificant and could therefore be neglected (Appendix 2).

Bulk Liquid Temperature

The bulk liquid temperature T_∞ was taken as the average of the three temperatures measured by the three thermocouples suspended in the bulk liquid at approximately one inch above the heat transfer surface.

Liquid Subcooling

Liquid subcooling θ_{sat} was calculated as the difference between the saturation temperature T_{sat} and the bulk liquid temperature T_∞ according to

$$\theta_{sat} = T_{sat} - T_\infty \qquad (7.2)$$

Bubble Waiting Time

The bubble waiting time t_w for a particular bubble was calculated using the relationship

$$t_w = [(n_2 + 1) - n_1] \Delta t \qquad (7.3)$$

where n_1 is the frame number at which the preceding bubble just disappeared, (n_2+1) the frame number at which the bubble just appeared and Δt the time interval between frames. The average value of Δt was determined to be 1.1482 m s. The derivation of the waiting time relationship and the interframe time interval can be found in Appendix 3 and Appendix 4 respectively.

The average bubble waiting time t_w at a given site was calculated by dividing the sum of the individual bubble waiting times by the total number of bubble emissions at that site.

In the analysis of the film strips, the first three to four feet at the beginning and end were disregarded to allow for acceleration and deceleration effects. With a particular frame arbitrarily selected to represent zero

time datum, the rest of the film was projected one frame.
at a time and for a given site the frame number at which a
bubble disappeared and the frame number preceding the frame
at which a subsequent bubble appeared were recorded in
sequence. This procedure was repeated for each active site
and individual waiting times were calculated. The average
waiting time t_w at a given site was then determined.

Although it was found that a relatively large
number of nucleation sites were activated on the region
of the glass surface photographed, bubble waiting time data
was taken for only twelve sites because the rest of them
emitted only a few bubbles. Because it was desired to obtain
representative values of waiting time, sites with little
activity were disregarded in the analysis.

CHAPTER 8
RESULTS

The experimental data is presented in this chapter with little comment. Analysis and discussion of the data are presented in the next chapter. The thermometric and bubble waiting time data are tabulated in Appendix 5 and Appendix 6 respectively.

Figure 27 shows the characteristic boiling curve for dichloromethane boiling on a glass surface at each of three levels of subcooling investigated. The boiling curves are plotted in the form of measured heat flux Q/A versus temperature difference $(T_w - T_\infty)$.

Figures 28 to 30 show the distribution of the active sites and maximum bubble size observed at the different levels of subcooling and heat flux investigated. The sites for which waiting time data was taken are identified by letters A to L. The region of the heat transfer photographed was 10.55 mm long by 7.46 mm wide and the diagrams of Figure 28 to 30 therefore represent a 6.5 enlargement.

Figures 31 to 42 show plots of bubble waiting time t_w as a function of measured heat flux Q/A with liquid subcooling $(T_{sat} - T_\infty)$ as a parameter for the twelve active sites investigated. The sites are not presented in alphabetical order but rather in order of abundance of bubble emissions.

The diagrams show that bubble waiting time t_w decreases
as heat flux Q/A increases and liquid subcooling. $(T_{sat} - T_\infty)$
increases.
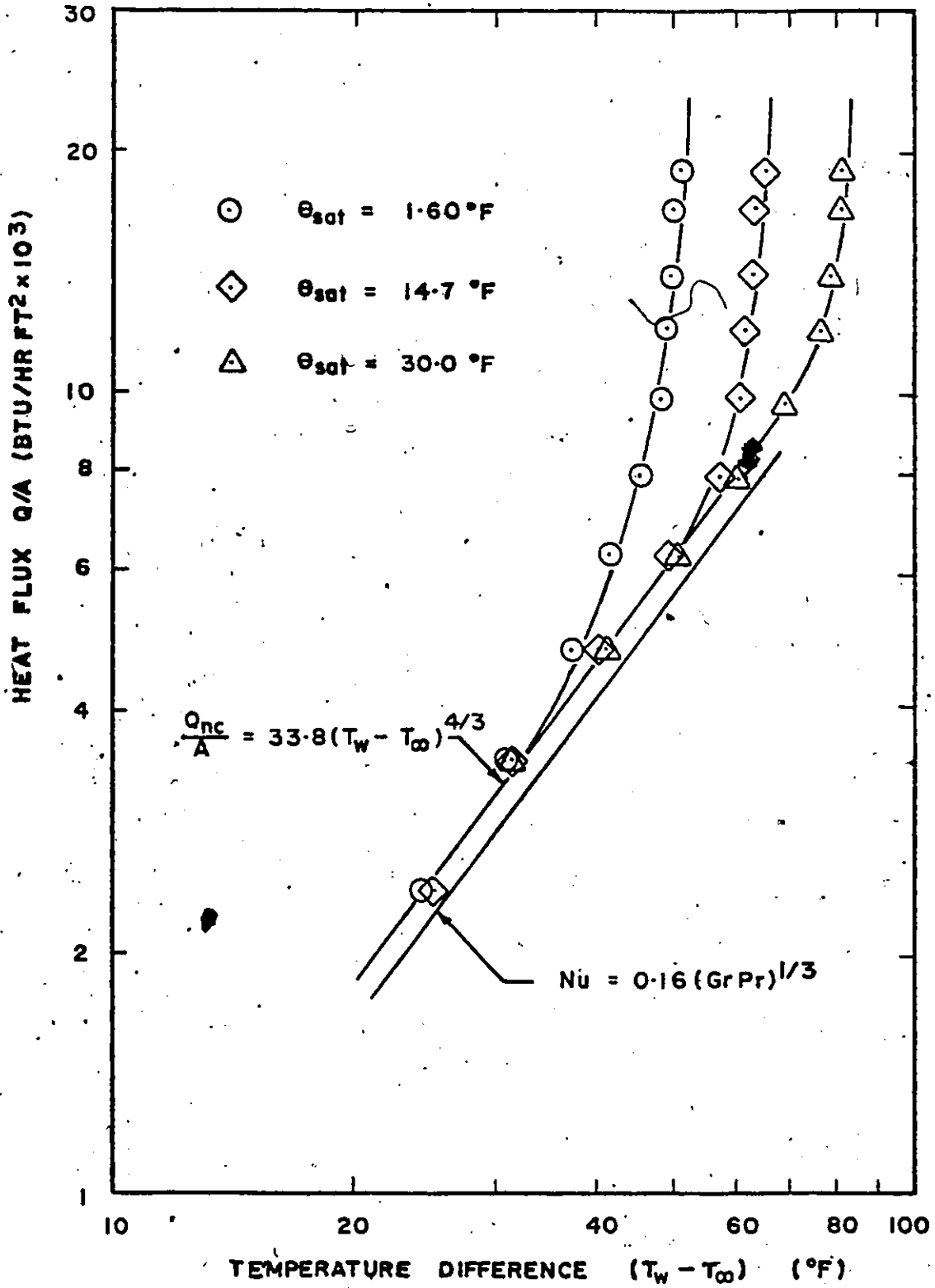
Figure 27 Boiling Characteristic Curve.
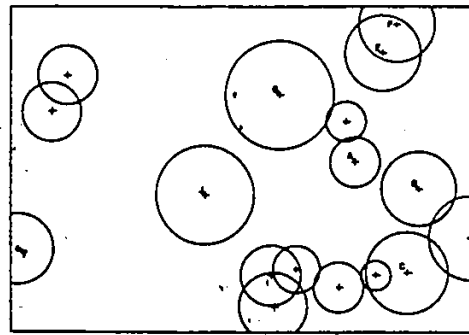
Figure 28 Distribution of Active Nucleation Sites at Subcooling of
1.60 °F (Small Letters Identify Sites).
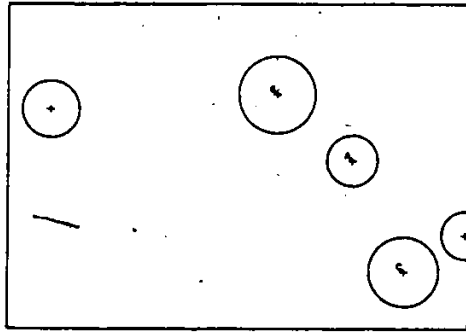
Q/A = 7903 BTU/HR FT^2
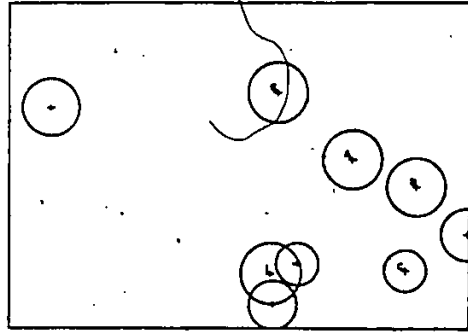
Q/A = 9757 BTU/HR FT^2
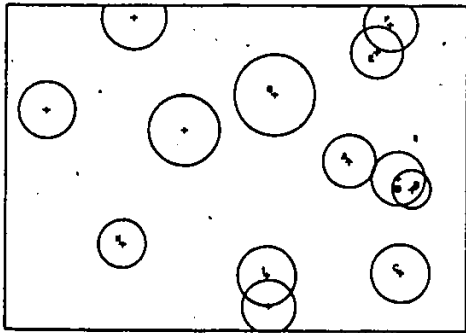
Q/A = 11806 BTU/HR FT^2
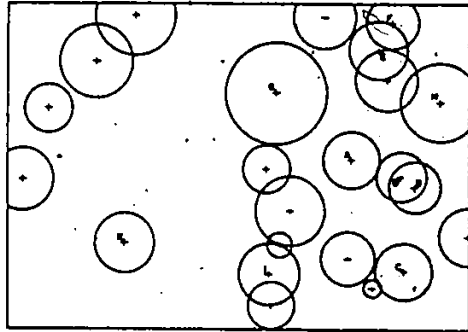
Q/A = 14050 BTU/HR FT^2
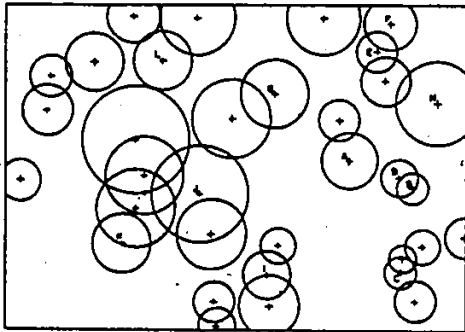
Q/A = 16490 BTU/HR FT^2
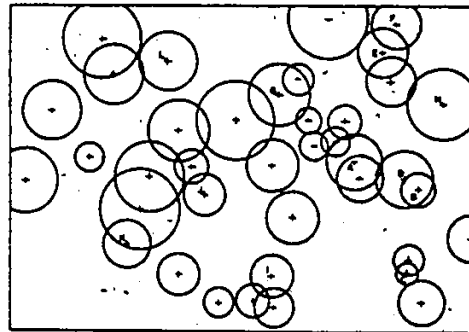
Q/A = 19124 BTU/HR FT^2

Figure 29 Distribution of Active Sites at Subcooling of 14.7 °F (Small Letters Identify Sites).

Q/A = 9757 BTU/HR FT^2 Q/A = 11806 BTU/HR FT^2

Q/A = 14050 BTU/HR FT^2 Q/A = 16490 BTU/HR FT^2

Q/A = 19124 BTU/HR FT^2
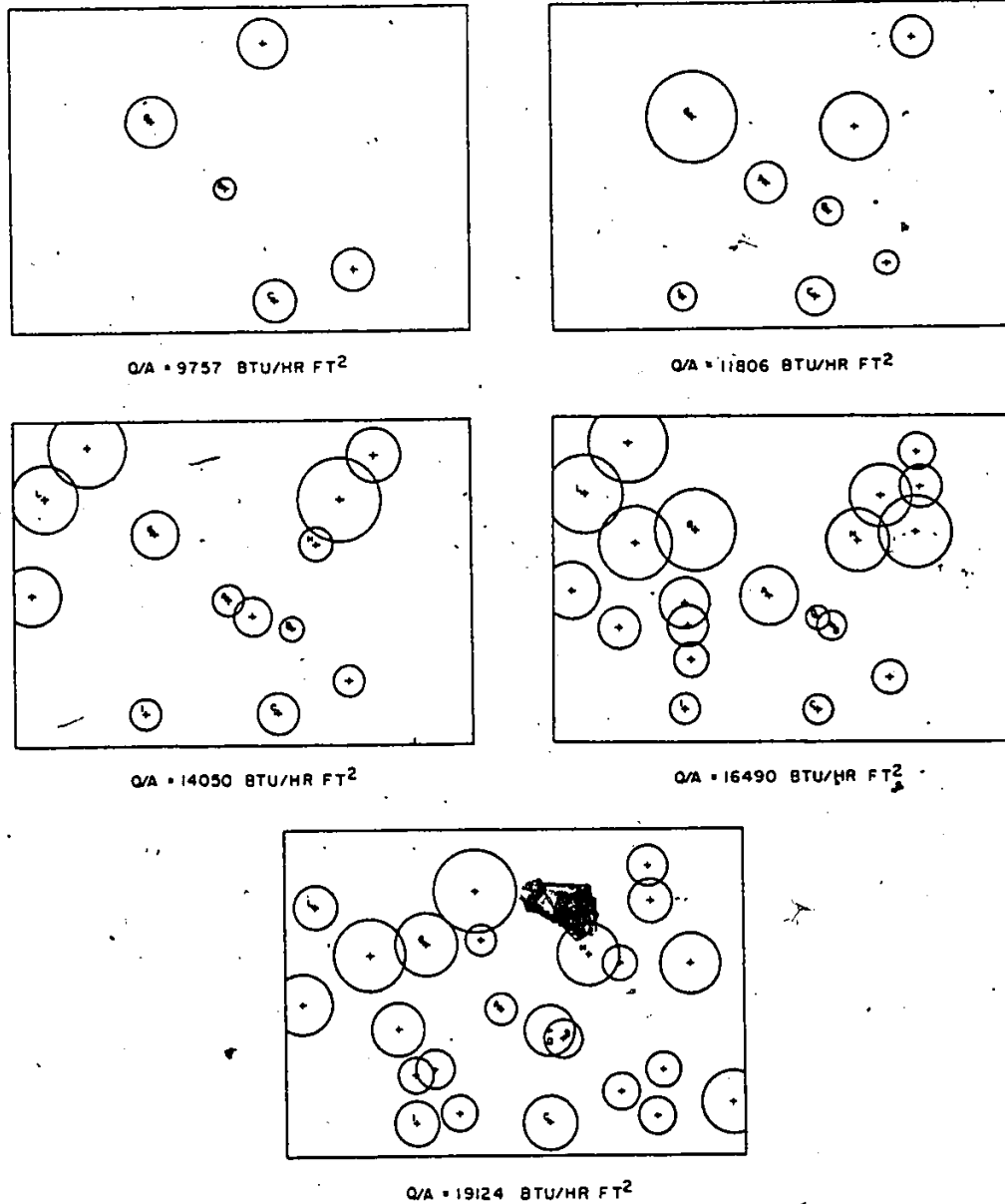
Figure 30 Distribution of Active Sites at Subcooling of 30.0 $^\circ$F (Small

Letters Identify Sites).
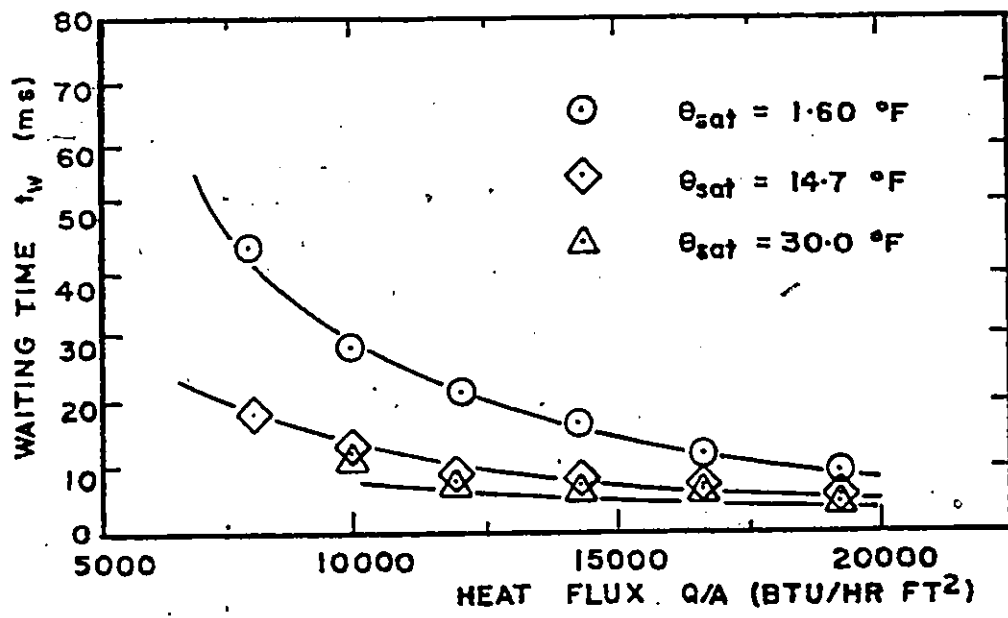
Figure 31 Bubble Waiting Time Results for Site A.
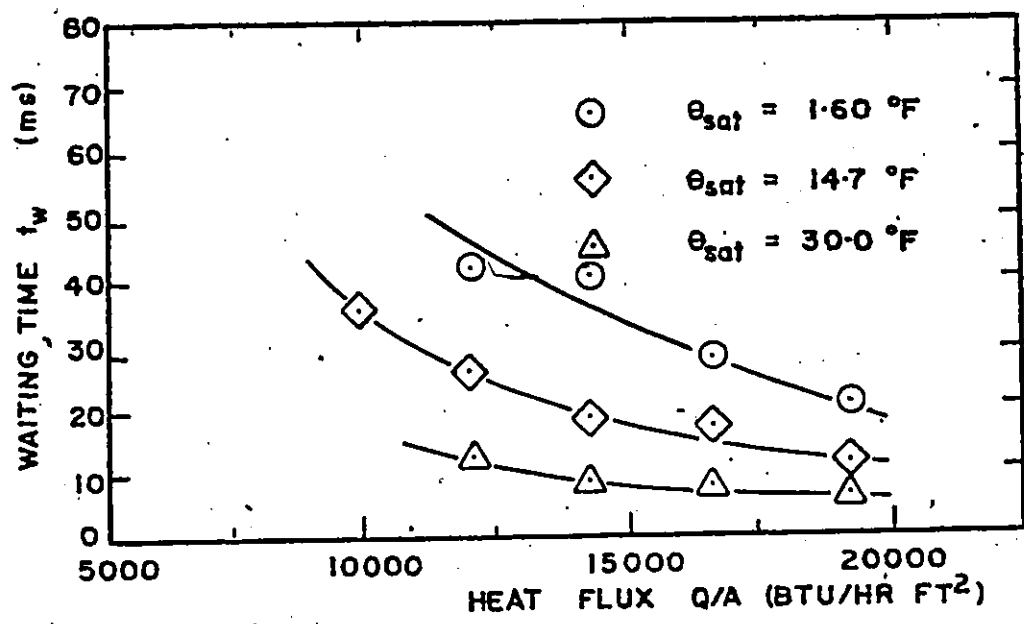
Figure 32 Bubble Waiting Time Results for Site B.
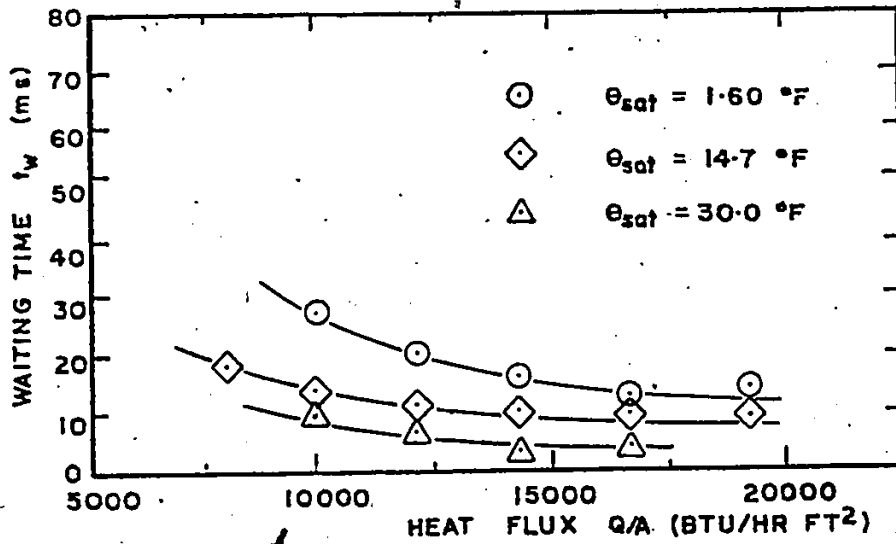
Figure 33 Bubble Waiting Time Results for Site C.
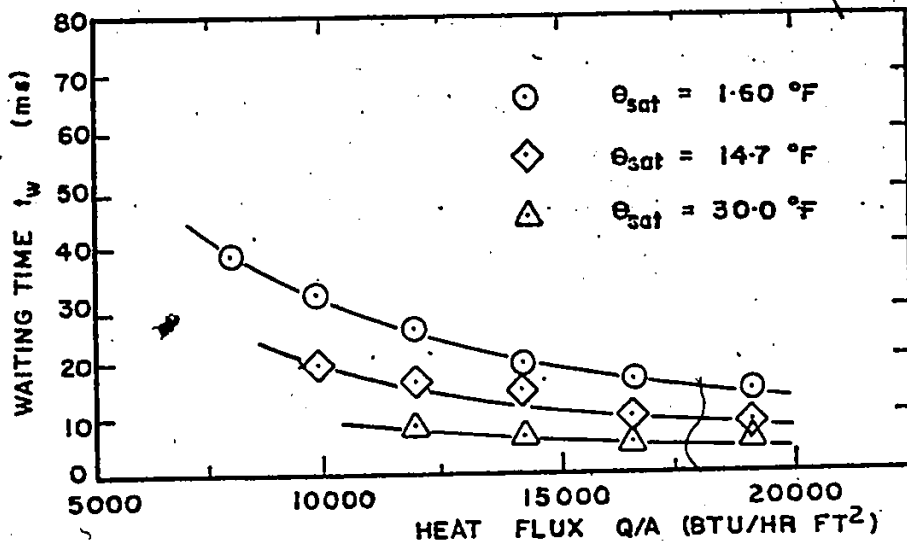
Figure 34 Bubble Waiting Time Results for Site I.
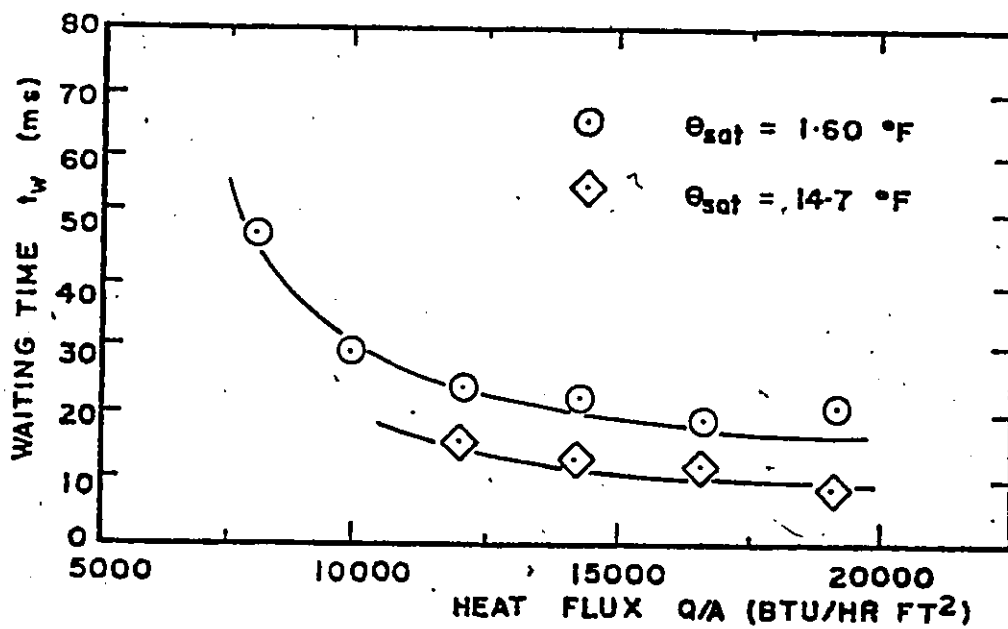
Figure 35   Bubble Waiting Time Results for Site E.
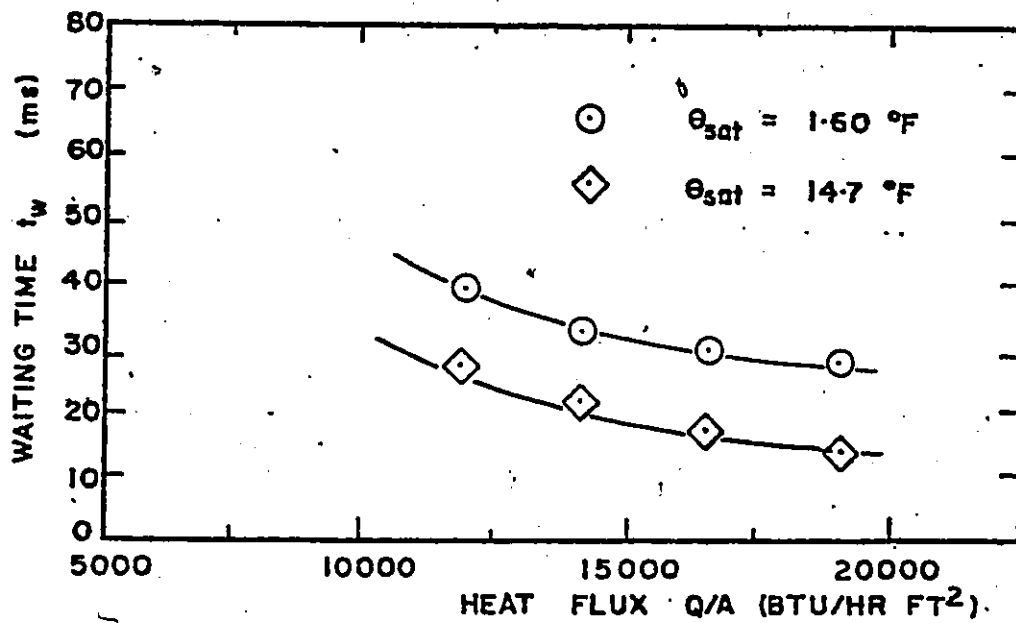
Figure 36   Bubble Waiting Time Results for Site F.
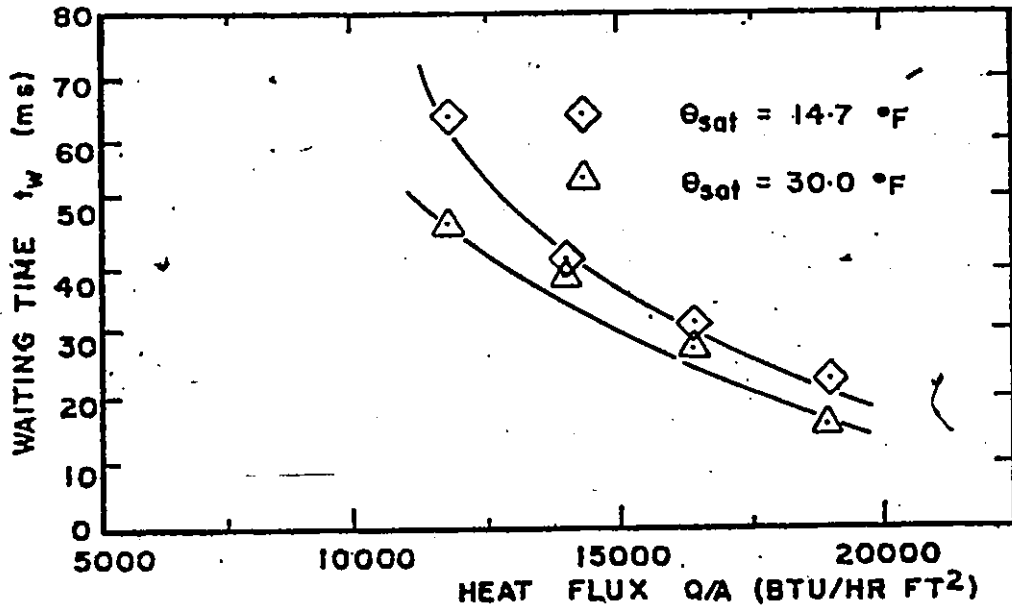
Figure 37 Bubble Waiting Time Results for Site G.
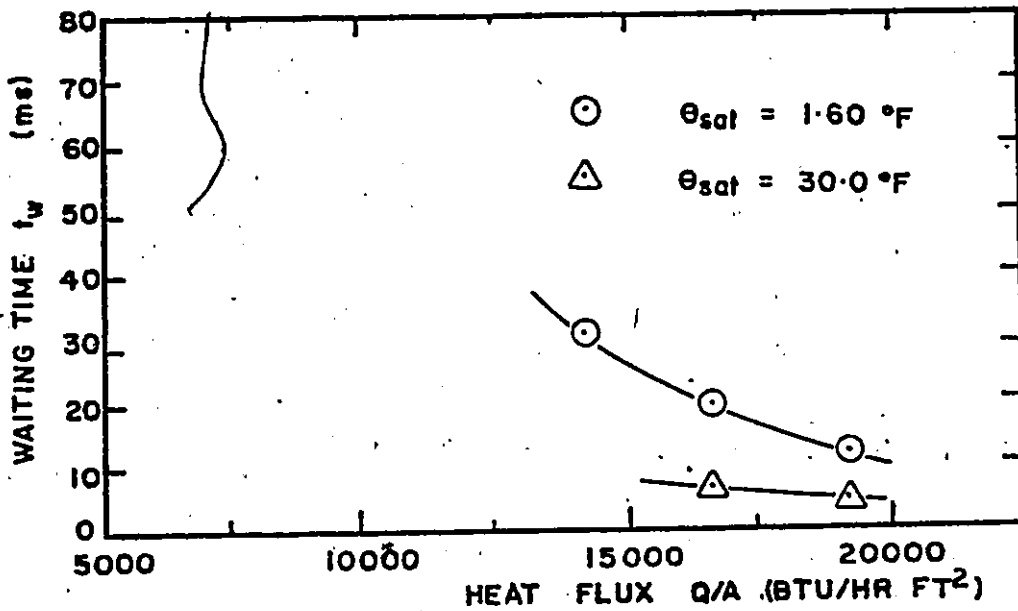
Figure 38 Bubble Waiting Time Results for Site L.
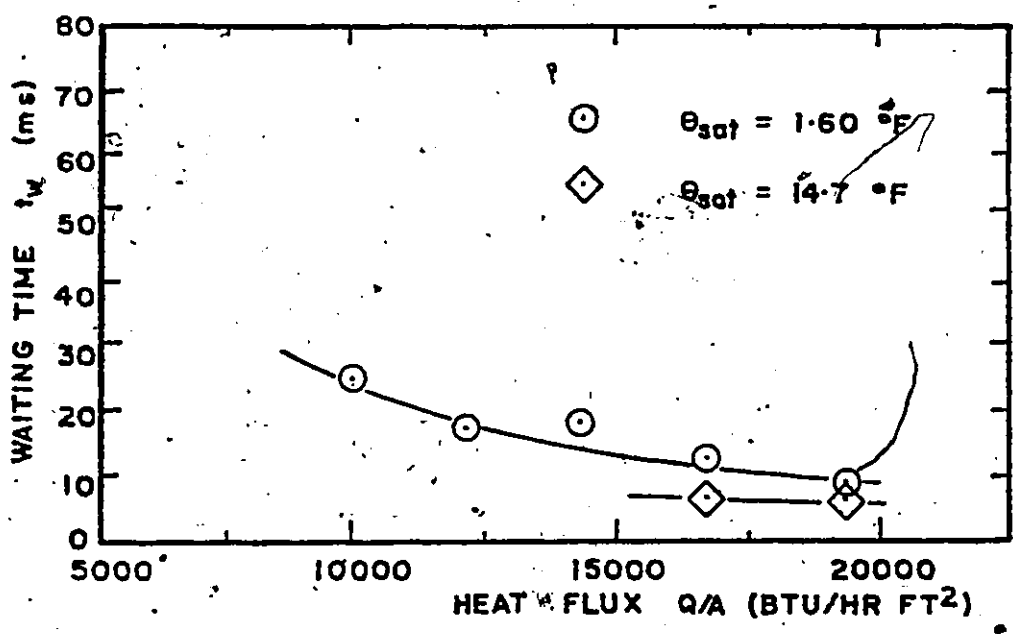
Figure 39 Bubble Waiting Time Results for Site J.
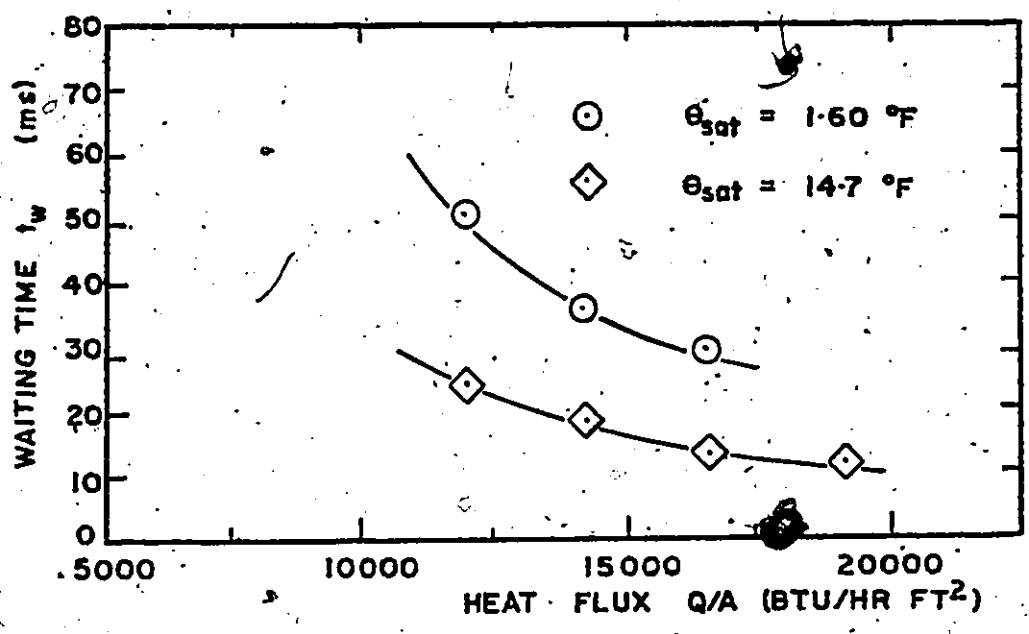
Figure 40 Bubble Waiting Time Results for Site K.
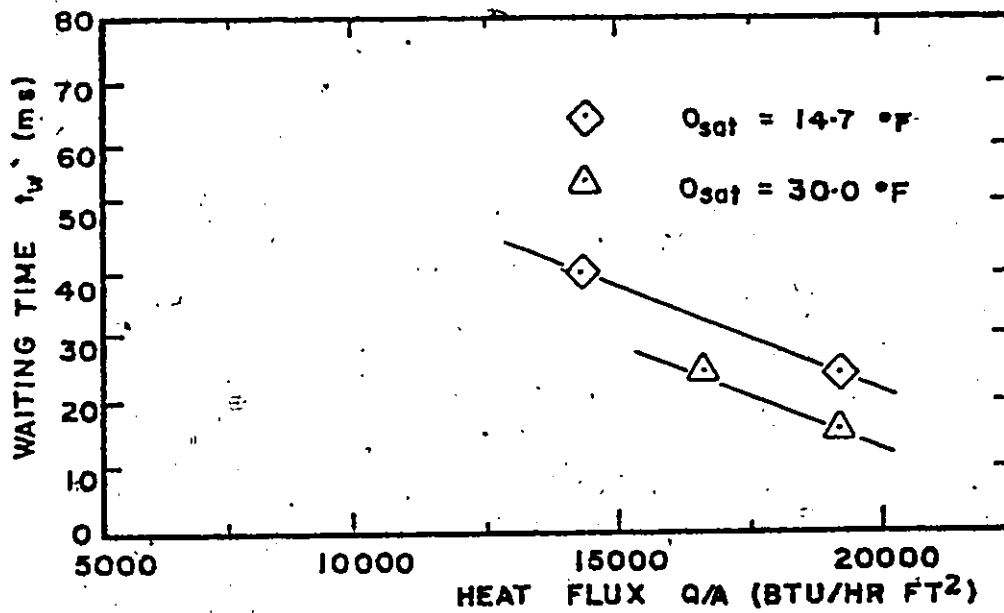
Figure 41   Bubble Waiting Time Results for Site D.
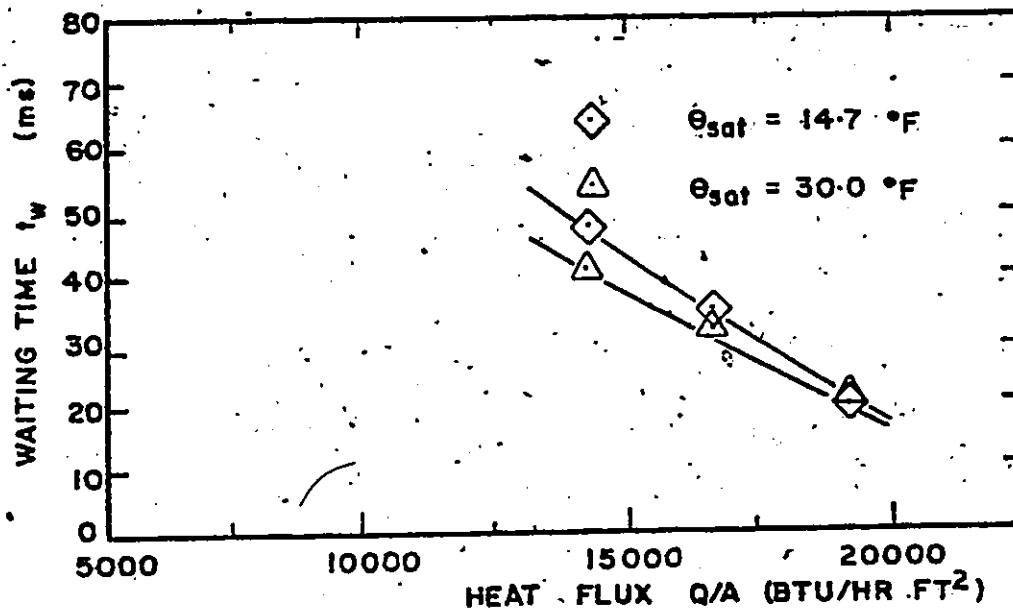
Figure 42   Bubble Waiting Time Results for Site H.

CHAPTER 9

ANALYSIS AND DISCUSSION

9.1 Introduction

In this chapter the boiling characteristic curves, active site distribution and maximum bubble diameter results presented in Chapter 8 will be discussed briefly. The mechanism and theories of bubble nucleation covered in detail in Chapter 3 will then be reviewed and the bubble waiting time results of Chapter 8 examined in light of these theories.

9.2 Boiling Characteristic Curves

Figure 27 shows the characteristic boiling curves for dichloromethane boiling on a glass surface at one atmosphere pressure and at subcoolings of $1.6^{\circ}F$, $14.7^{\circ}F$ and $30.0^{\circ}F$. Although it is customary to present boiling data as a plot of measured heat flux Q/A as a function of wall superheat $(T_w - T_{sat})$, the procedure of plotting heat flux Q/A as a function of temperature difference $(T_w - T_\infty)$ has the advantage of delineating the effect of subcooling. Consequently, in Figure 27, each curve diverging from the straight line representing natural convection represents a different level of subcooling. The straight line representing natural convection heat transfer can be expressed [45]

$$\frac{Q_{nc}}{A} = C_o \, (T_w - T_\infty)^{4/3}$$

.(9.1)

where the constant C_0 was calculated to be 33.8 BTU/hr ft^2(^{O}F)$^{4/3}$

From natural convection theory [45]

$$Nu = 0.16 \ (Pr \ Gr)^{1/3} \tag{9.2}$$

which can be re-expressed as

$$\frac{Q_{nc}}{A} = [0.16 \ (\frac{g\beta_\ell \rho_\ell^2 k_\ell^2 C_\ell}{\mu_\ell})^{1/3}](T_w - T_\infty)^{4/3} \tag{9.3}$$

With the properties of dichloromethane at one atmosphere, the value of the constant $[0.16(g\beta_\ell \rho_\ell^2 k_\ell^2 C_\ell / \mu_\ell)^{1/3}]$ was calculated to be 28.0 BTU/hr ft^2(^{O}F)$^{4/3}$. Therefore, equation (9.3) becomes

$$\frac{Q_{nc}}{A} = 28.0 \ (T_w - T_\infty)^{4/3} \tag{9.4}$$

Figure 27 shows good agreement between equations (9.1) and (9.2) and therefore establishes some confidence in the present work.

9.3   Active Site Distribution and Maximum Bubble Size

Figures 28, 29 and 30 show the distribution of active sites on the heat transfer surface and maximum bubble size observed for the six levels of heat flux and three levels of subcooling investigated. Although no quantitative analysis is presented, the active site distributions appear to be random as discussed in the literature [19, 20] and yet, at the same time, there is ample evidence of "patchwise boiling" which is the tendency of nucleation sites to cluster on the heat transfer surface. Explanations for patchwise boiling imply that the probability of an active site being located at

a random spot on the heat transfer surface is in many cases
influenced by other active sites already in existence in
the neighborhood of potentially active sites. This is
inconsistent with the observation that local active site
populations are distributed according to the Poisson's
equation which require that the event in question be
completely random and not influenced by events which have
already occurred. It is therefore possible that "patchwise
boiling" may only appear as clustering of active nucleation
sites when, in reality, it represents a completely random
phenomenon.

Figures 28, 29 and 30 show that the average density
of active sites increases rapidly as heat flux increases
and subcooling decreases. It can also be seen that there
is a general tendency for maximum bubble diameter to
decrease as heat flux and liquid subcooling increases.

9.4   Bubble Waiting Time

In Chapter 3 the mechanism of bubble nucleation was
discussed and it was shown that bubble growth begins when
the local thermal boundary layer has grown to a sufficient
thickness such that the criterion equation for bubble growth

$$\theta(b,t) = \theta_v \tag{3.77}$$

is satisfied. On the assumption that diffusion is the only
mode of heat transfer to the thermal boundary layer, the
expression

$$\frac{T(y,t) - T_\infty}{(Q/A)\sqrt{\kappa_\ell t}/k_\ell} = 2 \text{ ierfc } z \qquad (3.22)$$

was derived to predict the growth of, and temperature distribution in, the thermal layer. It was shown in Section 3.4.1 that if equation (3.22) does describe the behaviour of the local thermal boundary layer then the bubble waiting time t_w would be obtained by solving the expression

$$\theta_{sat} + \frac{A}{r_n} = 2 \frac{(Q/A)\sqrt{\kappa_\ell t_w}}{k_\ell} \text{ ierfc}(\frac{b}{2\sqrt{\kappa_\ell t_w}}) \qquad (9.5)$$

Using the properties of dichloromethane at one atmosphere, a computer program CURFIT (Appendix 8) was developed [42] to solve equation (9.5) and generate plots of waiting time t_w as a function of heat flux Q/A. Some representative plots are shown in Figure 20. The diagram shows that bubble waiting time decreases as heat flux increases and subcooling decreases. The first result follows the trend of the present experimental data as depicted in Figures 31 to 42. However, the second result contradicts the data. The situation is that equation (9.5) predicts a sharp increase in bubble waiting time t_w with increasing subcooling when the experimental observation shows just the opposite effect. Since equation (9.5) was derived on the assumption of a pure conduction mode of heat transfer in the liquid boundary layer and since it does not predict bubble waiting time adequately it is quite reasonable at this point to conclude that diffusion may not be the only mode of heat transfer.

Best, Burow and Beer [30] indicated that their optical investigation pointed to a convective contribution of heat transfer of significant magnitude in the formation of a thermal boundary layer of a boiling liquid. It was felt that this convective contribution cannot be neglected in a meaningful formulation of a bubble nucleation model. In accordance with this, it was proposed in Chapter 3, Section 3.2, that there exists an unsteady inwardly directed flow field, shown in Figure 17, in the layer of liquid adjacent to the heat transfer surface and in the near vicinity of active sites. It was explained that the convective transport of heat was promoted by this unsteady flow. On the basis of this convective component of heat transfer, combined with diffusion into the liquid from the heat transfer surface, a model of bubble nucleation was formulated. The result of this model showed that the local thermal boundary layer grows according to

$$\frac{d\phi^2}{d\tau} - \frac{1 - e^{-\tau}}{\tau - (1 - e^{-\tau})} \cdot \phi^2 [0.574(\frac{\phi}{X}) - 0.082(\frac{\phi}{X})^3 + 0.020(\frac{\phi}{X})^4] = 12$$

(3.63)

The theory was then incorporated in the criterion equation for bubble nucleation, equation (3.77), to give

$$\frac{1}{3} \frac{Q/A}{k_\ell} \Delta(t) \left[1 - 3(\frac{b}{\Delta(t)}) + 3(\frac{b}{\Delta(t)})^2 - (\frac{b}{\Delta(t)})^3\right] = \theta_{sat} + \frac{A}{r_n}$$

(3.88)

By substitution of $\Delta(t)$ from equation (3.63) into equation (3.88) the bubble waiting time t_w could be determined.

In the experimental part of the present investigation, the organic liquid dichloromethane was boiled on a glass heating surface. Organics are known to have small contact angles and, in accordance with Lorenz, Mikic and Rohsenow [40] it was thought that the nucleus sits in the cavity mouth such that the liquid-vapour interface makes contact with the cavity as shown in Figure 43. For this situation it can be seen that

$$b = 2 \; r_n \qquad\qquad (3.85)$$

With constant C assumed to be $1.5*10^{-3}$ inches in Equation (3.62) and the properties of dichloromethane at one atmosphere pressure, a computer program WAIT5 (Appendix 9) was developed [42] to generate plots of waiting time t_w as a function of heat flux according to equation (3.63) and (3.88). Representative results of this program are depicted in Figure 21.

Equation (3.63) and (3.88), which result from the bubble nucleation model formulated on the basis of a conduction-convection mode of heat transfer, relate five variables: nucleus radius r_n, time constant t_c, liquid subcooling θ_{sat}, heat flux Q/A and bubble waiting time t_w. Out of these five variables, only the latter three could be measured in the experimental part of the investigation. Since both nucleus radius r_n and time constant t_c were unknowns, testing of the model required an indirect approach.

The situation is such that if one value of time constant t_c can be established for each of the three levels

Figure 43 Bubble Nucleus And History of Waiting Time.

$$\Theta_b = T_b - T_\infty$$
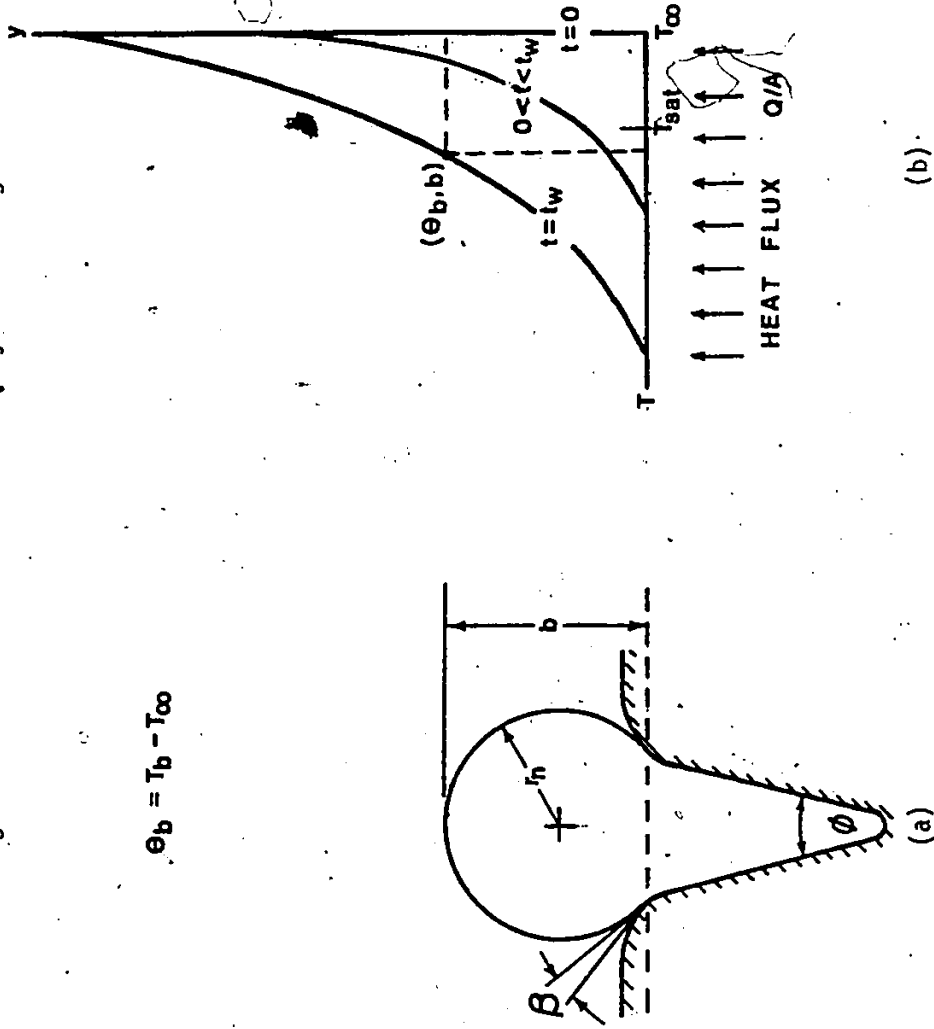
Figure 43(a) Nucleus Sitting Within Cavity.

Figure 43(b) History of Bubble Waiting Time for Conduction-Convection Model of Heat
Transfer.

of subcooling investigated, then the nucleus radius r_n can be determined for each of the twelve active sites for a known value of bubble waiting and heat flux. Having the value of r_n now, the model can be used to predict bubble waiting time t_w at any of the three levels of subcooling for which t_f is determined. If the predictions compare well with the experiments, then it would be reasonable to believe that the model is realistic and valid.

In testing the model, computer program WAIT5 was used to generate curves of waiting time t_w versus heat flux Q/A with liquid subcooling θ_{sat}, time constant t_c and nucleus radius r_n as parameters at each of the three levels of subcooling investigated: 1.6^0F, 14.7^0F and 30.0^0F. The value of t_c was established as 0.10 m s at 1.60^0F subcooling by adjusting the values of r_n for the twelve active sites investigated until a constant value of t_c enabled the theoretically predicted waiting times to agree with the experimentally determined waiting times at the six levels of heat flux. With the twelve values of r_n now established, the value of t_c was determined at 14.7^0F subcooling by adjusting it until a single value of 1.50 m s permitted close agreement between theory and experiment at the six levels of heat flux. A similar procedure showed t_c to be 20.0 m s at 30.0^0F. Good agreement between theory and experiment is shown in Figures 44 to 48 for five representative sites.

A close examination of Figures 44 to 48 shows that, in addition to a reasonably good agreement between the pre-
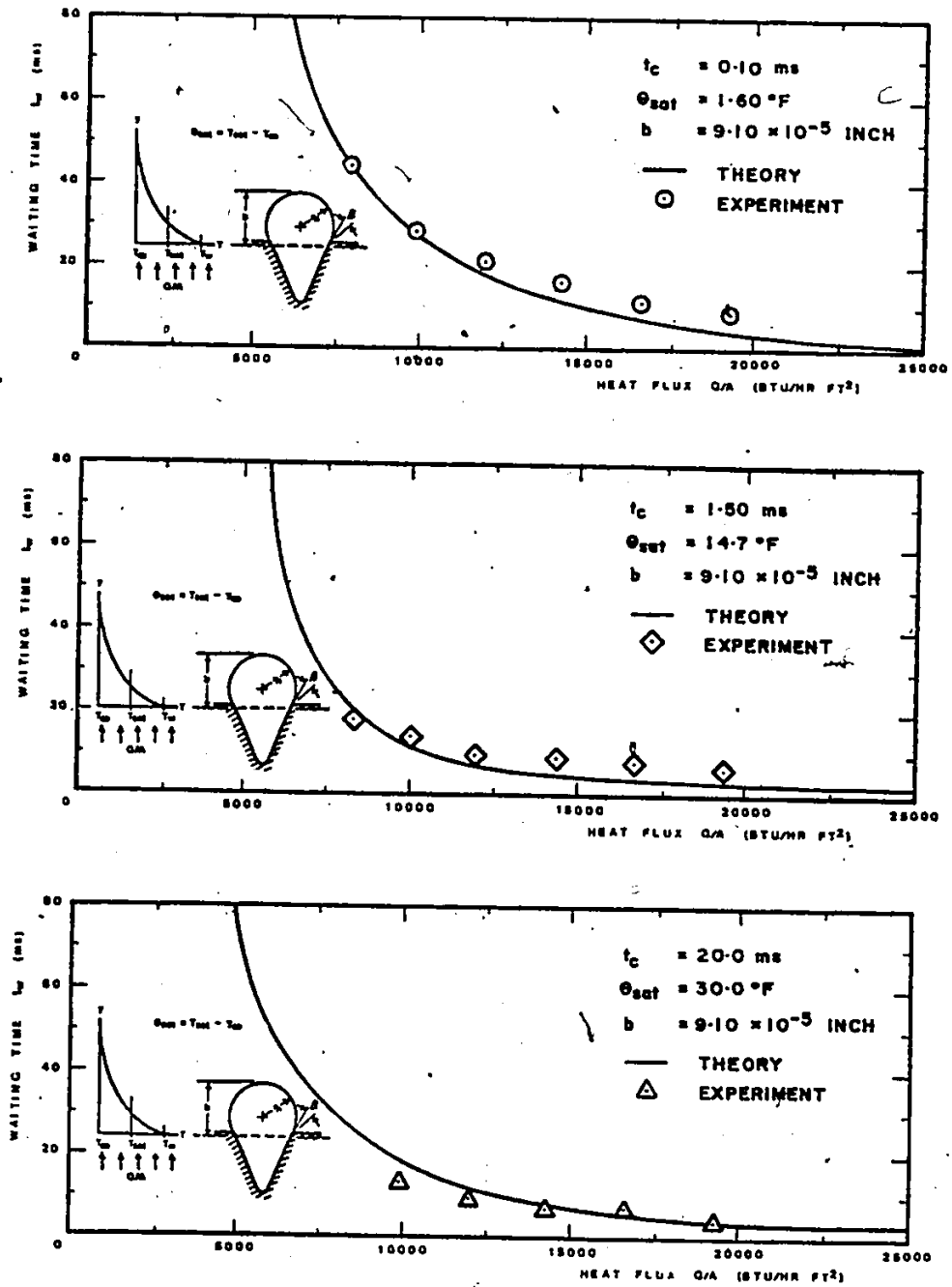
Figure 44   Agreement Between Theory and Experiment for Site A.
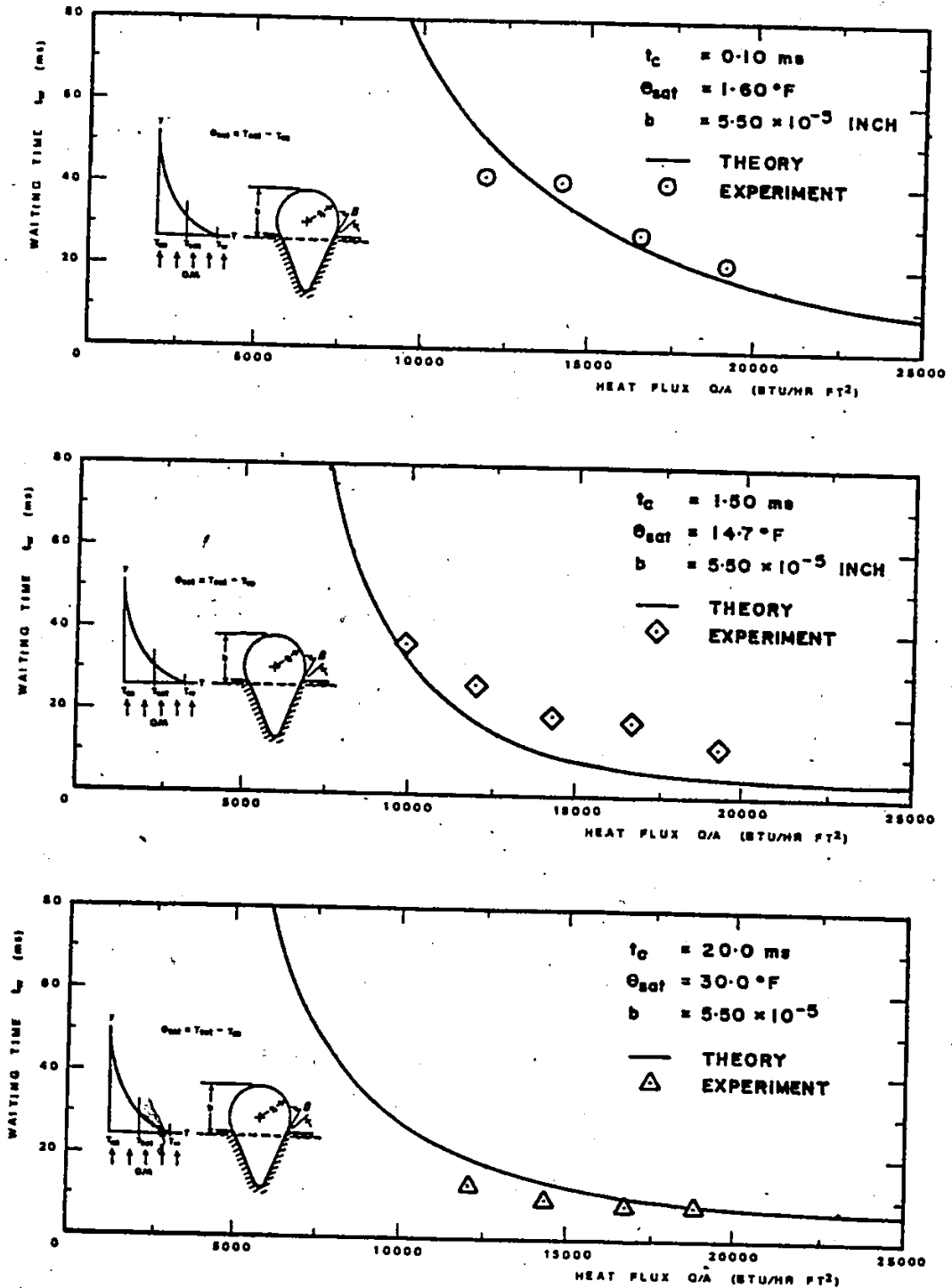
Figure 45   Agreement Between Theory and Experiment for Site B.
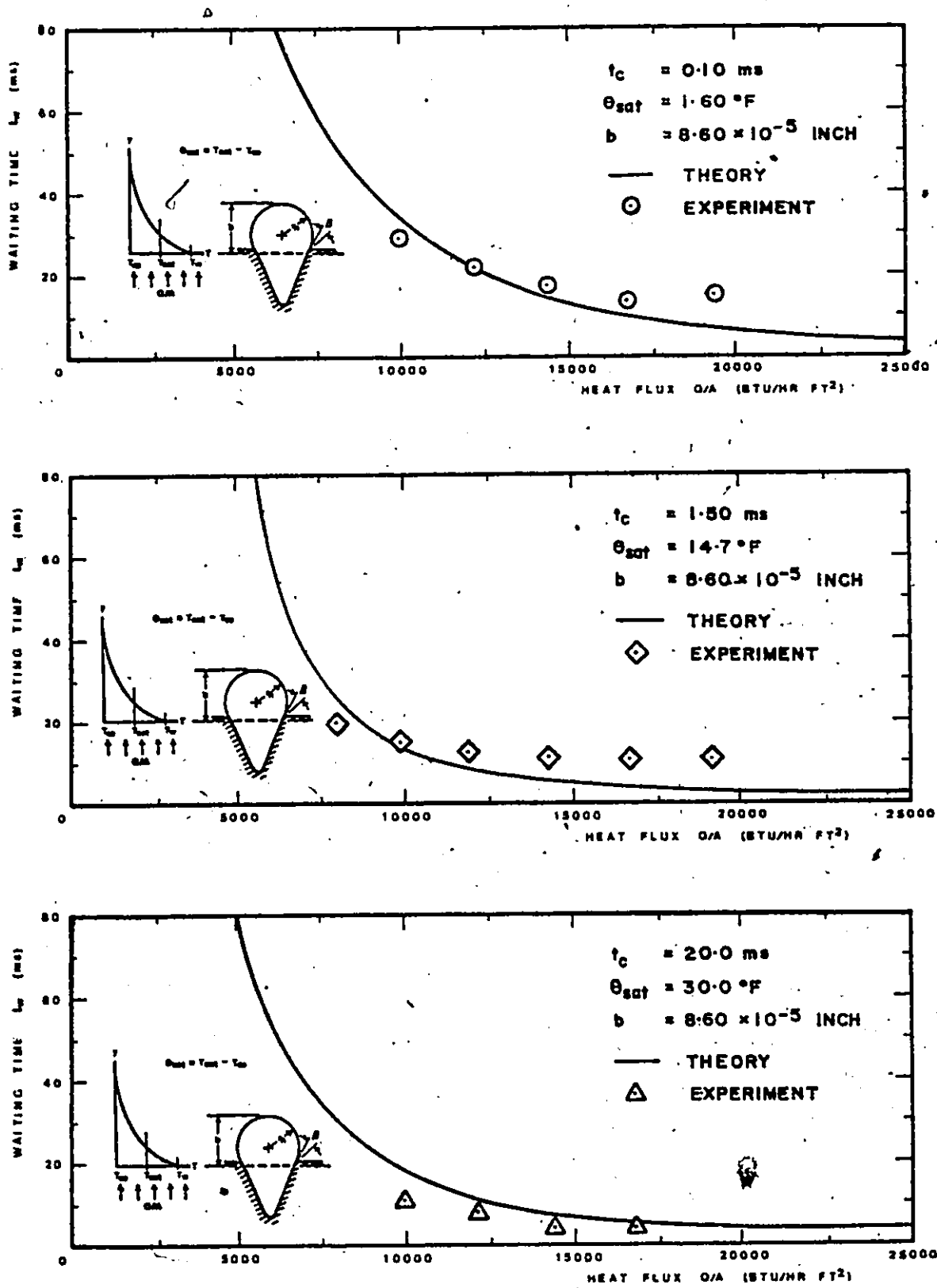
Figure 46   Agreement Between Theory and Experiment for Site C.
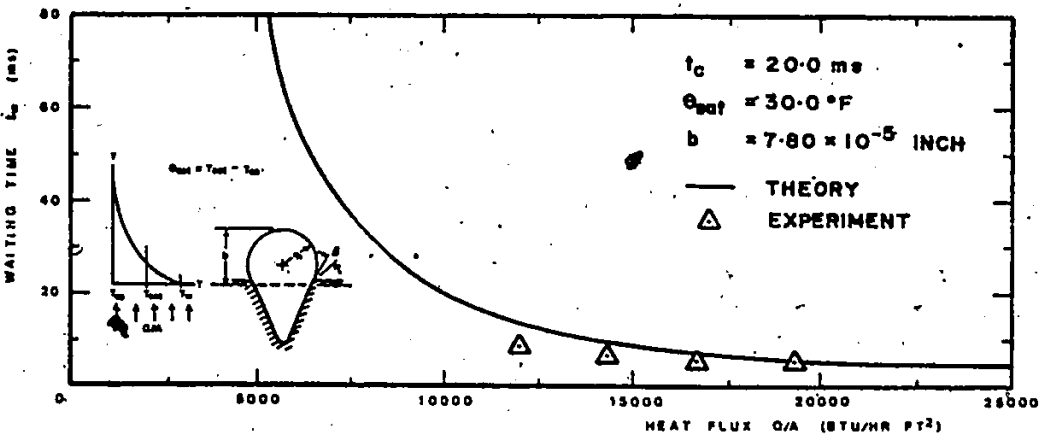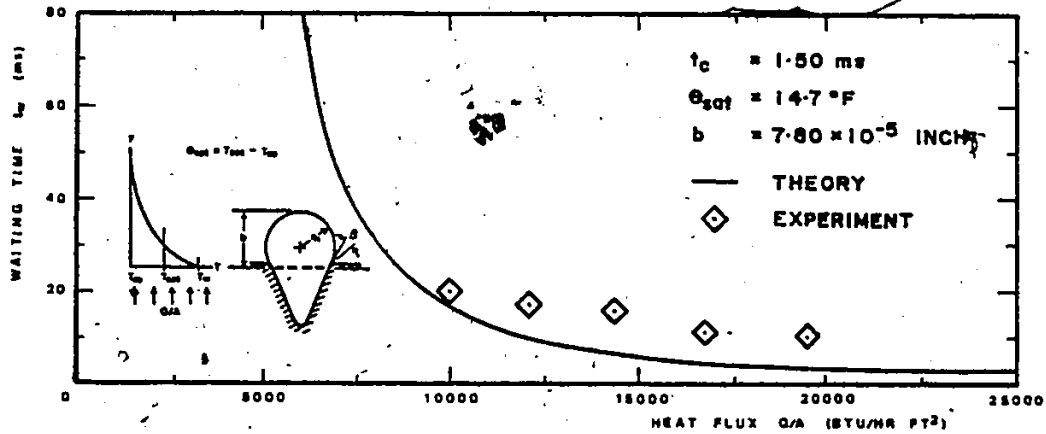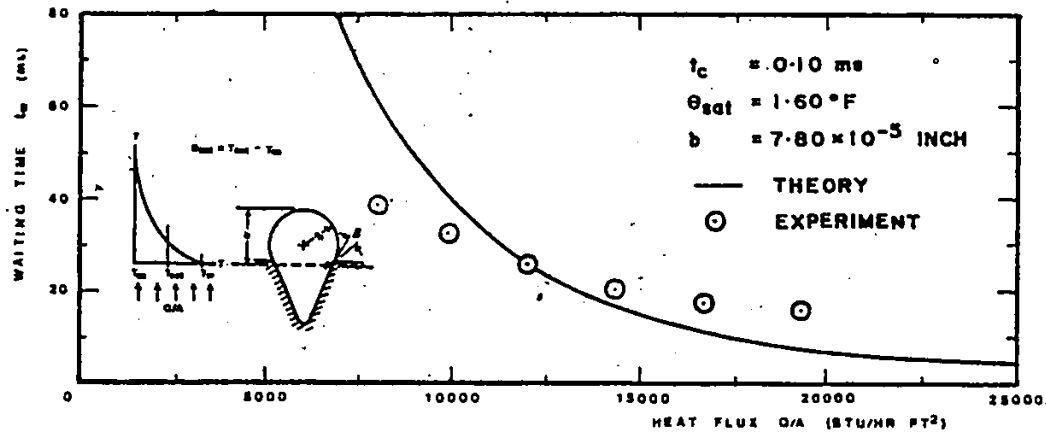
Figure 47   Agreement Between Theory and Experiment for Site I..
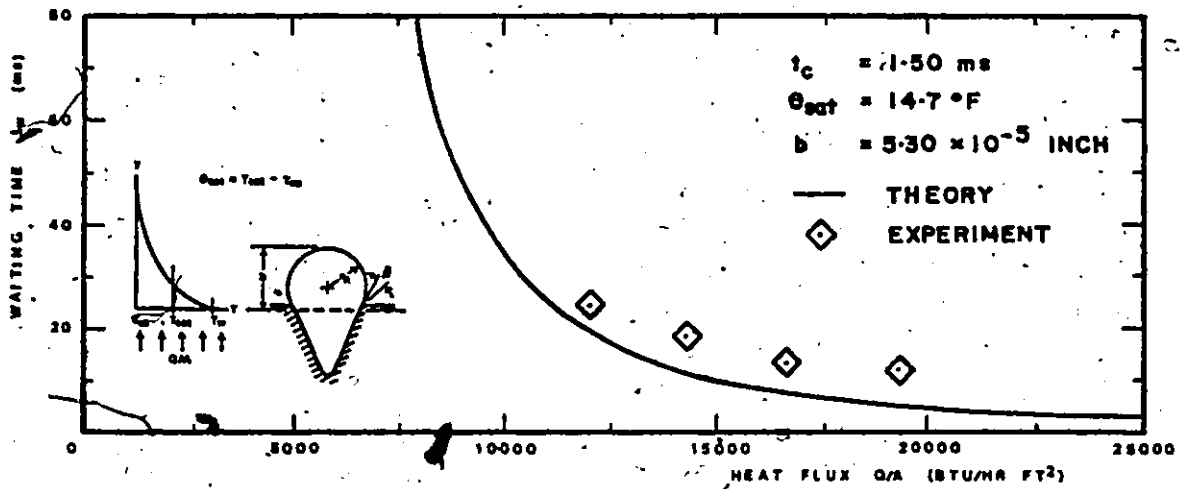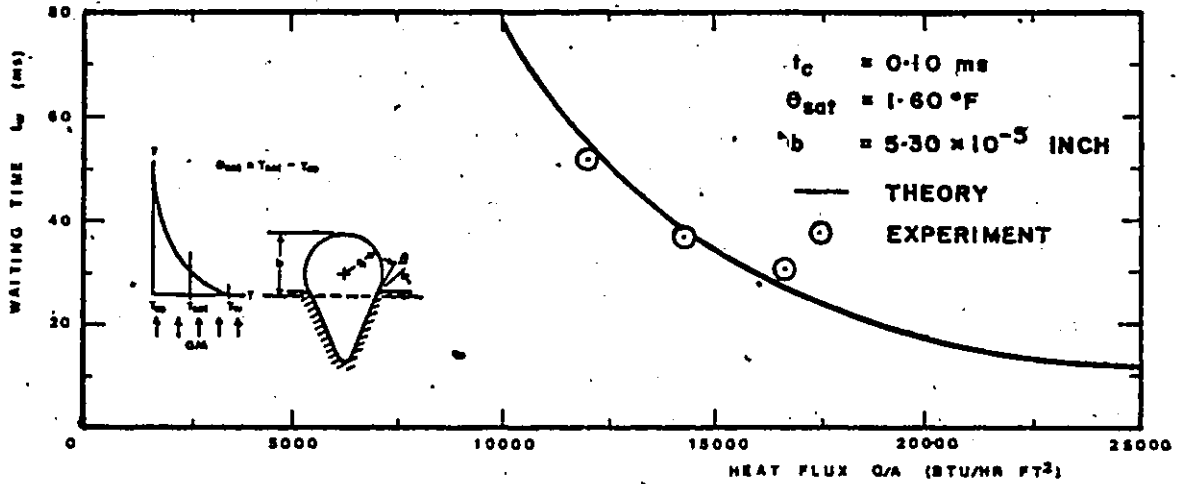
Figure 48   Agreement Between Theory and Experiment for Site K.

diction of bubble waiting times by the model and experimentally determined bubble waiting times, the value of t_w approaches very large values at a heat flux Q/A of approximately 6000 BTU/hr ft^2. The implication of this is that boiling should cease at about this level of heat flux if the nucleation model is realistic. Although precise experimental data is lacking, cessation of boiling occurred when the potential difference across the heating surface was approximately 40 volts, corresponding to a heat flux of 6250 BTU/hr ft^2.

In summary, the model of bubble nucleation formulated on the basis of a pure conduction mode of heat transfer to the liquid layer adjacent to the heat transfer surface was shown to predict bubble waiting time in boiling that were inconsistent with experimental data. Another bubble nucleation model was then formulated which incorporated a convective contribution, together with conduction heat transfer which appears to be present in the vicinity of active sites. The model was used to predict bubble waiting times that agreed reasonably well with experimentally determined values. It would therefore seem that some mode of heat transfer acts in conjunction with diffusion to promote bubble nucleation and the results of the present investigation suggest that convective energy transport is responsible.

CHAPTER 10

CONCLUSIONS

1. The investigation presents a set of measurements for nucleate boiling at atmospheric pressure using dichloromethane (methylene chloride) on a stannic oxide coated glass surface for ten levels of heat flux varying from approximately 2500 BTU/hr ft^2 to approximately 20,000 BTU/hr ft^2 and three levels of subcooling varying from 1.6^{o}F to 30.0^{o}F.

2. The results are comprised essentially of a set of measurements of average bubble waiting time for twelve active sites at six levels of heat flux varying from approximately 8000 BTU/hr ft^2 to approximately 20000 BTU/hr ft^2 and three levels of subcooling varying from 1.6^{o}F to 30.0^{o}F.

3. Bubble waiting time decreases as heat flux increases and subcooling increases.

4. A bubble nucleation model formulated on the basis of pure conduction of heat into the liquid layer adjacent to the heat transfer surface is not capable of predicting bubble waiting time.

5. A bubble nucleation model incorporating both conduction and convection of heat to the liquid in the vicinity of

active sites was found to be capable of predicting

bubble waiting time.

6. The growth of the thermal boundary layer, and subsequently

bubble nucleation, appears to be controlled by both diffu-

sion and convection of heat to the liquid in the vicinity

of active sites.

APPENDIX 1

VAPOUR PRESSURE CURVE FOR DICHLOROMETHANE

114.
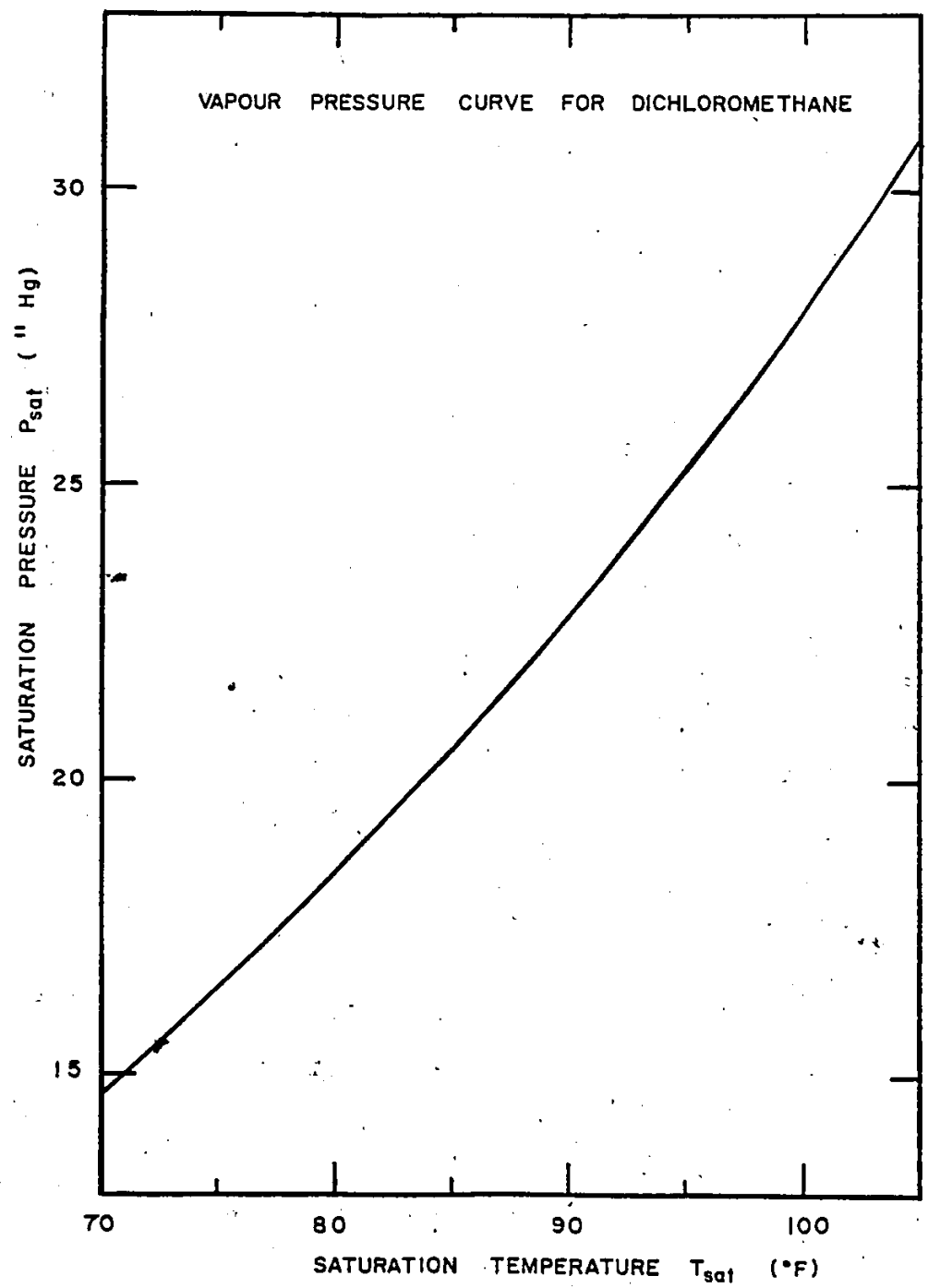
Figure 49   Vapour Pressure Curve for Dichloromethane.

APPENDIX 2

UNCERTAINTY ANALYSIS

APPENDIX 2

UNCERTAINTY ANALYSIS

A.2.1 Introduction

The following sections describe the uncertainty of measurements involved with the calculation of surface temperature, heat flux and bubble waiting time.

A.2.2 Surface Temperature

The surface temperature T_w was measured by a thermocouple "epoxied" to the underside of the test specimen. The correction for the temperature drop across the test specimen was determined by Judd [38] to be $0.69^\circ F$. Since the maximum wall temperature T_w measured in this investigation was $155.8^\circ F$, the uncertainty would be 0.44%.

A.2.3 Heat Flux

The uncertainty in the measured heat flux due to the uncertainty of the voltmeter and ohmmeter readings was determined by using the following equation:

$$\delta f = \left\{ \left| \frac{\partial f}{\partial x_1} \right|^2 (\delta x_1)^2 + \left| \frac{\partial f}{\partial x_2} \right|^2 (\delta x_2)^2 + \ldots + \left| \frac{\partial f}{\partial x_n} \right|^2 (\delta x_n)^2 \right\}^{\frac{1}{2}} \qquad A.2.1$$

where f = result computed

δf = uncertainty in f

117.

δx_n = uncertainty in the nth variable

x_n = nth variable

The uncertainty in the voltmeter reading was 1 Volt and that of the ohmmeter 1 Ohm. The uncertainty in the input energy was therefore 3.54%.

The uncertainty due to the loss of heat to the air space below the glass surface $Q_{underside}$ was computed using the relationship [46]

$$h_{av} = 0.12 \left(\frac{\Delta T}{L_c}\right)^{1/4} \qquad\qquad A.2.2$$

where L_c = $\dfrac{\text{surface area of glass plate}}{\text{perimeter of glass plate}}$

ΔT = difference between the temperature measured by the thermocouple "epoxied" on the underside of the glass surface and the ambient temperature.

With the use of equation A.2.2 the heat loss at the underside of the test specimen under the most severe conditions of the experiment was calculated as

$$Q_{underside} = 1.38 \text{ BTU/hr}$$

The uncertainty due to heat conduction to the base plate through the rubber gasket separating the heating surface from the base plate Q_{edges} was calculated using the relationship

$$Q_{edges} = kA \frac{\Delta T}{x}$$

where   k = 0.070 BTU/hr ft ^{O}F is the thermal conducti-

vity of the rubber gasket material.

x = 0.025 in is the thickness of the rubber gasket.

ΔT = temperature difference between the glass sur-
face and the vessel base plate.

A = area of contact between glass surface and vessel
base plate.

Assuming that conduction was undirectional through the gasket
into the vessel base plate and that the temperature of the
base plate was equal to the bulk liquid temperature T_∞, equa-
tion A.2.3 showed that the heat loss to the base plate was

$$Q_{edges} = 20.14 \text{ BTU/hr}$$

Considering the heat loss from the test specimen to
be the sum of $Q_{underside}$ and Q_{edges}, then

$$Q_{loss} = (1.38 + 20.14) \text{ BTU/hr}$$
$$= 21.52 \text{ BTU/hr}$$

This represents an uncertainty of 6.2% of the input energy.

A.2.4 Bubble Waiting Time

Because of the discontinuous nature of the framing
movie camera, the image of a bubble is recorded only at
discrete time intervals. Typically, at the beginning of an
emission cycle one frame would show no bubble at a particular
site and the next frame would show a bubble already of some

size. Similarly, towards the end of the cycle, one frame
would show a bubble of some size followed by a frame with
no bubble at the site being analyzed. With this situation
existing, the uncertainty in calculating waiting time with
the use of equation 7.3 was estimated to be one interframe
time interval Δt. The average value of Δt was computed to
be 1.1492 m s. With an average value of bubble waiting time
t_w of 25 m s, the uncertainty in the calculated values of
t_w is of the order of 4.6%.

APPENDIX 3

DERIVATION OF THE BUBBLE WAITING

TIME EQUATION

APPENDIX 3

DERIVATION OF THE BUBBLE WAITING TIME EQUATION

As explained in Appendix 2, because of the discontinuous nature of the framing movie camera the image of a bubble is recorded only at discrete time intervals. Consider a film strip showing the disappearance of a bubble at frame #n_1 and the appearance of a subsequent bubble at the same site at frame #(n_2+1) as shown in Figure 50. At one extreme the bubble waiting time could be

$$t_{w_{max}} = [(n_2+1) - (n_2-1)]\Delta t \qquad\qquad A.3.1$$

At the other extreme, the waiting time could be

$$t_{w_{min}} = (n_2-n_1)\Delta t \qquad\qquad A.3.2$$

Since

$$t_{w_{max}} \geq t_w \leq t_{w_{min}} \qquad\qquad A.3.3$$

equations A.3.1 and A.3.2 can be combined to give

$$t_w = \{[(n_2+1) - n_1] \pm 1\}\Delta t \qquad\qquad A.3.4$$

where the uncertainty is ± 1 Δt. Neglecting the uncertainty

$$t_w = [(n_2+1) - n_1]\Delta t \qquad\qquad A.3.5$$

BUBBLE

FRAME # n_1 SHOWING
THE DISAPPEARANCE
OF A BUBBLE

INCREASING n

FRAME # n_2 PRECEDING
FRAME # (n_2+1)

FRAME # (n_2+1) SHOWING
THE APPEARANCE OF A
SUBSEQUENT BUBBLE
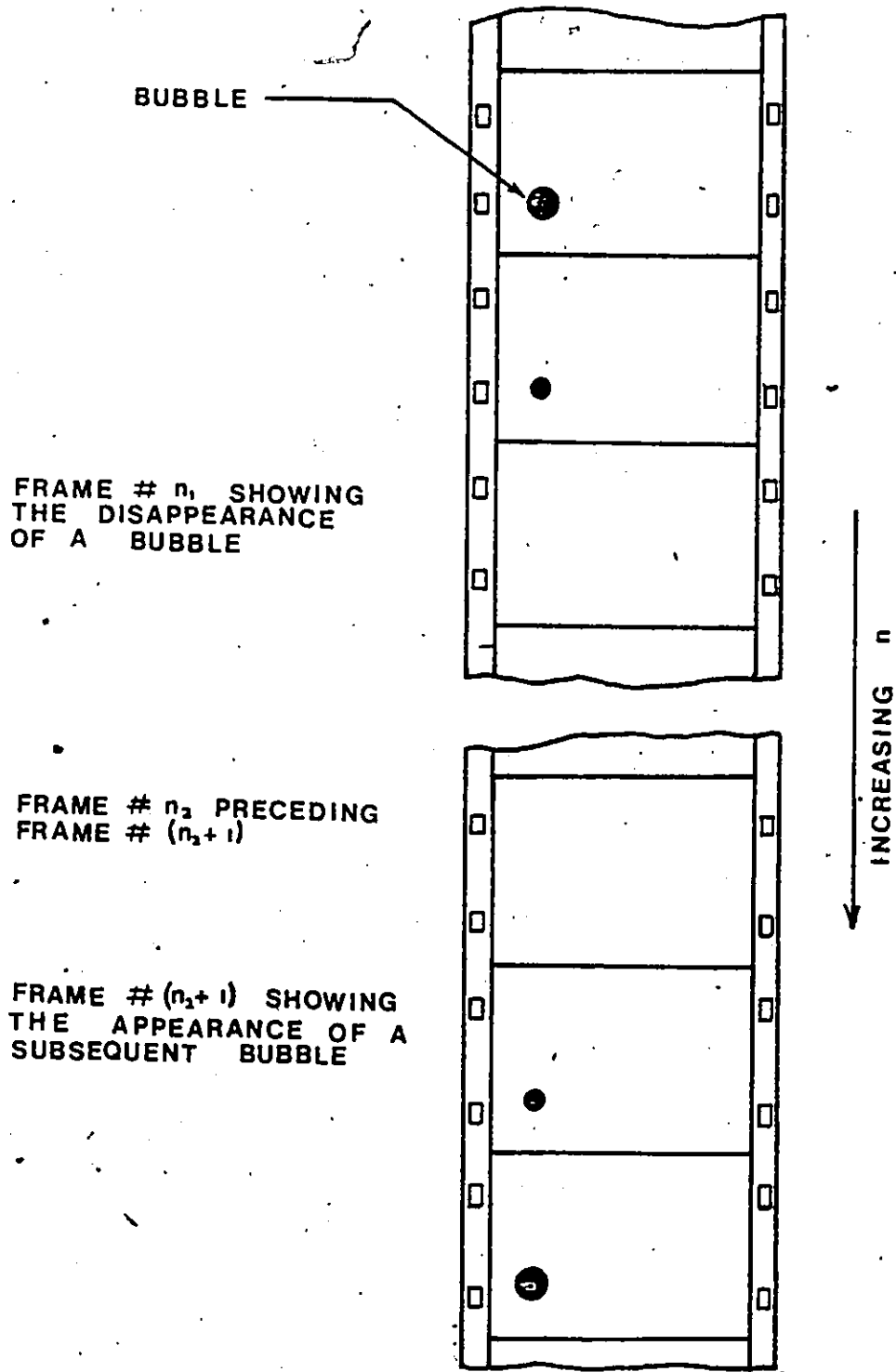
Figure 50   Bubble Images as Recorded on Film.

APPENDIX 4

FRAMING RATES

124.

APPENDIX 4

FRAMING RATES

Although the framing rate of the camera was nomi-
nally set at 1000 frames/second, the actual framing rates
as determined from an analysis of the timing marks on the
film strips were somewhat less as indicated in the table
below.

TABLE A.4.1   FRAMING RATES

FILM	FRAMING RATE (FRAMES/SEC)
1	872.8
2	858.3
3	889.5
4	867.1
5	866.7
6	870.8

125.

APPENDIX 5

THERMOMETRIC DATA

TABLE A.5.1   THERMOMETRIC DATA FOR DICHLOROMETHANE
                BOILING ON A GLASS SURFACE AT A PRESSURE
                OF 29.95" Hg AND SUBCOOLING OF 1.6°F

Q/A (BTU/hr ft^2)	T_W (°F)	T_∞ (°F)	$(T_W - T_\infty)$ (°F)
19124	153.6	101.9	51.7
16490	152.1	101.8	50.3
14050	151.1	101.9	49.2
11806	151.1	102.0	49.1
9757	150.3	101.6	48.7
7903	147.3	101.5	45.8
6245	143.3	101.4	41.9
4751	139.1	101.3	37.8
3513	133.2	101.2	32.0
2439	125.0	100.8	24.2

TABLE A.5.2   THERMOMETRIC DATA FOR DICHLOROMETHANE
BOILING ON A GLASS SURFACE AT A PRESSURE
OF 30.00" Hg AND SUBCOOLING OF 14.7°F.

Q/A (BTU/hr ft^2)	T_W (°F)	T_∞ (°F)	$(T_W - T_\infty)$ °F
19124	152.8	88.1	64.7
16490	152.3	89.1	63.2
14050	152.3	89.0	63.3
11806	150.4	88.9	61.5
9757	149.5	89.0	60.5
7903	146.1	89.0	57.1
6245	138.4	89.1	49.3
4751	129.2	89.0	40.2
3513	120.2	88.8	31.4
2439	113.7	89.2	24.5

TABLE A.5.3   THERMOMETRIC DATA FOR DICHLOROMEHANE
              BOILING ON A GLASS SURFACE AT A PRESSURE
              OF 30.25" Hg AND SUBCOOLING OF 30.0°F.

Q/A (BTU/hr ft^2)	T_W ($^\circ$F)	T_∞ ($^\circ$F)	$(T_W - T_\infty)$ $^\circ$F
19124	155.8	74.1	81.7
16490	155.0	73.9	81.1
14050	152.8	74.0	78.8
11806	150.3	73.8	76.5
9757	143.3	74.0	69.3
7903	134.9	74.0	60.9
6245	126.5	74.0	51.9
4751	115.6	74.3	41.3
3513	106.5	74.9	31.6

APPENDIX 6

BUBBLE WAITING TIME DATA

TABLE A.6.1   BUBBLE WAITING TIME DATA AT 1.60°F SUBCOOLING

	HEAT FLUX Q/A (BTU/hr ft^2)					
SITE	7903	9757	11806	14050	16490	19124
A	43.8	28.1	21.8	16.8	12.1	9.2
B	—	—	42.3	40.9	28.1	21.0
C	—	28.2	20.7	16.6	13.0	14.6
D	—	—	—	—	—	—
E	48.0	29.4	24.4	22.6	19.2	21.4
F	—	—	39.5	33.4	30.1	28.7
G	—	—	—	—	—	—
H	—	—	—	—	—	—
I	38.8	32.0	25.9	20.9	17.5	15.7
J	—	26.2	18.2	18.9	13.8	10.4
K	—	—	51.0	37.2	30.5	—
L	—	—	—	30.0	20.4	12.2

TABLE A.6.2   BUBBLE WAITING TIME DATA AT 14.7^{O}F SUBCOOLING

	HEAT FLUX Q/A (BTU/hr ft^2)					
SITE	7903	9757	11806	14050	16490	19124
A	19.2	14.7	10.3	8.8	8.1	6.3
B	—	36.2	26.7	19.7	18.0	12.7
C	18.7	14.9	12.1	11.3	10.0	10.3
D	—	—	—	42.7	—	24.0
E	—	—	18.1	16.0	15.4	9.5
F	—	—	26.4	20.6	15.9	13.0
G	—	—	65.4	42.6	33.2	24.4
H	—	—	—	48.2	35.5	20.5
I	—	19.4	16.6	15.0	10.7	10.3
J	—	—	—	—	7.6	7.6
K	—	—	24.8	19.1	13.8	12.6
L	—	—	—	—	—	—

TABLE A.6.3   BUBBLE WAITING TIME DATA AT 30.0°F SUBCOOLING

SITE	HEAT FLUX Q/A (BTU/hr ft^2)					
	7903	9757	11806	14050	16490	19124
A	—	12.1	8.8	6.7	7.3	4.8
B	—	—	12.4	9.2	8.1	6.2
C	—	10.3	7.4	4.3	5.4	—
D	—	—	—	—	25.5	17.4
E	—	—	—	—	—	—
F	—	—	—	—	—	—
G	—	—	48.0	40.9	28.9	17.1
H	—	—	—	40.5	31.5	22.2
I	—	—	9.1	7.5	6.2	6.0
J	—	—	—	—	—	—
K	—	—	—	—	—	—
L	—	—	—	—	5.6	3.9

APPENDIX 7

PROPERTIES OF DICHLOROMETHANE AT
ATMOSPHERIC PRESSURE

APPENDIX 7

PROPERTIES OF DICHLOROMETHANE AT ATMOSPHERIC PRESSURE

Saturation Temperature, T_{sat} $= 563^{o}R$

Liquid Density, ρ_{ℓ} $= 80.4 \; lb_m/ft^3$

Vapour Density, ρ_{v} $= 0.203 \; lb_m/ft^3$

Liquid Specific Heat, C_{ℓ} $= 0.28 \; BTU/lb_m \, ^{o}F$

Liquid Thermal Conductivity, k_{ℓ} $= 0.0869 \; BTU/hr \, ft \, ^{o}F$

Latent Heat of Vapourization, h_{fg} $= 139 \; BTU/lb_m$

Surface Tension, σ $= 1.63 \times 10^{-3} \; lb_f/ft$

Liquid Thermal Diffusivity, κ_{ℓ} $= 1.05 \times 10^{-6} \; ft^2/sec$

Liquid Coefficient of Cubical Expansion, β_{ℓ} $= 8.28 \times 10^{-4}/^{o}F$

Liquid Coefficient of Viscosity, μ_{ℓ} $= 0.878 \; lb_m/ft \, hr$

APPENDIX 8

COMPUTER PROGRAM FOR CALCULATING AND PLOTTING
BUBBLE WAITING TIME AS A FUNCTION OF HEAT FLUX -
CONDUCTION MODEL OF BUBBLE NUCLEATION

```
        PROGRAM CURFIT
C       THIS VERSION OF PROGRAM CURFIT INCORPORATES
C       CONSTANTS CALCULATED USING THE PROPERTIES
C       OF CH2C12 AT ONE ATMOSPHERE PRESSURE
        DOUBLE PRECISION P,Q
        DIMENSION A(5),B(5)
        REAL IERFC,NUM
        DATA A/5*0.0/,B/5*0.0/
        DATA Q/'        '/
        COMMON/STATUS/ISTAT(16)
        DO 25, I=1,100
C       TYPE 1
1       FORMAT(//,' CONTACT ANGLE = ',$)
C       ACCEPT 2, PHI
2       FORMAT(F4.1)
        TYPE 3
3       FORMAT(' SUBCOOLING = ',$)
        ACCEPT 4, SUB
4       FORMAT(F4.1)
        TYPE 5
5       FORMAT(' HEAT FLUX   WAITING TIME ')
        TYPE 6
6       FORMAT('   *****        **.*      ')
        N = 0
7       N = N + 1
        READ(5,8) P,B(N)
8       FORMAT(2X,A5,9X,F4.1)
        IF(P.EQ.Q) GO TO 10
        DECODE(5,9,P) A(N)
9       FORMAT(F7.0)
        GO TO 7
10      CALL INIT
        IX = 50
        IY = 20
        CALL GRID(IX,IY)
        CALL PLOT55(2,7,0,ISTAT)
        CALL LABEL('0            5000            10000
     1    HEAT FLUX (BTU/hr(ft.ft))        25000',
     2' 100         50            ')
        CALL PLOT55(9,0,0,ISTAT)
        CALL PLOT55(12,,'WAITING TIME (ms)',ISTAT)
        CALL PLOT55(9,49,1,ISTAT)
C       TYPE 11,PHI
11      FORMAT(' CONTACT ANGLE = ',F4.1,' DEGREES ')
        CALL PLOT55(9,49,3,ISTAT)
        TYPE 12,SUB
12      FORMAT(' SUBCOOLING = ',F4.1,' FAHRENHEIT ')
        CALL PLOT55(1,0,,ISTAT)
        DO 13, J=1,N-1
        IA = IFIX(A(J)/50.0)
        IB = IFIX(2.0*B(J))
13      CALL PLOT55(3,IA,IB,ISTAT)
14      CALL PLOT55(9,49,5,ISTAT)
        TYPE 15
15      FORMAT(' NUCLEUS SIZE = ',$)
        ACCEPT 16, P
16      FORMAT(A5)
        IF(P.EQ.Q) GO TO 24
        DECODE(5,17,P) SIZE
17      FORMAT(F4.1)
```

```
      IF(SIZE.EQ.0) GO TO 24
      X = 1.00E-3*(2.00)
      Y = SIZE*1.0E-4
      CALL PLOT55(1,1,,ISTAT)
      CALL PLOT55(7,0,0,ISTAT)
      CALL PLOT55(8,512,0,ISTAT)
      TW = 118.0
18    ITW = IFIX(2.0*TW)
      Z = 7.773E-4*SQRT(TW)
      ARG2 = Y/Z
      SUM = ARG2
      DENOM = 1
      N = 0
19    N = N + 1
      TERM = 2*N + 1
      NUM = 2.0**N
      DENOM = DENOM*TERM
      ADDSUM = (NUM/DENOM)*((ARG2)**TERM)
      RATIO = ADDSUM/SUM
      IF(RATIO.LT.1.0E-6) GO TO 20
      SUM = SUM + ADDSUM
      GO TO 19
20    ERFC = 1.0 - 1.12838*EXP(-ARG2*ARG2)*SUM
      IERFC = 0.56419*EXP(-ARG2*ARG2) - ARG2*ERFC
      FLUX = 1.04280*(X/Y + SUB)/(Z*IERFC)
      IF(FLUX.GE.25000.0) GO TO 21
      IFLUX = IFIX(FLUX/50.0)
      CALL PLOT55(3,IFLUX,ITW,ISTAT)
      TW = TW -1.0
      IF(TW.EQ.0) GO TO 21
      GO TO 18
21    READ(5,22) KR
22    FORMAT(A2)
      CALL PLOT55(9,49,6,ISTAT)
      CALL PLOT55(12,,'              ',ISTAT)
      GO TO 14
24    CALL CLEAR
25    CONTINUE
      STOP
      END
```

APPENDIX 9

COMPUTER PROGRAM FOR CALCULATING AND PLOTTING
BUBBLE WAITING TIME AS A FUNCTION OF HEAT FLUX -
CONDUCTION-CONVECTION MODEL OF BUBBLE NUCLEATION

139.

```
        PROGRAM WAIT5
C       THIS VERSION OF PROGRAM WAIT5 INCORPORATES
C       CONSTANTS CALCULATED USING THE PROPERTIES
C       OF CH2CI2 AT ONE ATMOSPHERE PRESSURE
        DOUBLE PRECISION P,Q
        DIMENSION A(7),B(7),DELTA(120)
        REAL INC
        DATA A/7*0.0/,B/7*0.0/
        DATA Q/'         '/
        COMMON/STATUS/ISTAT(16)
        DO 25, I=1,100
        TYPE 1
1       FORMAT(//,' TIME CONSTANT  = ',$)
        ACCEPT 2,TC
2       FORMAT(F6.3)
        TYPE 3
3       FORMAT(' SUBCOOLING = ',$)
        ACCEPT 4, SUB
4       FORMAT(F4.1)
        TYPE 5
5       FORMAT(' HEAT FLUX    WAITING TIME ')
        TYPE 6
6       FORMAT('    XXXXX          XX.X      ')
        N = 0
7       N = N + 1
        READ(5,8) P,B(N)
8       FORMAT(2X,A5,9X,F4.1)
        IF(P.EQ.Q) GO TO 10
        DECODE(5,9,P) A(N)
9       FORMAT(F7.0)
        GO TO 7
10      CALL INIT
        IX = 50
        IY = 20
        CALL GRID(IX,IY)
        CALL PLOT55(2,7,0,ISTAT)
        CALL LABEL('0             5000              10000
     1      HEAT FLUX (BTU/hr(ft.ft))          25000',
     2' 100       50                    ')
        CALL PLOT55(9,0,0,ISTAT)
        CALL PLOT55(12,,'WAITING TIME (ms)',ISTAT)
        CALL PLOT55(9,49,1,ISTAT)
        TYPE 11,TC
11      FORMAT(' TIME CONSTANT =   ',F6.3,' ms ')
        CALL PLOT55(9,49,3,ISTAT)
        TYPE 12,SUB
12      FORMAT(' SUBCOOLING = ',F4.1,' FAHRENHEIT ')
        CALL PLOT55(1,0,,ISTAT)
        DO 13, J=1,N-1
        IA = IFIX(A(J)/50.0)
        IB = IFIX(2.0*B(J))
13      CALL PLOT55(3,IA,IB,ISTAT)
14      CALL PLOT55(9,49,5,ISTAT)
        TYPE 15
15      FORMAT(' NUCLEUS SIZE = ',$)
        ACCEPT 16, P
16      FORMAT(A5)
        IF(P.EQ.Q) GO TO 24
        DECODE(5,17,P) SIZE
17      FORMAT(F4.2)
```

```
      IF(SIZE.EQ.0) GO TO 24
      X = 1.00E-3*(2.00)
      Y = SIZE*1.0E-4
      IF(TC.EQ.0.0) TC = 0.001
      DT = (0.1/TC)
      PHISQR = 12.0*DT*(ALOG(DT)+10.0)
      INC = 0.0
      TAU = DT
      TERM = (1.0-EXP(-DT))
      COEFF = (TERM/(TAU-TERM))
      RATIO = 1.0
      DO 18, J=1,1180
      PHISQR = PHISQR + INC
      PHI = SQRT(PHISQR)
      N = ((J-1)/10)+1
      DELTA(N) = 3.887E-4*SQRT(TC)*PHI
      INC = DT*(COEFF*PHISQR*
     1(0.5741*(RATIO)-0.0816*(RATIO**3)+0.0204*(RATIO**4))+12.0)
      TAU = TAU + DT
      TERM = (1.0-EXP(-TAU))
      COEFF = (TERM/(TAU-TERM))
      CHI = (3.85/SQRT(TC))*(TAU-TERM)
      RATIO = PHI/CHI
      IF(RATIO.GT.1.0) RATIO = 1.0
18    CONTINUE
      CALL PLOT55(1,1,,ISTAT)
      CALL PLOT55(7,0,0,ISTAT)
      CALL PLOT55(8,512,0,ISTAT)
      TW = 118.0
19    ITW = IFIX(2.0*TW)
      ARG = Y/DELTA(IFIX(TW))
      IF(ARG.LT.1.0E-10) ARG = 1.0E-10
20    FUNC = 1.0-3.0*(ARG)+3.0*(ARG*ARG)-1.0*(ARG*ARG*ARG)
      FLUX = 3.12840*(X/Y+SUB)/(DELTA(IFIX(TW))*FUNC)
      IF(FLUX.GE.25000.0) GO TO 21
      IFLUX = IFIX(FLUX/50.0)
      CALL PLOT55(3,IFLUX,ITW,ISTAT)
      TW = TW - 1.0
      IF(TW.EQ.0) GO TO 21
      GO TO 19
21    READ(5,22) KR
22    FORMAT(A2)
      CALL PLOT55(9,49,6,ISTAT)
      CALL PLOT55(12,,'                    ',ISTAT)
      GO TO 14
24    CALL CLEAR
25    CONTINUE
      STOP
      END
```

NOMENCLATURE

SYMBOL	DESCRIPTION	UNITS
A	Total Area of Heat Transfer Surface	ft^2
	Parameter $A = \dfrac{2\sigma T_{sat}}{\rho_v h_{fg}}$	$ft\ ^\circ R$
a	Local Area of Heat Transfer Surface	ft^2
b	Height of Bubble Nucleus Above Point of Contact of Liquid-Vapour Interface With Heat Transfer Surface	inch
C	Specific Heat	$BTU/lb_m\ ^\circ F$
	Constant $C = V_\infty t_c$	inch
C_1	Constant $C_1 = \dfrac{1 + \cos\beta}{\sin\beta}$	
C_2	Constant $C_2 = \dfrac{1}{\sin\beta}$	
C_3	Constant $C_3 = \dfrac{C_1}{C_2}$	
D	Bubble Departure Diameter	inch
E	Potential Difference	Volts
f	Bubble Emission Frequency	sec^{-1}
g	Gravitational Constant	ft/sec^2
h	Heat Transfer Coefficient	$BTU/hr\ ft^2\ ^\circ F$
h_{fg}	Latent Heat of Vapourization	BTU/lb_m
k	Thermal Conductivity	$BTU/hr\ ft\ ^\circ F$
L_c	Ratio L_c = Area of Heat Transfer Surface/Perimeter of Heat Transfer Surface	ft

142.

m	Mass	lb_m
N	Total Number of Active Sites	
Na	Population of Active Sites or Local Area a	
$\overline{Na}$	Average Population of Active Sites on Area a	
N/A	Active Site Density	
$\overline{N}$	Average Population of Active Sites on Area A	
n_1	Frame Number at which Bubble just Disappeared	
n_2+1	Frame Number at which Subsequent Bubble just Appeared.	
P	Pressure	lb_f/ft^2
$P_U(Na)$	Probability that a Random Local Area a has a Population Na	
Q/A	Heat Flux	$BTU/hr\ ft^2$
q	Parameter $q = \sqrt{s/\kappa_\ell}$	
R	Electrical Resistance	Ohms
r	Radial Coordinate	
r_c	Cavity Mouth Radius	inch
r_n	Bubble Nucleus Radius	inch
$\overline{S}$	Mean Nearest Neighbor Distance between Active Sites	inch
$\sqrt{\overline{S^2}}$	Root-Mean-Square Nearest Neighbor Distance between Active Sites	inch
S_{mp}	Most Probable Nearest Neighbor Distance between Active Sites	inch
s	Laplace Transportation of Time	
T	Temperature	$^oF,\ ^oC,\ ^oR$
ΔT	Temperature Difference between Underside of Glass Specimen and Ambient	^oF

t	Time	sec
t_c	Time Constant	sec
t_g	Bubble Growth Time	sec
t_w	Bubble Waiting Time	sec
Δt	Interframe Time Interval	sec
U_δ	Velocity of Flow at Base of Bubble	in/sec
u	Horizontal Component of Velocity	in/sec
V_∞	Terminal Rise Velocity of Bubble	in/sec
v_{fg}	Specific Volume Change of Vapourization	ft^3/lb_m
x	Horizontal Cartesian Coordinate	
y	Vertical Cartesian Coordinate	
Z	Dimensionless Distance $Z = [y/(2\sqrt{\kappa_\ell t})]$	
Z_{Na}	Number of Local Areas a having a Local Population Na	
β	Liquid Contact Angle Coefficient of Cubical Expansion	$^oF^{-1}$
δ	Hydrodynamic Boundary Layer Thickness Extrapolated Superheat Layer Thickness	inch inch
Δ	Local Thermal Boundary Layer Thickness	inch
δ_1	Thermal Boundary Layer Thickness at a Distance from Active Nucleation Sites	inch
δ_2	Local Thermal Boundary Layer Thickness	inch
η	Ratio $y/\Delta(t)$	
θ	Temperature Difference $\theta = T - T_\infty$	^oF
$\bar{\theta}$	Laplace Transformation of θ	
θ_{sat}	Liquid Subcooling $\theta_{sat} = T_{sat} - T_\infty$	^oF

θ_w	Wall Superheat $\theta_w = T_w - T_{sat}$	^oF
κ	Thermal Diffusivity	ft^2/hr
μ	Coefficient of Viscosity	$lb_m/ft\ hr$
ξ	Ratio $y/\delta(t)$	
ϕ	Parameter $\phi = \Delta(t)/\sqrt{\kappa_\ell t_c}$	
ρ	Density	lb_m/ft^3
σ	Surface Tension	lb_f/ft
τ	Dimensionless Time $\tau = t/t_c$	
χ	Parameter $\chi = \delta(t)/\sqrt{\kappa_\ell t_c}$.	

SUBSCRIPT	DESCRIPTION
b	Bubble
c	Cavity
ℓ	Liquid
n	Nucleus
sat	Saturation
v	Vapour
w	Wall
∞	Bulk

REFERENCES

1. Fisher, J. C., "The Fracture of Liquids", Journal of Applied Physics, Vol. 19, Nov. 1948, pp. 1062-1067.

2. Turnbull, D., "Kinetics of Heterogeneous Nucleation", Journal of Chemical Physics, Vol. 18, No. 2, Feb. 1950, pp. 198-203.

3. Bankoff, S. G., "Ebullition From Solid Surfaces in the Absence of a Pre-existing Gaseous Phase", Trans. ASME, Vol. 79, 1957, pp. 735-740.

4. Bankoff, S. G., "Entrapment of a Gas in the Spreading of a Liquid over a Rough Surface", A.I.Ch.E. Journal, Vol. 4, No. 1, March 1958, pp. 24-26.

5. Knapp, R. T., "Cavitation and Nuclei", Trans. ASME, Vol. 80, 1958, pp. 1315-1324.

6. Griffith, P. and Wallis, J.D., "The Role of Surface Conditions in Nucleate Boiling", Chem. Eng. Progress Symp. Series, Vol. 55, 1959, pp. 49-63.

7. Clark, H. B., Strenge, P. S. and Westwater, J. W., "Active Sites for Nucleate Boiling", Chem. Eng. Progress Symp. Series, Vol. 55, 1959, pp. 103-110.

8. Nix, G. H., Vachon, R. I. and Hall, D. M., "A Scanning and Electron Microscopy Study of Pool Boiling Surfaces", Heat Transfer 1970, Fourth Int. Heat Transfer Conference, Paris-Versailles, 1970, B1.6.

9. Nail, J. P., Vachon, R. I. and Morehouse, J., "An SEM Study of Nucleation Sites in Pool Boiling from 304 Stainless-Steel, Journal of Heat Transfer, Trans. ASME, May 1974, pp. 132-137.

10. Berenson, P. J., "Experiments on Pool Boiling Heat Transfer", Int. Journal of Heat and Mass Transfer, Vol. 5, 1962, pp. 985-999.

11. Marto, P. J., Moulson, J. A. and Maynard, M. O., "Nucleate Pool Boiling of Nitrogen with Different Surface Conditions", Journal of Heat Transfer, Trans. ASME, Series C, Vol. 90, No. 2, Nov. 1968, pp. 437-444.

- 146.

12. Jakob, M., "Heat Transfer", Vol. 1, Wiley, New York, 1949.

13. Corty, C. and Foust, A. S., "Surface Variables in Nucleate Boiling", Chem. Eng. Progress Symp. Series, Vol. 51, No. 17, 1955, pp. 1-12.

14. Kurihara, H. M. and Myers, J. E., "The Effect of Superheat and Surface Roughness on Boiling Coefficient", A.I.Ch.E. Journal, Vol. 6, No. 1, March 1960, pp. 83-91.

15. Nishikawa, K., Trans. Soc. Mechanical Engineers, Japan, Vol. 20, 1954.

16. Hsu, S. T. and Schmidt, F. W., "Measured Variables in Local Surface Temperatures in Pool Boiling of Water", Journal of Heat Transfer, Trans. ASME, August 1961, pp. 254-260.

17. Hatton, A. P. and Hall, I. S., "Photographic Study of Boiling on Prepared Surfaces", Proceedings of the Third Int. Heat Transfer Conference, Chicago, 1966.

18. Vachon, R. I., Tanger, G. E., Davis, D. L. and Nix, G.H., "Pool Boiling on Polished and Chemically Etched Stainless Steel Surfaces", Journal of Heat Transfer, Trans. ASME, Vol. 90, 1968, pp. 231-237.

19. Gaertner, R. F., "Distribution of Active Sites in Nucleate Boiling of Liquids", Chem. Eng. Progress Symp. Series, Vol. 59, No. 41, 1963, pp. 52-61.

20. Sultan, M. A. E., "Spatial Distribution of Active Sites and Bubble Flux Density", M.Eng. Thesis, McMaster University, 1977.

21. Shoukri, M. S. M., "Nucleation Site Activation in Saturated Boiling", M.Eng. Thesis, McMaster University, 1974.

22. Brown, W. T., "Study of Flow Surface Boiling", Ph.D. Thesis, Mech. Eng. Dept., M.I.T., 1967.

23. Hsu, Y. Y., "On the Size Range of Active Nucleation Cavities on a Heating Surface", Journal of Heat Transfer, Trans. ASME, Aug. 1962, pp. 207-216.

24. Heled, Y. and Orell, A., "Characteristics of Active Nucleation Sites in Pool Boiling", Int. Journal of Heat and Mass Transfer, Vol. 10, 1967, pp. 553-554.

25. Wiebe, J. R. and Judd, R. L., "Superheat Layer Thickness Measurements in Saturated and Subcooled Nucleate Boiling", Journal of Heat Transfer, Trans. ASME, Nov. 1971, pp. 455-461.

26. Han, C. and Griffith, P., "The Mechanism of Heat Transfer in Nucleate Pool Boiling", Part I, Int. Journal of Heat and Mass Transfer, Vol. 8, 1965, pp. 887-904.

27. Hsu, Y. Y. and Graham, R. W., "An Analytical and Experimental Study of the Thermal Boundary Layer and Ebullition Cycle in Nucleate Boiling", NASA TN D-594, 1961.

28. Yamagata, F. H., Nishikawa, K. and Matsouka, H., "Nucleate Boiling of Water on the Horizontal Heating Surface", Kyusu Imperial University, Faculty of Engineering Memoirs, Vol. 1, 1955, pp. 97-163.

29. Marcus, B.D. and Dropkin, D., "Measured Temperature Profiles Within the Superheated Boundary Layer Above a Horizontal Heating Surface in Saturated Nucleate Pool Boiling of Water", Journal of Heat Transfer, Trans. ASME, Series C, Vol. 87, No. 3, Aug. 1965, pp. 333-341.

30. Best, R., Burow, P. and Beer, H., "Die Warmeubertragung Beim Sieden Unter Dem Einfluss Hydrodynamischer Vorgange", Int. Journal of Heat and Mass Transfer, Vol. 18, 1975, pp. 1037-1047.

31. Rohsenow, W., "A Method of Correlating Heat Transfer Data for Surface Boiling of Liquids", Trans. ASME, Vol. 74, Aug. 1952, pp. 969-976.

32. McFadden, P. W. and Grassman, P., "The Relation Between Bubble Frequency and Diameter During Nucleate Pool Boiling", Int. Journal of Heat and Mass Transfer, Vol. 5, 1962, pp. 169-173.

33. Cole, R., "A Photographic Study of Pool Boiling in the Region of Critical Heat Flux", A.I.Ch.E. Journal, Vol. 6, No. 4, Dec. 1960, pp. 533-558.

34. Hahne, E. and Grigull, V., "Heat Transfer in Boiling", Ch. 3, Academic Press, New York, 1977.

35. Cochran, T. H. and Aydelott, J. C., "Effects of Subcooling and Gravity Level on Boiling in the Discrete Bubble Region", NASA TN D-3449, 1966.

36. Ellion, M. E., "A Study of the Mechanism of Boiling Heat Transfer", Memo #20-88, Jet Propulsion Laboratory, California Institute of Technology, March 1954, p. 72.

37. Gunther, F. G., "Photographic Study of Surface Boiling Heat Transfer to Water with Forced Convection", Trans. ASME, Vol. 73, 1951, p. 115.

38. Judd, R. L., "Influence of Acceleration on Subcooled Nucleate Boiling", Ph.D. Thesis, University of Michigan, 1968.

39. Shoukri, S. M. S., "The Influence of Surface Conditions in Nucleate Boiling", Ph.D. Thesis, McMaster University, 1977.

40. Lorenz, H. G., Mikic, B. B. and Rohsenow, W. M., "The Effect of Surface Conditions on Boiling Characteristics", Proceedings of the Fifth Int. Heat Transfer Conference, Japan, Vol. IV, 1974.

41. Arpaci, V. S., "Conduction Heat Transfer", Addison-Wesley Publishing Company, Massachusetts, 1966, pp. 350-351.

42. Judd, R. L., Private Communication.

43. Johnson, M. A., de la Pena, J. and Mesler, B. B., "Bubble Shapes in Nucleate Boiling", Chem. Eng. Progress Symp. Series, No. 64, Vol. 62, 1966, pp. 1-5.

44. Voutsinos, C. M., "Laser Interferometric Investigation of Microlayer Evaporation for Various Levels of Subcooling and Heat Flux", M.Eng. Thesis, McMaster University, 1976.

45. Judd, R. L. and Hwang, K. S., "A Comprehensive Model for Nucleate Pool Boiling Heat Transfer Including Microlayer Evaporation", Journal of Heat Transfer, Vol. 98, No. 4, Nov. 1976, pp. 623-629.

46. McAdams, W. H., "Heat Transmission", 3rd Edition, McGraw-Hill Book Company, New York, 1954, p. 180.